UNIVERSITY OF SOUTHAMPTON

FACULTY OF PHYSICAL SCIENCES AND ENGINEERING

School of Electronics and Computer Science

Sensory Feedback for Artificial Hands

by

Noor Hazrin Hany Bt Mohamad Hanif

Thesis for the degree of Doctor of Philosophy

November 2015

UNIVERSITY OF SOUTHAMPTON

ABSTRACT

FACULTY OF PHYSICAL SCIENCES AND ENGINEERING

ELECTRONICS AND COMPUTER SCIENCE

Doctor of Philosophy

SENSORY FEEDBACK FOR ARTIFICIAL HANDS

by Noor Hazrin Hany Bt Mohamad Hanif

Executing daily chores with missing limbs is undoubtedly very challenging. For a person who has lost his lower arm, it is highly desirable to replace this loss with a device that not only identical in appearance, but closely mimics its capabilities. While there are many prosthetic products of multiple functionalities in the current market, the capability of the device to replicate the tactile sensory system, the sensation largely felt at the fingertips and palm, is often neglected.

The motivation of this work is to provide a sense of embodiment to prosthetic users by supplementing their devices with a sensory feedback to the residual arm using haptic technology. A piezoelectric sensor attached to a fingertip of a Southampton Hand, is used to acquire vibration signals as a textured surface slides past the finger. With an upgraded data acquisition strategy, the piezoelectric sensor has been able to detect signal frequencies generated during the exploratory movement that reliably correlate to all the widths of grooves and ridges of the surface textures under investigation. The same signal frequencies become input signals to the Eccentric Rotation Mass (ERM), a haptic actuator selected to produce vibration to the upper arm, in accordance with the sensation felt by a finger when exploring the surface textures. A prototype that includes the ERM miniature motor and a specially designed brass platform has been fabricated to work at 250 Hz, the optimum frequency of mechanoreceptors underneath the skin of the upper arm. Results from the psychophysical investigation demonstrated that participants were able to associate the vibration patterns perceived at their upper arms with the surface textures felt on their fingertips. The findings from this work provide optimistic possibility that touch sensations that was previously lost could be ‘felt’ by the users. This would undeniably enhance their appreciation towards a well-designed device that feels more natural due to its ‘life-like’ quality.

Table of Contents

List of Figures

List of Tables

Declaration of Authorship

I, Noor Hazrin Hany Mohamad Hanif declare that this thesis entitled 'Sensory Feedback for Artificial Hands' and the work presented in it are my own and has been generated by me as the result of my own original research.

I confirm that:

1. This work was done wholly or mainly while in candidature for a research degree at this University;
2. Where any part of this thesis has previously been submitted for a degree or any other qualification at this University or any other institution, this has been clearly stated;
3. Where I have consulted the published work of others, this is always clearly attributed;
4. Where I have quoted from the work of others, the source is always given. With the exception of such quotations, this thesis is entirely my own work;
5. I have acknowledged all main sources of help;
6. Where the thesis is based on work done by myself jointly with others, I have made clear exactly what was done by others and what I have contributed myself;
7. Parts of this work have been published as listed in Section 1.4.

Signed:

NOOR HAZRIN HANY BT MOHAMAD HANIF

Date: 18th November 2015

Acknowledgements

"So, undoubtedly, along with the hardship there is ease. Undoubtedly, along with the hardship there is ease." *(Al-Inshirah: 5-6)*

First and foremost, my deepest gratitude goes to Allah s.w.t. for giving me the deen, the faith, the health and the strength to successfully complete this thesis. Without His permission and help, I would have not been able to achieve this stage of my PhD journey.

Secondly, I would like to express my sincerest appreciation to my main supervisor, Dr Paul Chappell, for his valuable suggestions, guidance, support and patience that have tremendously helped my research work. A big thanks too, to my second supervisor and co-researcher, Professor Neil White and Dr Andy Cranny, for their technical advices.

I would also like to acknowledge the Malaysian Government and International Islamic University Malaysia (IIUM) for the opportunity and financial sponsorship in pursuing my doctoral study.

Special thanks also goes to all the technical supports in the Electronics & Computer Science Laboratory/Workshop, particularly Eric Webb, Barry Bailey, Mark Temple and David Kemmish. I am also grateful to the wonderful people who participated in the psychophysical investigation.

In addition, I would like to express my deepest appreciation to my parents, parents-in-law and the rest of my family members and friends for their continuous prayers, endless encouragement and non-stop assistance that inspire me to complete my studies.

I am forever grateful to have my husband, Mohd Fazli, and our two beautiful children, Sarah and Aariz, sharing with me, this PhD journey. Their unconditional love, prayers, understanding and patience have kept me motivated to fulfil my childhood ambition. This thesis is especially dedicated to them.

Nomenclature

ζ	Damping ratio
ω	Angular velocity [rpm]
ω_n	Natural frequency [rad/s]
χ^2	Chi-squared
B	Viscous friction coefficient
C_d	Decoupling capacitors [F]
C_f	Feedback capacitance [F]
C_{load}	External capacitor [F]
C_s	Sensor capacitance [F]
E_a	Voltage supply [V]
f_c	Cut-off frequency [Hz]
‘g’	Gravity of earth [9.81 ms-2]
GND	Ground
G_X, G_Y, G_Z	Accelerations in X, Y and Z directions (g)
I_a	Armature current [A]
J	Rotor moment of inertia [kgm^2]
K_b	Back EMF constant [Vs/rad]
K_T	Torque constant [Mm/A]
L_a	Armature inductance [H]
m	Mass of eccentric rotation mass [g]

m_o	Mass of motor [g]
R_a	Armature resistance [Ω]
R_b	Bias resistance [Ω]
R_g	Gain resistor [Ω]
V_{out}	Voltage output [V]
$V_{outX,}$ $V_{outY,}$ $V_{outZ,}$	Voltage outputs in X, Y and Z directions [V]
V_{st}	Voltage in self-test mode [V]
V_X, V_Y, V_Z	Voltages in X, Y and Z directions [V]

Abbreviations

DAQ	Data Acquisition
DC	Direct Current
DPDT	Double Pole Double Throw
EMG	Electromyography
ERM	Eccentric Rotation Mass
FFT	Fast Fourier Transform
GUI	Graphical User Interface
LED	Light Emitting Diode
LRA	Linear Resonant Actuator
MEMS	Micro-electromechanical systems
PVC	Polyvinylchloride
PVDF	Polyvinylidenefluoride
PWM	Pulse Width Modulation
PZT	Lead zirconate titanate
RMS	Root Mean Square
SNR	Signal-to-noise-ratio
SPDT	Single Pole Double Throw
SSF	Supplementary Sensory Feedback
VI	Virtual Instrument

Chapter 1 Introduction

Prosthetic hands are designed to aid users in their daily living. Also known as artificial hands, they are generally utilised to replace the missing arm above the elbow (known as transhumeral prosthesis) or below an elbow (known as transradial prosthesis), due to reasons such as birth defects, diseases or accidents [1].

There are currently various types of prosthetic devices in the market, ranging from the passive prostheses, body-powered prostheses as well as electric prostheses. The passive prostheses are purely for cosmetic purposes, while the body-powered and electric prostheses are designed to replicate the actual functions of the missing limbs such as holding a cup, gripping a ball or moving an object from one place to another. For example, the bebionic3 is equipped with 14 different types of grip patterns and hand positions for users to manipulate objects [2]. Another type of artificial hand in the current market is the i-LIMB hand, that allow users to move all five fingers separately by responses picked up from tiny electrodes attached on the forearms [3]. Another commercial artificial hand is the user friendly OttoBock hand, which is enhanced with an EMG signal processor that aids the user in gripping objects at a faster response time [4].

However, although they may have numerous functions, the prosthetic devices are usually under-utilised, and even rejected due to various reasons such as excessive mass, unattractive appearance, user discomfort and slow in movement, among others. According to a report by Biddiss and Chau [5], the rejection rates for body-powered and electric prostheses are as high as 87% and 75% respectively. The three commercial hands mentioned in the previous paragraph, have masses between 350-615 g, which are mostly above the 400 g of mean weight of human hands (from distal to wrist) [6]. User discomfort generally relates to the mass of the hand. Some prosthetic devices have a similar mass to normal hands, but the attachment methods sometimes make the system

a little uncomfortable. Unattractive appearance is generally due to the mechanical parts and joints but many manufacturers nowadays have included PVC or silicone gloves to envelope the hands and to give a 'natural' look for the users. The report in [6] also mentioned that although the hands managed to achieve power, precision, lateral or finger point grasps, the users are less satisfied with the grasp speed. A study by Vinet suggests that a speed of 0.8 s for the grasping action is appropriate for prosthetic hands [7].

Although the rejection rates for prosthetic devices are very high, it has been reported as well that the sensory feedback capability is one of the major decision factor in accepting the device, especially in electric prosthesis. Users are accustomed to sound made by the motor as well as vibration through a close fitting socket [5]. This auditory feedback allows a user to be aware of the current movement of his artificial hand without relying heavily on visual attention. According to a psycho-physiological assessment , users are subjected to mental stress when they are solely relying on their visual feedback in manipulating their artificial arm [8]. The stress that a person experienced was reduced when they were provided with auditory feedback and significantly improved when both cues were included. The mental stress was determined via the heart rate ratio taken from Electrocardiogram (ECG) measurements.

Sensory feedback could also be an important feature to artificial hand design. This response should be able to mimic the exteroceptive and proprioceptive sensations in a normal human being, in which superficial and deep sensations on the skin are recognized just by touching the object [9]. This sensation could act as a good input for rehabilitation process as other motor skills are trained via perceived sensations. Raspopovic demonstrated the capability of sensory feedback for hand prostheses by stimulating the nerve fascicles at the residual upper arm using information obtained from the sensors located at the artificial hand [10]. The nerve stimulation resulted in users to accurately identify the stiffness and shape of different objects. As objects could be identified and discriminated, users will also be able to respond appropriately to the objects they manipulate.

Realizing the importance of sensation, there has been research into adding a sensory feedback capability in a prosthetics design. The feedback control of a prosthetic device has long been deliberated in the past. The feedback system could be categorized into three parts, which are supplementary sensory feedback (SSF), artificial reflexes and control interface feedback [11]. SSF is largely in terms of vibration or

electrical stimulation, among others, in supplementing the missing or under-used sensory channels. Riso thoroughly discussed possible methods in acquiring a sense of touch by directing the sensation to the peripheral afferent nerves within the remaining limb using electrical stimulation [12]. The artificial reflex gives the user a cue to react to certain conditions, such as generating vibration in the thumb area to detect potential slippage of object in hand. The control interface feedback, on the other hand, manipulates the output response of the user via the input felt by them (through mechanical or hydraulic linkages).

1.1 Research Justification

This research work focuses on providing supplementary sensory feedback to the prosthetic users to replace their missing sensory systems. Several articles, mainly on the grasp force and slippage have been reported for this purpose. Force, pressure and temperature sensors have been designed within the prosthetic device to ensure more control by the user in manipulating the grasped object [13], [14], [15] while a slip sensor made it possible for object slippage prevention [16], [17].

It is until recently that researchers have become interested in designing artificial hands that enable users to discriminate surface textures. This feature is very useful for prosthetic users as they have lost their most sensitive tactile sensory system, located at their fingers and palm [18]. Adding this capability would undeniably make the device feel more natural and 'life-like'. It would also promote the sense of embodiment to the users and would greatly enhance their appreciation towards a well-designed prosthetic device Furthermore, touch sensations are very much superior in terms of sensitivity as compared to visual, or even auditory senses [18], [19].

Research has been carried out in the discrimination of surface texture to some extent [20], [21] but very little progress has been made towards creating a sensory feedback to the users. The capability of the device to decipher the surface texture are commonly conveyed through some graphical user interface (GUI), which would require bulky equipment, and again, may lead to mental stress [8]. The existence of sensory feedback has proven its capability in enabling users to effectively manipulate objects without relying to visual and auditory sensation [10].

On the other hand, there are investigations into creating artificial senses, also widely known as haptic feedback, to the residual limb, such as vibration, skin stretch or

pressure [22], [23] but little is done in mimicking surface textures. The closest applications to the surface texture detection with haptic feedback are smart mobile phone alerts or virtual reality games [24], [25] but not many of these applications have been utilised with the prosthetic devices.

The information crossover between the detection of surface textures with haptic sensation should make a more meaningful experience for upper limb prosthetic users. Therefore the tactile and haptic premises for prosthetic hands should be integrated, and thus became the motivation of this research.

1.2 Research Aims

The aims of this research work are:

1. To identify the most suitable actuators to deliver supplementary sensation to the upper arm and to validate the capabilities of the selected actuator through simulation and experiments;
2. To acquire signals from surface textures using the piezoelectric sensor of the Southampton Hand and to process the signals to determine the dimensions of the texture;
3. To link the information gathered from the surface texture and recreate the sensation felt by the artificial finger by using a selected haptic actuator;
4. To evaluate the association between the generated haptic sensations perceived at the upper arm with the surface textures felt at the fingertips by conducting a psychophysics investigation.

1.3 Research Contributions

This thesis combined important features that made up a sensory feedback system for artificial / prosthetic hand, as follows:

1. Simulation and validation of the haptic characteristics of the selected eccentric rotation mass (ERM) miniature motor. The transfer function of the motor has been obtained and this was used to predict its transient responses. The experiments conducted on the motor have provided useful information about the frequency responses and effective vibration energy of the motor.

2. Signal acquisition of surface textures using piezoelectric sensors to determine the grating widths of the textures. The data acquisition strategies that include the construction of a voltage mode amplifier and the utilization of a high resolution data acquisition device have provided reliable output with low external noise. These capabilities have been demonstrated on four different types of surface textures.
3. Recreation of the sensation felt by sliding a finger across a textured surface. This supplementary sensation is in the form of vibration and was generated using the information gathered from the surface texture. With the implementation of the frequency measurement technique, a prototype has been fabricated to work at 250 Hz, which is the optimum frequency of the mechanoreceptors at the skin of the upper arm. With reference to input pulses applied to the haptic actuator, it has produced vibration output with less than 90 milliseconds time delay in total.
4. The vibrations generated and perceived at the upper arm should ideally have association with the surface textures. This has been validated by a psychophysical investigation that showed statistically significant relationship between the vibration patterns and the surface textures.

1.4 Published Papers

From the research work presented in this thesis, the following papers have been published:

1. **Mohamad Hanif, N. H. H**., Chappell, P. H., Cranny, A. and White, N. M., "Surface Texture Detection of Artificial Fingers" in *37th Annual International Conference of the IEEE Engineering in Medicine and Biology Society* (2015), Milan, Italy, pp. 8018-8021.
2. Chappell, Paul H., Muridan, Norasmahan, **Mohamad Hanif, N. Hazrin H.**, Cranny, Andy and White, Neil M. (2015), "Sensing texture using an artificial finger and a data analysis based on the standard deviation", *IET Journal of Science, Measurement & Technology*, 1-9.
3. **Mohamad Hanif**, **N. H. H. ,** Chappell, P. H., Cranny, A. and White, N. M., "Development of Vibrotactile Sensory Feedback For Prosthetic Hand Users"

in *IASTED International Conference Biomedical Engineering (BioMed 2014)*, Zurich, Switzerland, 23 - 25 Jun 2014, pp. 294-301.

4. **Mohamad Hanif**, **N. H. H. ,** Chappell, P. H., Cranny, A. and White, N. M., "Vibratory feedback for artificial hands," in *2013 International Conference on Electronics, Computer and Computation (ICECCO)*, 2013, pp. 247–250.

1.5 Thesis Structure

The structure of the remainder of this thesis is as follows:

Chapter 2 presents the research background and literature review on the previous and current work related to the prosthetic devices, tactile stimulation, as well as haptic devices. The technology gap was addressed and the research focus was emphasized following the review of existing literature.

Chapter 3 and Chapter 4 explain the simulation and experimentation carried out in generating haptic feedback, including detailed descriptions of the equipment, material as well as general design ideas. These chapters also present and discuss the results obtained from the simulation and experiments.

Chapter 5 discusses the strategies in acquiring surface signals and includes a detailed description of apparatus used. The types of surface textures and how the signals were gathered are described in Chapter 6. The signal analysis and calculations of the surface texture dimensions are also presented in this chapter.

Chapter 7 describes how the signals from the surface textures were manipulated to generate associated vibration patterns. The hardware and software configurations in linking the surface texture information to the haptic actuator are also explained. The output signals in terms of vibration output observed from oscilloscope waveforms are also discussed.

Chapter 8 explained the procedures in conducting the psychophysical investigations to associate the generated vibration patterns with the surface texture. The statistical analyses from the investigations are also discussed in this chapter.

Chapter 9 concludes the research work and highlights the potential future work of this project.

Chapter 2 Incorporation of Haptic Feedback into Prosthetic Devices

The sense of embodiment, or body ownership, makes an important factor for self-recognition. Typically an amputee may regard the prosthetic device attached to his residual arm/leg is not part of his body [26]. However, several research works have shown that the sense of embodiment with prosthetic devices could be improved when sensory feedback is restored [8][18][27]. The findings have thus become the goal for this work.

The focus of this research is to provide supplementary sensation to the residual upper arm when sliding an artificial finger across a surface texture. The sensation perceived on the arm should ideally be similar to that felt by a bare finger when moving across the texture. Different types of existing prosthetic devices have been reviewed to highlight the gap in the technology and the possible methods to address it. Section 2.1 presents various types of the device, including the Southampton Hand, which was used to acquire signals from the surface texture. The tactile sensing methods, both naturally and artificially, are described in Section 2.2. In identifying which sensation to be applied at the upper arm and to select the most suitable actuator, the various types of tactile sensations and the available haptic actuators in the market have been reviewed in Section 2.3.

2.1 Prosthetic Hand

This section describes the society's perception of prosthetic devices, types of devices in the market, various researches in enhancing the existing devices, as well as a description of a prototype hand made in University of Southampton, which has been used for this work.

2.1.1 Prosthetics in Society

The motivation for the vast development and rapid evolution of prosthetic devices is the growing needs of people that will benefit from the technology. According to a report by GlobalData, the global prosthetics market (including orthotics) was valued at USD 3 billion and was projected to grow at a compound annual growth rate (CAGR) at 6% from 2010-2017 [28]. There are many key players responsible for this market growth, and one of them is Otto Bock, a company that manufactures various arm prosthesis products [4].

In a separate report, the estimated prosthesis wearing population in the United Kingdom between the year 2011-2012 is nearly 60 000 people, in which approximately 5000 of them are new amputees (excluding the injured Armed Forces Personnel) [29]. 5% of this overall population are upper limb amputees, caused by extensive injury, diseases, abnormal cell growth or infections whereas about 3% of those in need of the upper limb prosthetic device are due to congenital defects [30]. Regardless of the cause, the disability significantly affects a person in many ways such as their physical ability, emotional wellbeing and as well social adaptability. It is therefore evident that the use of prosthetic devices has become very common and generally well accepted in society. The London 2012 Paralympics, for example, has successfully attracted a massive public awareness of people with disabilities, particularly disabled athletes, judging from its record breaking ticket sales, television viewing and sporting achievements [31]. The event has showcased more than 4000 athletes of various limb loss and disabilities to compete in 22 games [32].

According to the survey by Kyberd and Wartenberg, 76% of upper limb prosthetic users wear their the devices more than 8 hours a day while about 46% of them use the device for more than 12 hours daily [33]. The daily usage includes work, driving and even sport activities. There were some suggestions for improvement in terms of lighter weight, better appearance, less sound, more grip function as well as

additional sensory feedback. The lack of these attributes leads to high rejection rates of prosthetic devices as reported by Biddiss and Chau [5].

2.1.2 Research into Prosthetic Hands/ Artificial Hands

Spanning a period of more than 30 years, there have been many developments in an attempt to upgrading existing prosthetic hands. The list is exhaustive, hence only research hands that incorporate either haptic / tactile feedback or are capable in discriminating surface texture, are given consideration in this review.

A modified Ottobock prosthetic arm has been used to control the grasp force of a device using a haptic feedback simulator that incorporates vibrotactile and visual cues [14]. In this research, the performance of the users to match the assigned grip force, improved tremendously when the haptic responses were supplemented to the device. In another research, an artificial hand prosthesis (SmartHand) was designed to provide vibration (vibrotactile) and pressure / force (mechanotactile) sensory feedback on amputees' residual arms [34]. Given a 17 mN/mm^2 pressure or 0.36 N amplitude vibrations at 165 Hz, the task was to identify the locations of the stimulus between the five fingers. It was reported that it was harder to discriminate the vibrotactile stimuli as compared to the mechanotactile stimuli.

Kim and Colgate studied the recreation of different types of tactile stimulation which are pressure, vibration, temperature and shear force to provide intuitive haptic feedback that is utilised by amputees who have undergone targeted nerve reinnervation surgery [15]. A miniature haptic device has been created at a later stage of this project to aid people who have undergone the surgery for grip force control. The performance improved significantly in terms of task completion speed, but degrades when both pressure and shear stimuli were introduced simultaneously [35].

Another recent breakthrough is in the design of a bionic hand that could be wired to the patient's nervous systems that enables him to control his hand movement as well as receiving touch signals from the skin sensors[10]. By employing cathodal pulses of 10-300 μs with a current intensity between 10-100 μA, the patient is capable of feeling touch and tingling sensations [36]. Rager [37] worked with detection of object slip and used the information to reconstruct the force components generated during the slip event to simulate firing responses of skin mechanoreceptors. The outcome indicated that the firing patterns could be represented by electrical stimuli to provide tactile

feedback. Another approach in implementing tactile feedback to a prosthetic device was by using ultrathin stretchable silicone nanoribbon electronics as skin prosthesis [38]. The artificial skin was capable to detect strain, humidity, temperature as well as pressure, and passes the sensory signals to peripheral nerves using multi-electrode array.

It can be concluded from the published literatures that the research hands are either capable of generating haptic feedbacks to the users or identify surface textures to some extent, but there is not much link between the two important capabilities. The incorporation of tactile sensing feedback with surface textures recognition for prosthetic hands, would considerably increase the similarity of the device with the lower arm that was lost.

2.1.3 Prototype Hand made in University of Southampton

The Southampton Hand is both a research prosthetic hand and a control method that have been developed by the researchers at the University of Southampton that started since more than 50 years ago. The latest prototype of the hand has a mass of 400g [39], which is comparatively lighter than the reported values of other research hands [6]. Similar to human hands, it consists of four fingers and a thumb. The thumb is operated by two electrical motors while one motor is dedicated to each finger. All the fingers and thumb are made of six bar linkages with piezoelectric thick film sensors fabricated on them [40].

The hand has evolved from improvement of grasping tasks using an adaptive controller [41], to the myoelectric controlled hand prosthesis [42] to the additional sensors for automatic control [13] [39]. The latest work on the Southampton hand is the development of texture sensors to discriminate surface gratings [40]. The finger link system of the Southampton Hand is used to acquire information of the surface texture. The latest prototype of the Southampton Hand is shown in Figure 2-1.

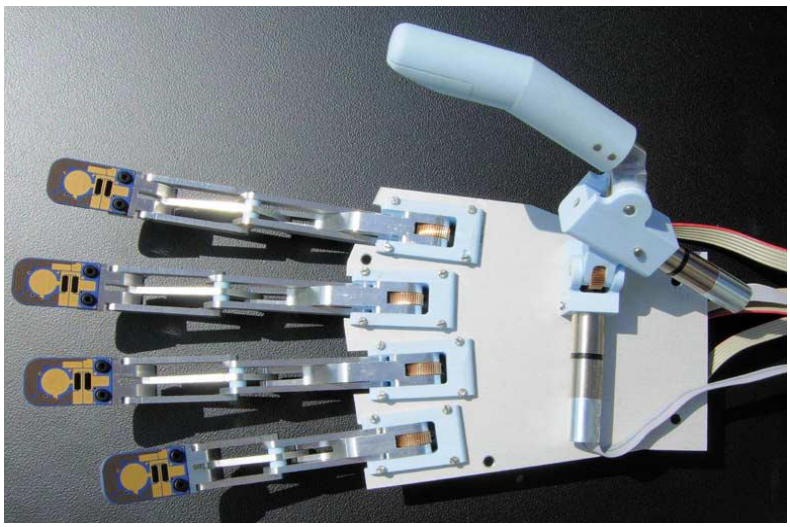

Figure 2-1: A prototype hand made in University of Southampton (reproduced from [16])

2.2 Tactile Sensing

Tactile sensing is the detection, measurement and interpretation of the spatial distribution of normal force applied on an object surface [43]. In order for artificial hands to achieve sensing capabilities as that of humans, the physiology of human skin should be understood first. In this review, emphasis is given on two different skin regions which are the skin that covers the fingertip and at the upper arm. The skin at the fingertips is responsible in sensing surface texture information. It is expected that the sensor of the prosthetic hand should be able to replicate the sensing capability of the actual fingertips. The signals gathered from the sensor will be transformed into another tactile sensation that should be perceived at the upper arm. Therefore the physiology of skin at the upper arm should also be known.

2.2.1 Physiology of Human Skin

The skin is a major organ of the body that forms about 8% of total body mass [44]. Within the skin, there are millions of mechanoreceptors that make up a very reliable somatosensory system. This system is responsible for detecting different types of senses that contact the skin, such as pain, moisture, heat, prick or various surface textures of the object. Should there be loss of other sensory modalities (e.g. sight or hearing), the skin would be able to make up for the loss by responding to the object being touched by the impaired person.

The cutaneous mechanoreceptors in the human skin are responsible for human tactile sensations. They are categorized by their adaptability in responding to a constant stimulus. A rapidly adapting (also known as fast adapting, FA) mechanoreceptors responds well to changes in stimulus position while a slowly adapting (SA) mechanoreceptors responds to constant indentation onto the skin surface [44]. There are four types of tactile cutaneous mechanoreceptors, which are Meissner, Merkel, Pacinian and Ruffini. Details of each mechanoreceptor are shown in Figure 2-2 and Table 2-1.

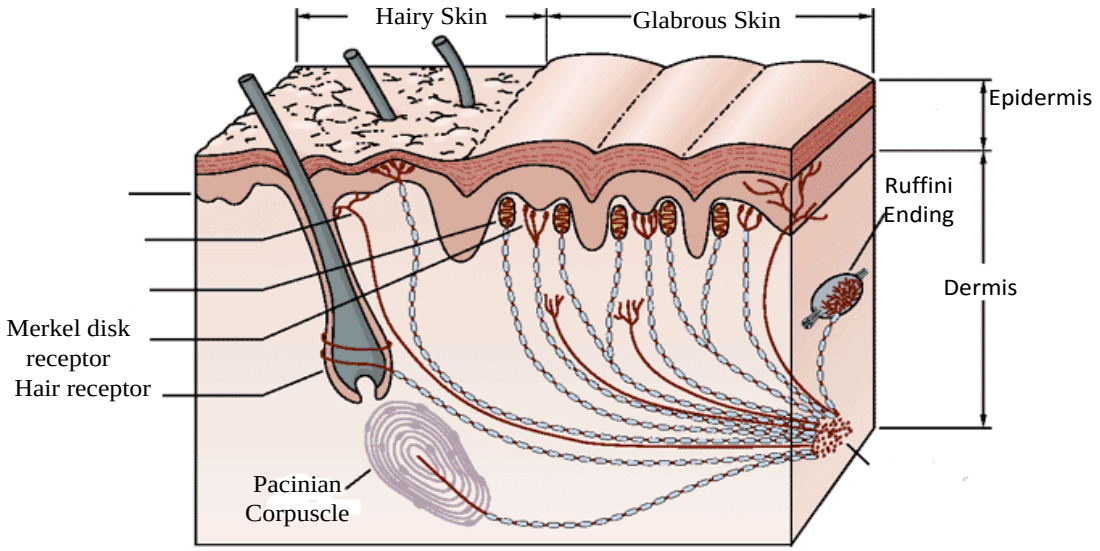

Figure 2-2: Locations of mechanoreceptors in the glabrous and hairy skin of human body (reproduced from [45])

Table 2-1: Details of the Tactile Cutaneous Mechanoreceptors

Mechanoreceptors	***Meissner***	***Pacinian Corpuscle***	***Merkel***	***Ruffini***
Adaptability [44]	Rapid (FA I)	Rapid (FA II)	Slow (SA I)	Slow (SA II)
Location [44]	Shallow, under the groove between the dermal papillae	Deep, underneath dermis and in deeper regions of body	Shallow, in the epidermis right under the papillary ridges of skin	Deep, lower parts of dermis
Capabilities [12], [44]	Detect object contact/ release/ slippage	Very sensitive to mechanical deformation / various surface texture at high frequencies	Distinguish details of the surface shape of the object through light pressure	Activated by shear force / skin stretch
Tactile perception	Distinguish fine surface textures (<100μm) [46]	Distinguish fine surface textures (<200μm) at 250 Hz [21]	Perceive course textures (>100μm) [46]	N.A.
Frequency Sensitivity	Low (10 – 50Hz) [44]	High (100 – 400 Hz) [44]	Low (0-30 Hz) [47]	Low (0-15 Hz) [47]

Sensory endings in glabrous skin (skin that covers palm, sole of foot and the flexor surfaces of fingers and toes) are extremely sensitive to cutaneous stimulation. However only glabrous skin on hand is used for tactile discrimination as the mechanoreceptors are located just beneath the skin layer [44]. People are able to distinguish the different roughness of a material with 5µm particles and the 9µm particles just by sliding their fingers on the material [19]. Depending on the sliding speed, angle between finger and material as well as the fingertip region, a fine surface with threshold as small as 2.2 µm could be discriminated [48].

Unlike the glabrous skin, the hairy skin, which is skin that covers the rest of the body, is less sensitive to vibration or pressure. This is due to the fact that not many mechanoreceptors are located within these areas, except the Pacinian mechanoreceptors which are located deep under the tissues surrounding joints and bones. However, at higher vibration frequencies, the skin sensitivity are similar to that of the glabrous skin [47]. This is contributed by the capability of the Pacinian corpuscles that could be activated by vibration frequencies as high as 400 Hz. Figure 2-3 shows the vibration detection threshold for human that corresponds to the frequency sensitivity of the mechanoreceptors. It can be observed from the figure that a person could detect as low as 1µm of indentation on skin at about 250Hz, with the aid of the Pacinian corpuscles that could be fired within the particular frequency band.

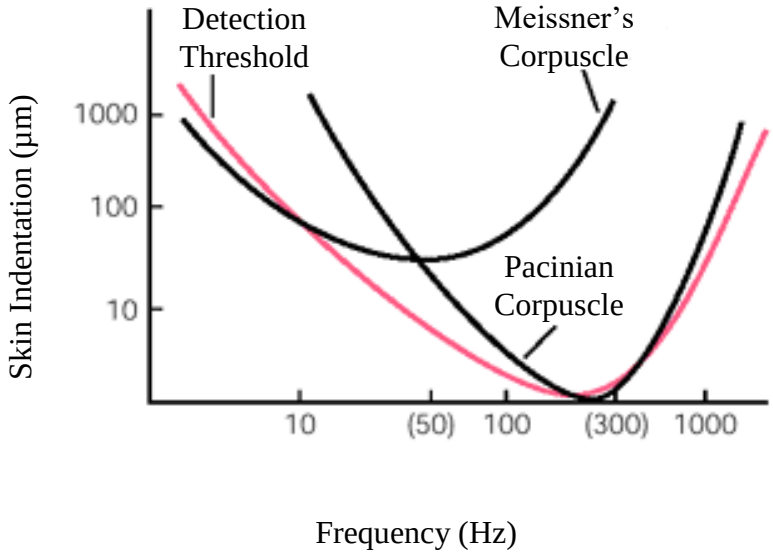

Figure 2-3: Vibration threshold responses in human body according to the firing frequencies of the mechanoreceptors (reproduced from [45])

A person's response through the skin to vibration stimuli depends on the frequency, amplitude and duration of vibration as well as the area of contactor stimulating the skin [49]. The best hairy skin sites to efficiently perceive vibrotactile stimuli would be near the wrist, elbow, spine or navel [49].

The optimal frequency sensitivity varies between 150 to 300 Hz depending on the location in the human body, in which the upper arm has the sensitivity of about 250 Hz [45]. The amplitude of vibration refers to the strength of vibration (usually measured in gravitational acceleration, *g*), and this has a linear relationship to the frequency of the vibration. The ability to detect the stimulus is higher when the duration of vibration increases from 80 to 320 ms, and for short pulses, stimuli longer than 200 ms is perceived as annoying [50]. Apart from that, the minimum acceleration threshold for detection on skin throughout 50 Hz to 250 Hz frequency range is 0.25 *g* [51]. Therefore it is important to manage the amount of vibration and its duration that act on the skin according to the application required.

2.2.2 Data Acquisition of Artificial Fingers

There have been significant and increased efforts over the past decades in matching the capabilities of human touch sensations for artificial hands. To ensure the most accurate and reliable information about the surface texture, factors such as the surface properties to be acquired, type of sensors as well as the experimental set up should be thoughtfully considered.

The experimental set-up also plays a major role in achieving excellent accuracy for data acquisitions. For example, the sliding velocity and acceleration of the fingers have a great effect on the vibration frequency between the surface and the finger. The generated frequency should match the frequency bandwidth of the data acquisition unit in ensuring all the information is not lost [19]. In accordance to the Shannon-Nyquist theorem, to ensure reliable reconstruction of the sampled data, the sampling rate of the data acquisition unit should be at least twice of the sampled data. However, in most cases, this is barely adequate and the sampling rate should be much more higher than twice of the sampled data to take into account possible harmonics [52]. This particular characteristic is of tremendous importance as different textures provide different vibration frequencies or intensities [53].

Another important factor in achieving the most accurate representation of the surface texture is the signal-to-noise-ratio (SNR). In some cases, the required magnitude output of the sensor is comparatively lower than the generated interference. It is therefore useful to include signal conditioning units with high SNR to amplify small signals as well as appropriate filters to avoid aliasing during the signal reconstruction process [53].

The applied force onto the surface texture is also of equal importance. The contact normal force should be in an optimal range to avoid undetected information if the force is too low or too high, resulting damage to the sensor or the object. A person can judge whether the force exerted to the texture is too high or too low with his bare finger. However unless the artificial hands is equipped with a smart feedback system, a value need to be set to ensure optimum force exerted onto the texture. Okamura used a PID force controller to ensure a constant 2N of force during the sliding operation [54] .

As with the human fingers, the position of the finger itself when sliding across the surface texture is also crucial. As published in [48], the top fingertip of human finger is more sensitive than the centre fingertips during the step-height test (Figure 2-4). This is possibly attributed by the location of active sensory nerves within the top fingertips. This similar concept is applicable for artificial fingers; the nearer the surface to the sensor, the more sensitive it is in acquiring the required information.

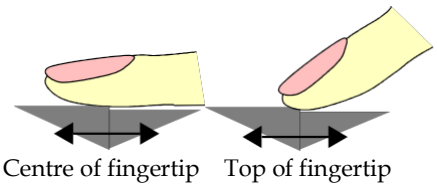

Figure 2-4: Fingertip regions (reproduced from [48])

The data acquisition part of this work is a continuation and modification of previous work by Muridan [40], which looked into the characteristic of the generated output signals in determining surface texture of an object. In Muridan's work, perspex grating of different roughness were attached on a specially built aluminium block and were moved past the fingertip sensor of a Southampton Hand at varying constant velocities. The output voltage has been analysed using the Fast Fourier Transform (FFT) and mean standard deviation to produce patterns that directly corresponds to that of the gratings [40] , [55].

The piezoelectric sensor embedded at the fingertip that was used in Muridan's work, has been designed by Cranny [13] and Cotton [16]. This sensor consists of

piezoelectric force sensor that could detect initiation of object slip, piezoresistive strain sensor to adjust the hand grip as well as thermistor paste for temperature detection. The piezoelectric material is of the PZT type (lead zirconate titanate) as it has a good thermal characteristic and high sensitivity, which is useful for prosthetic applications. The characteristics of the sensor, although initially designed for different purposes, have shown promising results for surface texture detection [40], [55]. The piezoelectric sensor layout is as shown in Figure 2-5.

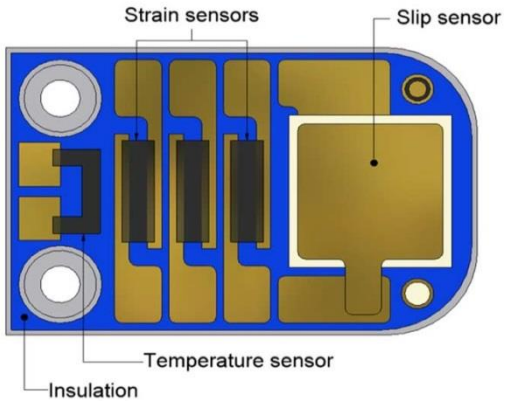

Figure 2-5: Piezoelectric sensor layout (reproduced from [16]). See Figure 5-3 for the one used in this work.

Instead of using real surfaces, the perspex gratings were specially fabricated to specific widths of ridges and grooves. This was done to ease the task in comparing the measurement of widths from the signal gathered by the sensor with the actual width. Apart from that, as the widths of the grooves and ridges were varied in a repeating pattern, the signal acquisition capability of the sensor could also be assessed systematically.

The widths of the ridges and grooves of the gratings in one spatial period play an important role in perceived roughness. As reported in [20], wider groove width leads to better estimation of roughness perception while wider ridges results in lower estimation of perceived roughness. Textures with spatial periods greater than 200 μm is considered to be rough while lower than that are considered to be fine textures. Figure 3-3 highlights the groove, ridge and spatial period in gratings.

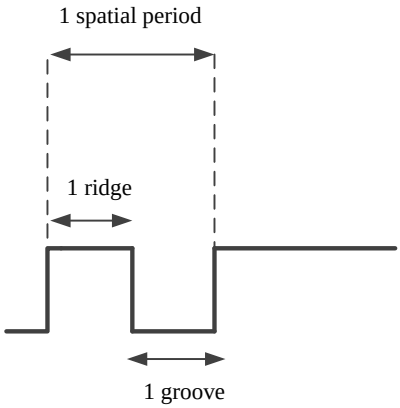

Figure 2-6: Physical parameters of a grating

The two Perspex gratings described in Muridan's work [40], [55] are both considered to be rough (spatial periods of 644 µm and 430 µm). The coarser grating has a repeating pattern of grooves every 469 µm with 175 µm groove width while the finer grating has a repeating pattern every 258 µm with groove width of 172 µm.

As described in Section 1.3 of this thesis, the sensitivity of the sensor from Muridan's work [40] has been improved to gather even more information from the surface textures. Other surface textures with different grating widths were also added into this work. Further to this, the information from the surface textures was then translated as a haptic feedback to the upper arm. In other words, the sensation felt when sliding the prosthetic finger across the surface texture were recreated and stimulated at a different part of the body. The methodologies and results from this follow-up research work are explained in the following Chapter 3 to Chapter 8 of this thesis.

2.3 Haptic Feedback

In dealing with activities of daily living or special tasks, a person may be faced with unwanted situations when the particular objects could not be touched with their bare hands. This could be due to the delicacy, size or intricateness of the object that has a high risk to be damaged if improperly handled. There are also occasions that the object to be manipulated is way out of reach. To address these situations, virtual objects are created to mimic the actual properties of the object. The incorporation of the sense of touch and control through kinaesthetic or tactile sensation of the virtual objects is called haptic feedback. This technology is deemed to be very important as the capability to touch generates reliable outcomes and leads to a greater satisfaction. The applications of haptic feedback range from smart phone gadgets [24], educational

simulation of force exertion onto virtual objects [56], stroke rehabilitation devices [57] as well as useful visualization for space explorations [58]. The sense of touch is also very useful during minimally invasive surgery in identifying blood vessels and other anatomical structures [59].

In this work, haptic feedback is used to represent the sensation felt by a prosthetic finger when sliding across a surface texture. With the aid of a haptic actuator, the sensations were recreated from the signals gathered by the sensors of the prosthetic finger, and stimulated at a different part of the body.

2.3.1 Tactile Sensations for Haptic Actuators

Haptic actuators are devices that are designed to recreate the kinaesthetic or tactile sensation. Kinaesthetic sensations are generated by activating the receptors within the muscles, joints and tendons while tactile sensations are generated through the activation of mechanoreceptors in the human skin [60]. As this research looks at discriminating surface textures, an emphasis will be placed on activating the sensory nerves on the human skin. These nerves are fired via various interactions on the skin such as friction, skin stretch, normal indentation, vibration, heat, shear, electrocutaneous and suction pressure [61].

The sensation of friction could be created by applying a motor operated cylinder around a finger [47] [62]. The rotation of the motor in opposite directions stimulates the mechanoreceptors around the fingertip, shown in Figure 2-7. This supplementary sensory system is particularly useful for slip detection.

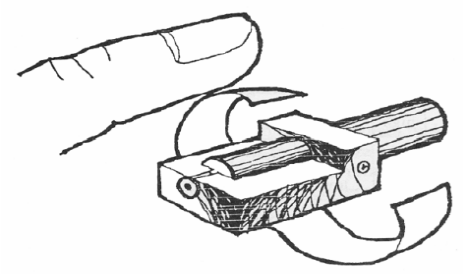

Figure 2-7: Motor operated cylinder strapped against finger to stimulate finger mechanoreceptors when it rotates (reproduced from [62])

Normal indentation or pressure generally evokes the sensitivity of the Merkel mechanoreceptor under the human skin. Raisamo has stated that, the absolute sensitivity threshold for fingertips and upper arm are 0.686 mN and 1.47 mN

respectively [47]. Possible haptic device that is able to exert pressure onto human skin is shape memory alloys [63]. When current passes through the device, it will change its shape and eventually constrict and create pressure to the finger that is wrapped within the alloy. Stanley and Kuchenbecker have used a Velcro band, servomotor and a force sensing resistor (FSR) to efficiently correlate variation of pressures exerted by users [23]. In a separate research work, the capability for feedback discriminations were proven through the application of pressure stimulations on the residual limbs of transradial amputees [34].

Suction pressure typically creates the sensation that the skin is being pushed. According to a psychophysical investigation by Makino, when a suction pressure was exerted on the fingertips of ten participants, nine responded that they felt as if their skins at the fingertips were pushed by a stick [64]. This was in accordance with works by Srivinasan that stated skin mechanoreceptors are more sensitive to strain energy denstity rather than the direction of the strain stimulus [65].This sensation is also useful for slip detection. The suction pressure however induces intense shearing stress on skin that could inflict pain to the users [64]

Vibration is most commonly used to supplement missing or inadequate sensory systems. The detection of vibration on human skin is dependent on the driving frequency of the associated vibration device. The frequency sensitivity varies depending on the area of the body, but the optimal vibration detection frequency lies at 250 Hz [45]. The intensity of the vibration could be manipulated by adjusting the input waveforms. Square waves and sine waves could generate rough and smooth sensations respectively [66]. Research into this type of modality is published in [14], [22], [67], and [49], among others. Most have proven the effectiveness of using this type of sensation, but Demain suggests that the vibration intensity should be controlled as prolonged exposure may cause long-term nerve and tissue damage [66].

Several researchers have compared the capability of vibrotactile stimulation with skin stretch, such as published in [23] and [68]. It was found out that hairy arms are more sensitive to tangential forces as compared to normal forces. Research published by Bark et al compares the relative and absolute position errors for applied stretch and vibration on skin [68]. It was shown that the stimulation via skin stretch has the lowest errors as opposed to vibratory stimulations.

Another possible way to stimulate the skin mechanoreceptors is through heat. Although it might be a good idea to have this type of feedback, the temperature range

should be within 30 - 36ºC to avoid extreme pain or thermal damage. Furthermore, human skin may not detect the changes in temperature if it is less than 0.5ºC/minute until it becomes very hot [69]. Therefore careful considerations should be taken into account when using this tactile stimulation.

Electrocutaneous stimulation works by passing electric current through skin. The sensations vary from tingles to searing pain depending on amount of input current and voltage. The stimulation depolarises nerves rather than stimulating a skin sensor. Due to possibility of pain, this method is not favoured among consumers and mostly used as research prototypes [47]. One recent work that utilizes this method is the design of a bionic hand wired to the patient's nervous systems. This device enables him to control his hand movement as well as receiving touch signals from the skin sensors [10].

Another type of tactile stimulation is the investigation of spatial resolution, where two points of contact on human skin defines the tactile sensitivity [66]. This is the minimum distance at which the presence of two stimuli is felt on the skin. The fingertips have the greatest discriminative capacity, which is at about 2 mm, while the palm and arm are 10 mm and 40 mm respectively [70]. The Braille display, used by the visually impaired, is a common example of actuators that utilizes this type of stimulation. The pins in the display are pushed up by piezoelectric actuators or solenoid [47].

2.3.2 Vibration Actuators

The focus of this literature survey is focused on vibration actuators as vibration is responsible in detecting the properties of a surface texture. At the right frequency and velocity, the vibrations felt at the fingertips during its sliding motion make it possible for texture discrimination. As it is better to have a modality match to achieve intuitive haptic feedback [15], it is desirable to process, transform and amplify the vibration sensation felt at the fingertips so that the vibrations will also be felt at the residual upper arm. Furthermore, this stimulation is more suitable to discriminate rough or smooth sensations, if it is not at all painful and could be manipulated to be within the acceptable intensity band to avoid nerve or tissue damages. Also, work by D'Alonzo [71] showed that the vibration supplementary sensation promotes a sense body-ownership of the attached artificial hand in transradial amputees.

With varying vibrations in terms of strength, frequency and pattern, the haptic actuators are very capable in providing users valuable tactile information. This mechanism is widely applied in mobile phones and pagers, to alert the users on incoming calls or messages. This mechanism is also commonly included in joysticks, to imitate the virtual sensation during video gaming sessions.

There are various models of haptic actuators currently available in the market, typically categorized into three different types, which are eccentric rotating mass actuator (ERM), linear resonant actuator (LRA) and piezo actuator.

An ERM Vibration motor is a DC motor with an asymmetric mass attached to the shaft. As the ERM rotates, the centripetal force of the eccentric mass drives a net centrifugal force that leads to movement of the motor from its initial position. Repeated rotations of the ERM create a constant displacement of the motor, and are considered as vibration [72].

To shorten the lag time of the motor, simple H-bridge circuitry is applied to the motor for active –braking mechanism. This is done by changing the polarity of the DC voltage of the motor, which in turn changes the direction of motor rotation. Similarly, to reduce the rise time of the motor, Pulse Width Modulation (PWM) is applied to quickly rotate the motor at a higher voltage [72].

Unlike the ERM, the Linear Resonant Actuator is made of a spring-mounted mass and vibrates in a linear motion. It requires sinusoidal input with a frequency that should match the resonant frequencies of the system, or at least to be driven within a narrow band of their resonant frequencies [73]. This characteristic makes it easier for vibration control, in which it could be adjusted by changing the amplitude of the sinusoid driver signal [72]. The disadvantage of this type of actuator that it only work within a narrow band (±2 Hz), and frequency drift will reduce the vibration tremendously [74].

Piezoelectric actuators could be in the form of disks or rectangular strips, and could be configured in single or multiple layers. In multiple layers configuration, stronger haptic response could be achieved [75] but it would require a higher driving peak-to-peak voltage [73]. This type of actuator vibrates when it is bent or deformed by the differential voltage applied at both ends of the actuator. The piezo actuators are regarded as high-definition (HD) haptics due to their faster rise times, higher bandwidth

(crisp), lower audible noise as well as stronger vibration [73]. Table 2-2 summarizes the comparisons between all three haptic actuators.

Table 2-2: Characteristics of the Eccentric Rotating Mass (ERM) Actuator, Linear Resonant Actuator (LRA) and Piezoelectric Actuator

Characteristics	***ERM***	***LRA***	***Piezoelectric***
Drive Voltage (V)	Low: 0.5 – 5.5 (peak) [76]	Low: 0.3 - 2 (RMS) [77]	High: 100 – 200 (peak-to-peak) [78]
Response Time (milliseconds) [74]	~ 50	~ 30	0.5
Vibration Method [79]	A motor with rotating eccentric mass (tri-directional vibration)	Spring mass system that oscillates in linear motion (unidirectional vibration)	Piezoelectric beam that bends when voltage is applied (unidirectional vibration)
Cost [80]	Low	Low	High
Advantages [74]	Easy to drive, low cost	Faster response time than ERM	Quick response time, wide frequency bandwidth
Limitation	Slow response [73]	Requires exact frequency as its resonant frequency [80]	Requires very high driving voltage, difficult to be integrated [80]
Common Applications [73], [80]	Cell Phones / Handheld devices	Smart Phones	Touchpads / Phones / Games

Judging from their capabilities and limitations, the ERM is deemed as the most suitable actuator to provide vibration to the upper arm. This is because it is low cost, with a reasonable response time, simple configuration and only requires low voltage. This actuator can also be adjusted to match the desired 250 Hz bandwidth specification.

The ERM will be located at the upper arm although the spine or navel would have a greater vibrotactile sensitivity [49]. This is mainly because the residual arm is nearer to the prosthetic device, hence the wiring is shorter.

2.4 Conclusions

This chapter has highlighted the expansion of research into the prosthetic/ artificial hands. Many researches have shown that the devices are able to provide haptic feedback or capable to decipher surface textures, but very little research has been carried out in integrating both properties together.

The capabilities of human mechanoreceptors in acquiring signals were reviewed to see how they could be replicated in artificial hands. Based on the literature on the data acquisition of artificial hands, the piezoelectric sensors have shown encouraging results in detecting different widths of surface gratings. This gives reassurance in exploring the capabilities further with this sensor. From a study of the literature it has also been found that the optimum frequency of the Pacinian corpuscle, the mechanoreceptors located deep underneath the skin of an upper arm is 250 Hz. This will be the frequency of operation when supplying the haptic feedback to the residual upper arm.

To decide on the type of supplementary sensation to be provided to the residual upper arm, various ways in activating the sensory nerves on the human skin have been reviewed. From the literature, the vibration sensation fits the criteria in replicating the sensation felt on finger. One of the reasons for this fitting criterion is that vibration is also generated during surface texture exploration. Therefore to achieve intuitive haptic sensation, a modality match is desired.

Chapter 3 Simulation of the Haptic Characteristics

From the review in the previous chapter, the most suitable supplementary sensation to be delivered to the residual arm would be vibration, which will be provided by an Eccentric Rotation Mass (ERM). Various factors were considered to pick the best available ERM in the market. To test its capability in producing the desired vibration sensation, the haptic characteristics of the ERM, specifically in terms of its transient responses, were simulated.

3.1 Selection of a Suitable Haptic Actuator

Some experiments and simulations have been carried out in generating suitable haptic feedback that should provide the same sensation felt when sliding a finger on a surface texture. There are various factors in deciding the most suitable actuator for this application. The selection factors include response time, bandwidth, voltage requirement, power consumption, cost, mass and ease of interface with controller. The detailed descriptions of each criterion are as tabulated in Table 3-1.

Going through the list of considerations, the Pico Vibe^{TM} vibration motor (model 304-111) from Precision Microdrives was selected as it fits the selection criteria satisfactorily. According to the product data sheet (Appendix A), the overall response time of the motor (including lag, rise and stop time) is 80 milliseconds and can produce vibration frequency within 0.1 to 300 Hz. The motor has a rated voltage of 3V, with a typical operating current and power consumption of 50 mA and 150 mW respectively. The body diameter and length are 4.6 mm and 11 mm respectively with a mass of 1.1 g.

The haptic device has a low unit cost of £4.20 which is considerably lower among other types of haptic actuator.

Table 3-1: Selection Criteria for Haptic Actuator

No.	*Selection Factors*	*Details*
1.	Response time	Within 1.0 to 1.5 s for overall task [6]
2.	Bandwidth	Should be able to produce 250 Hz, which is the optimum frequency for the activation of Pacinian corpuscle located at the skin of the upper arm [45]
3.	Voltage Requirement	The actuator will be handheld and battery operated, hence low voltage is preferred
4.	Power Consumption	Low
5.	Cost	Low
6.	Mass	Low, as it will be mounted onto human arm
7.	Size	Small

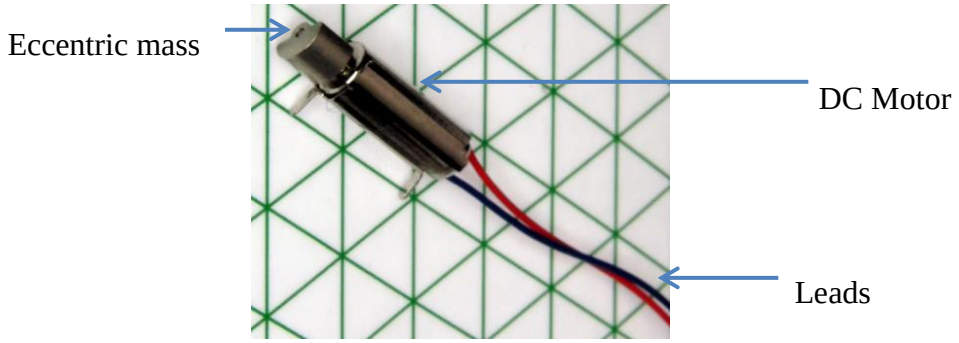

Figure 3-1: Pico Vibe^{TM} vibration motor, shown on 6mm isometric grid (reproduced from [81])

3.2 Transfer Function of the Haptic Actuator

An experiment was designed to obtain a transfer function that represents the motor as accurately as possible. This transfer function is useful as it will allow for simulation of the output responses of the motor in terms of speed, transient response and frequency as well as vibration amplitude when given an input voltage.

The required parameters in obtaining the transfer function are armature resistance, R_a (Ω), armature inductance, L_a (H), back EMF constant, K_b (Vs/rad),

torque constant, K_T (Nm/A), viscous friction coefficient, B (Nms/rad) and rotor moment of inertia, J (kgm^2) [82]. The armature resistance, R_a and armature inductance, L_a are easily measured using an inductor capacitance resistance (LCR) meter. The rotor moment of inertia, J is obtained by substituting the values of mass (m) and radius (r) of the motor to the following equation:

$$J = 0.5mr^2 \qquad (1)$$

To obtain the rest of the parameters, the motor was rotated freely and measurements were obtained when the rotation has become constant. In doing so, a power supply and a handheld digital tachometer (Premier Farnell ST-6236B) were used. The tachometer was used to measure angular velocity, ω (rpm) once the current, I_a (A) has become constant. This indicates that the system has reached steady state. The voltage supply, E_a, was set according to the motor's rated voltage, which is 3V. The following equations were used to obtain the required parameters:

$$E_a = I_a R_a + K_b \omega \qquad (2)$$

$$K_T = K_b \qquad (3)$$

$$B\omega = K_T I_a \qquad (4)$$

The experimental apparatus is as shown in Figure 3-2.

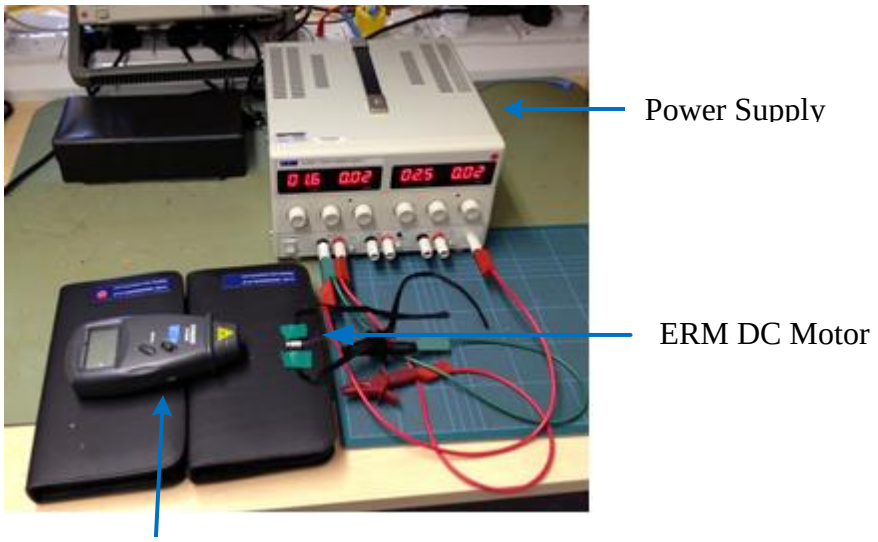

Figure 3-2: Experimental apparatus to obtain motor transfer function

Via explicit measurement of the DC motor, the physical parameters were determined, as shown in Table 3-2.

Table 3-2: Parameters for the Selected DC motor

No.	Parameters	Values
1	Armature resistance, R_a (Ω)	33.2
2	Armature inductance, L_a (μH)	80.1
3	Back EMF constant, K_b (Vs/rad)*	$7.6x10^{-4}$
4	Torque constant, K_T (Nm/A)*	$7.6x10^{-4}$
5	Viscous friction coefficient, B (Nms/rad)	$34.9x10^{-9}$
6	Rotor moment of inertia, J (kgm^2)	$5.63x10^{-10}$

*Neglecting the power loss by armature resistance, it follows that electrical power is equal to mechanical power of motor. Therefore $K_T = K_B$ in both theory and practice [83].

Using the parameters, the motor transfer function is obtained using the following armature-current controlled DC motor equation derived from [82] as follows:

$$G_v(s) = \frac{\omega}{V} = \frac{K_T}{[(R_a + sL_a)(Js + B)] + K_b K_T} \qquad (5)$$

where ω represents the resulting velocity (rad/s) while V is the input armature voltage (V). Through substitutions, the DC motor transfer function is:

$$G_v(s) = \frac{1.7e^{10}}{s^2 + 4.14e^5 s + 3.86e^7} \qquad (6)$$

This second-order DC motor characteristic is an overdamped low pass system, with natural frequency, ω_n, of 6216 rad/s and damping ratio, ζ, of 33.293.

3.3 Simulation of the Haptic Actuator

The next stage of this research work is to run MATLAB simulations using the derived motor transfer function. The simulation is divided into two parts. The first is to simulate the transient response of the DC motor while the second part is to simulate the amplitude of vibration. In the first part, the voltage supplied to the DC motor can be

varied according to the motor's specification to see how voltage affects the speed. Also the rise time and settling time for each of the instances can be observed.

In the second part of the simulation, the following parameters are used in Table 3-3 to estimate the vibration amplitude.

Table 3-3: Parameters for Vibration Amplitude Estimation

No.	***Parameters***	***Values***
1	Unit mass of motor, m_o	1.1 g
2	Mass of the eccentric rotating mass, m	0.5 g
3	Radius of eccentric mass, r	$2x10^{-1}$ m
4	Driving frequency of motor, ω_r	0 – 250 Hz (0 – 1570 rad/s)

The eccentric rotating mass of the motor is the offset (non-symmetric) mass attached to the DC motor shaft. This offset mass is responsible in generating vibration during the rotation of the motor due to the asymmetric centripetal force [72]. Figure 3-3 shows the eccentric rotating mass of a DC motor.

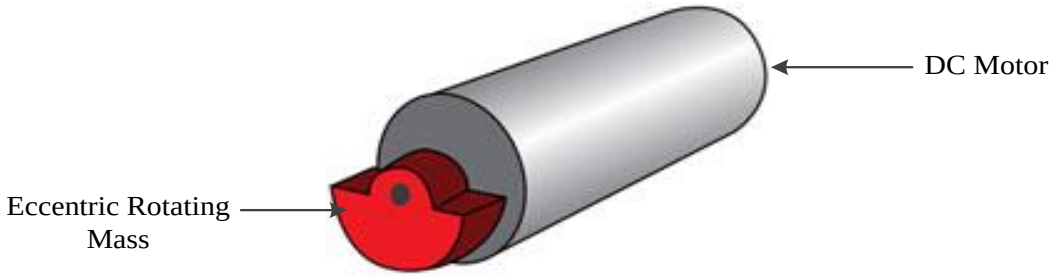

Figure 3-3 : Eccentric Rotating Mass of a DC motor (reproduced from [79])

3.3.1 Transient Response of the Haptic Actuator

Several output responses were generated by varying the input voltage to the system transfer function. By performing this MATLAB simulation, the transient response (settling time and rise time) was estimated as well as the resulting motor speed at a given voltage. The voltages were varied at 0.5 V step sizes, at which 0.6 V, 3 V and 3.6 V are the lowest, rated and maximum voltage respectively. The plots are as shown in Figure 3-4.

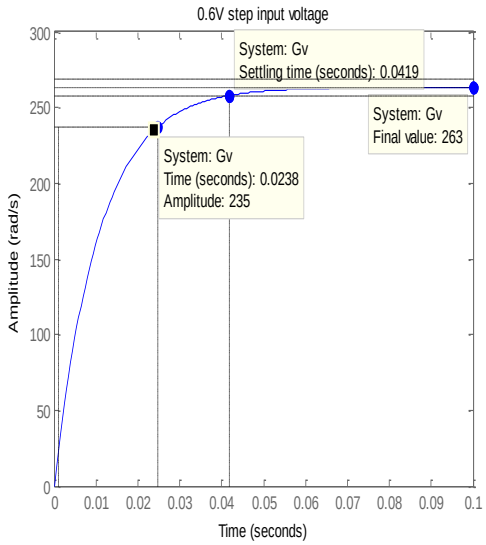

0.6 V Step Input Voltage

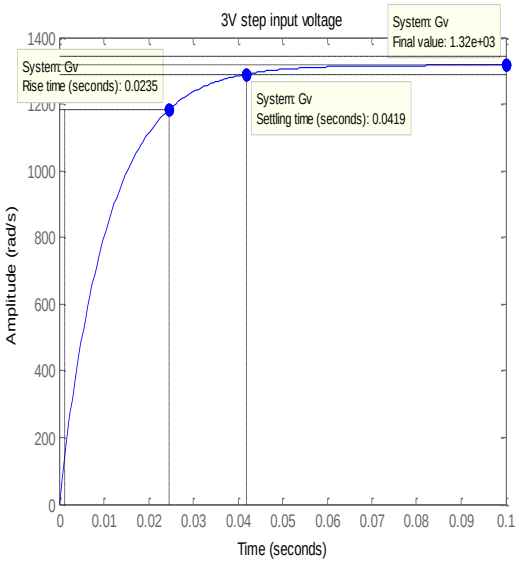

3 V Step Input Voltage

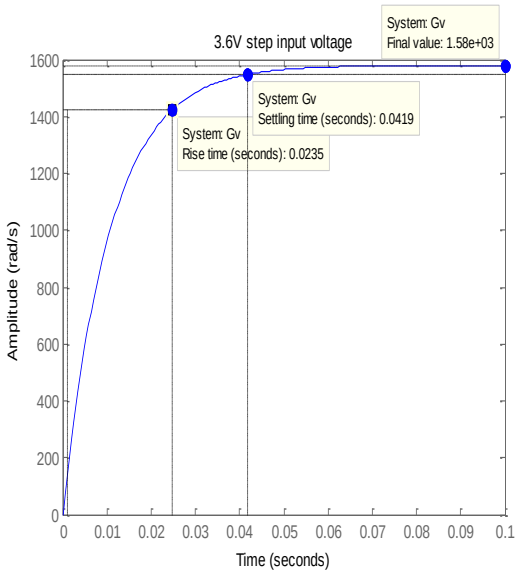

3.6 V Step Input Voltage

Figure 3-4: Transient responses at 0.6 V, 3 V and 3.6 V. The final motor speeds were recorded at 263 rad/s, 1320 rad/s and 1580 rad/s for 0.6 V, 3 V and 3.6 V respectively. The rise and settling time maintained at 24 milliseconds and 42 milliseconds.

3.3.2 Amplitude of Vibration

The amplitudes of vibration were simulated using the obtained values of the motor speed. The input voltages were varied in 0.5 V step sizes. The amplitudes were

recorded in terms of displacement (m), and acceleration (*g*). The plots for 3 V are as shown in Figure 3-5 .

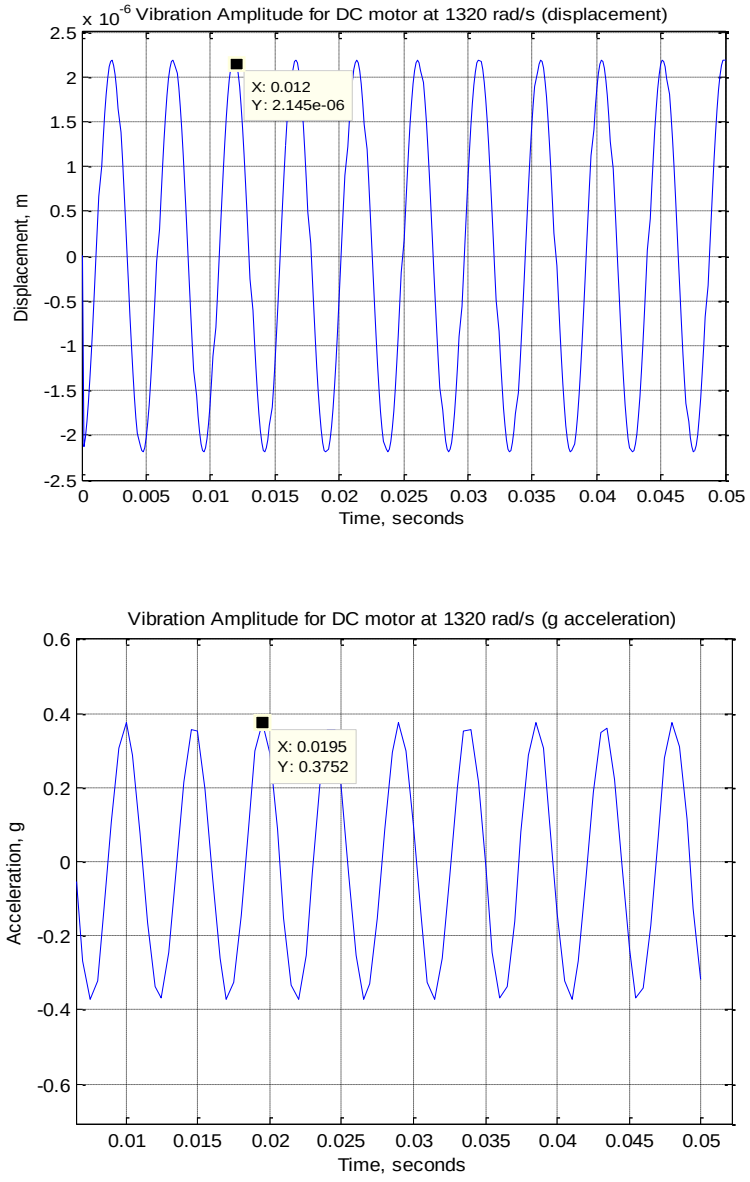

Figure 3-5: Displacement amplitude (4.2 µm peak-to-peak) and acceleration amplitude (0.76 *g* peak-to-peak) when voltage is supplied at 3 V, with motor speed of 1320 rad/s.

The relationships between variation of the input voltage (0.6 V - 3.6 V) to the generated speed as well as vibration amplitudes are as shown in Figure 3-6 and Figure 3-7.

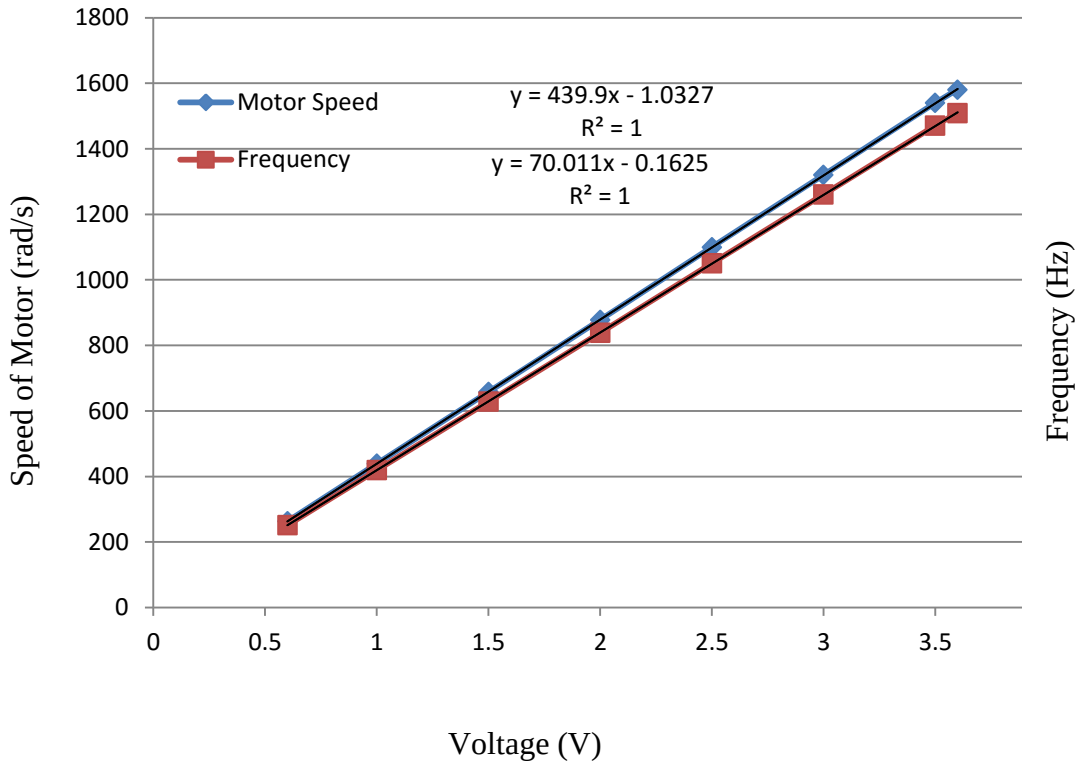

Figure 3-6: Speed of Motor (rad/s) and Frequency (Hz) vs. Voltage (V). The linear fits were obtained using Microsoft Excel software.

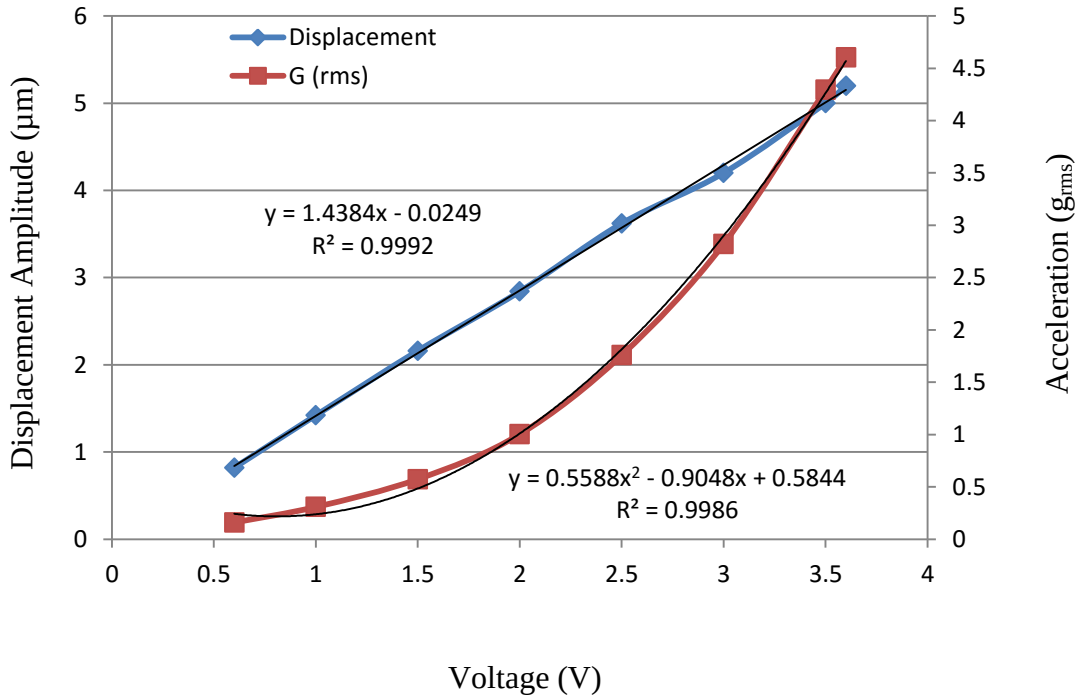

Figure 3-7: Displacement Amplitude (µm) and Acceleration (g_{rms}) vs. Voltage (V). The linear and quadratic fits were obtained using Microsoft Excel software.

The relationship between the input voltages to the transient responses, speed, frequency and vibration amplitude is as tabulated in Appendix B.

3.4 Discussion

The transfer function, as stated in equation (6), offers useful information regarding the selection of a miniature DC motor. This second order system has a very high natural frequency of 6216 rad/s (989.3 Hz), which indicates the system is very stable as the highest driving frequency to the system is about 1580 rad/s (251. 5 Hz). The motor also has a damping ratio of greater than 1, which means the system has an overdamped response. This steady behaviour ensures that there is no sudden jolt of sharp vibration felt at the arm during the initial rotation of the motor.

From the simulation outcomes in Figure 3-4, it can also be seen that the motor will be able to reach the desired speed within 42 milliseconds. The rise time, which is the time taken for the motor to achieve from 10% to 90% of its desired speed is about 24 milliseconds. These responses are well within target; it is stated that 0.8 – 1.5 s is adequate for prosthetic hands [6]. Should a faster response be needed, a Proportional-Derivative (PD) controller will be included as part of the design in the future.

The peak-to-peak amplitude of vibration has been simulated in terms of displacement (refers to skin indentation), as well as acceleration (Figure 3-5). Although each type of amplitude will be felt similarly on the skin, the way it is represented is useful for the vibration analysis. Displacement is mostly used for machines with rotating speeds lesser than 100 rad/s while lateral acceleration is used for higher rotating frequencies. The rotational acceleration is also one of the accepted practices in measuring vibration amplitude. A measured 1 *g* peak-to-peak acceleration is approximately $9.8 ms^{-2}$ peak-to-peak lateral acceleration [84].

As stated in [45], a person can detect about 10 mm skin indentation at frequency of 20 Hz. As the frequency increases to the optimal frequency of the Pacinian corpuscle, which is 250 Hz, the skin indentation can be detected as low as 1 μm. According to [76], the lowest level of vibration can be detected on human skin is 0.04 *g*. By referring to the Figure 3-6 and Figure 3-7 with this background information, the voltage input to the motor could be varied even from around 0.6 V up to 3.6 V to ensure sufficient vibration could be felt at the skin of the upper arm.

The simulation plots in Figure 3-6 show the linear relationship between the voltage versus the motor speed and its driving frequency. As the voltage increases, the rotation speed of the DC motor increases which leads to the increment of frequency. It can be seen that the motor generates frequencies between 42 Hz to 251 Hz depending on the input voltage. This is in accordance with [85] that states the Pacinian corpuscle in the hairy skin has a band-pass characteristic, which has a sensitivity between 65 to 400 Hz. As the frequency bandwidth of the skin falls within the frequency bandwidth generated by the motor, it imparts confidence that the skin will be able to detect the vibration of the motor in encoding the surface texture efficiently. As shown in Figure 3-7, the measured peak-to-peak accelerations were converted to the root mean square (RMS) acceleration to determine its effective vibration energy content. As the simulated vibrations were purely sinusoid, the RMS values were calculated with known value of peak acceleration, *pk*, using the following general formula:

$$RMS = 0.707 . pk \qquad (7)$$

The relationships between the voltage versus the displacement and acceleration have also been explored, as shown in Figure 3-7. The displacement amplitude linearly increased with increment of voltage input as expected. The quadratic (second order) behaviour of the acceleration in relation to the voltage input is also as predicted. This is because acceleration is a second order derivative to the displacement.

The only parameters that remained almost constant throughout the voltage variation were the settling and rise times. This could be explained by referring to the motor's root locus plot, generated using MATLAB, in Figure 3-8. As the gain is increased to 2.53×10^5 and beyond, the location of the pole will remain at -2.07. Pole locations show the transient responses for a system. The further away it is from the origin, the faster the transient response is [86]. For this case, as the pole location is constant at increasing gain, the transient responses are also constant as the voltage is increased. As the gain of the motor is already high (at 1.7×10^{10}), increasing the voltage does not have any effect to the transient response at all. Changing the voltage only affects the speed of motor. The simplest way to improve the transient responses of the motor is by adding another pole and zero to the system. The PD (Proportional-Derivative) and PID (Proportional-Integral-Derivative) are the common controllers used for improving transient responses [86].

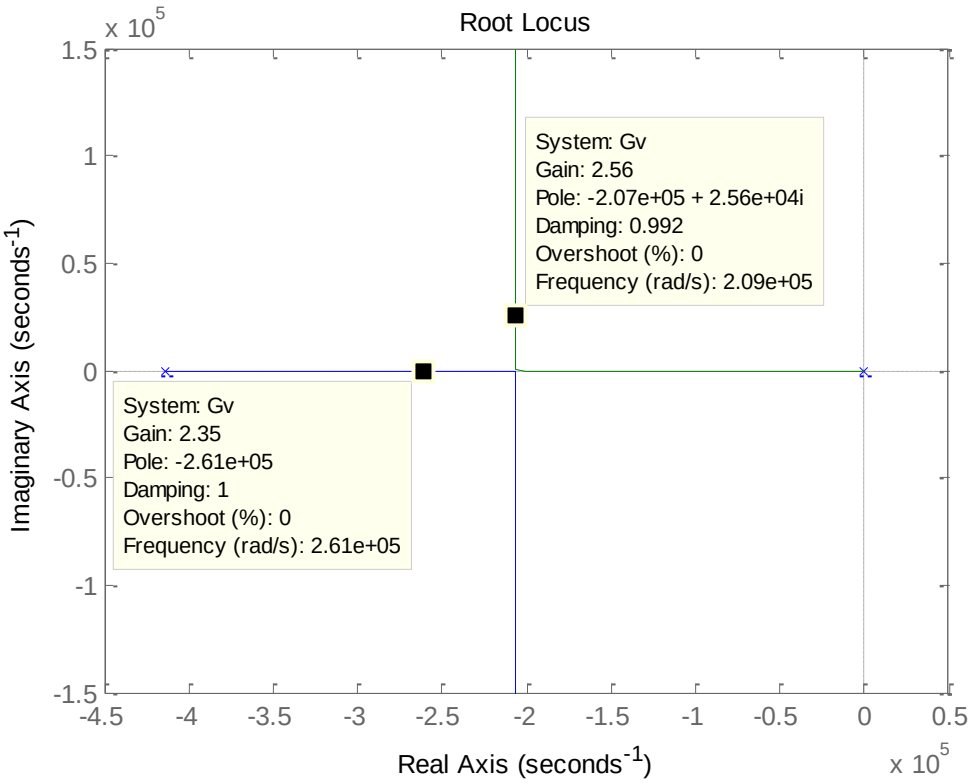

Figure 3-8: Root locus plot for the DC motor (processed in MATLAB)

3.5 Summary

This chapter described simulations that were used to predict the transient responses of the motor as well as its amplitude of vibration at a given input voltage. In order the simulation could be conducted, an experiment has been done to obtain the transfer function of the haptic system. Throughout the experimental and simulation work, adjustments of the input voltage were observed to affect the driving frequency of the actuator, which in turn generates the amplitude of vibration accordingly. The transient responses also provide some estimation in preparing the next haptic event, such as the time it may take when the step input is increased or decreased. This part of the research presented in this chapter has been presented and published in an IEEE conference [87].

Chapter 4 Validation of the Haptic Characteristics

To confirm the MATLAB simulation results, an experiment was designed to measure the amplitude of vibration generated by the miniature DC motor. Three devices have been identified to measure the amplitude of vibration produced by the miniature DC motor, which are laser interferometer, a wearable wireless sensor and a linear accelerometer. Each has been tested for its reliability and accuracy to obtain the best vibration measurement.

The laser interferometer (KEYENCE LC-2400W) is equipped with a sensor head that has the capability to measure the height and eccentricity of a specified object [88]. The sensor head is of the diffuse-reflective type and is equipped with LabView software to record the amplitude and frequency of vibration of the miniature DC motor. The motor was enclosed in a rigid plastic enclosure and was allowed to rotate freely on a designated platform under the beam of the laser. The vibration reading was obtained in millivolts and automatically converted to displacement amplitude (μm) by LabView.

However the sensitivity of the laser interferometer is 0.5μm, which was not sensitive enough to obtain accurate results of the vibration amplitude. Furthermore, even after recalibration, the outputs obtained during the experiment (peak-to-peak laser displacement and output voltage) were inconsistent and not repeatable. The possible reason for the inconsistency was due to the elasticity of the tape that holds the motor onto the platform.

To overcome the sensitivity and inconsistency issues, a wearable wireless sensor (model Shimmer3 from Shimmer), was used in place of the laser interferometer. This clinical grade sensor, commercially used for biophysical and motion sensing, is fitted with a 3-axis accelerometer that could be set to either ±1.5g or ±6g. The 3dB cut-off

frequencies are 400 Hz for the X and Y axes, and 300 Hz for the Z axis and the corresponding maximum sampling rate of the accelerometer is 1 kHz. Bluetooth is used to acquire the vibration signal and the data is automatically transferred to the computer via the Shimmer Connect software [89].

The Shimmer device was taped down onto the table using blue tack. The miniature DC motor was securely glued on top of the device. Measurements were taken from 0.5V-3.5V (at 0.5V step size). However, the Shimmer sensor was too sensitive to vibration to capture useful experimental results. The Fast Fourier Transform (FFT) of some of the collected data also showed that the frequency response of the vibration is much higher than that indicated by the simulation results and motor technical specification. The occurrences of very high instantaneous amplitudes were also observed during the actions of turning the motor on or off or of sudden movement.

4.1 Hardware Configuration of a Linear Accelerometer

To obtain an accurate vibration measurement, a linear accelerometer with minimum bandwidths of 2 kHz was selected. A linear accelerometer is a sensor that provides a voltage output proportional to the detected acceleration due to movement. The LIS3L02AS4 linear accelerometer was selected to measure the amplitude of vibration generated by the haptic actuator. It is a tri-axis (X, Y and Z directions) accelerometer with an IC interface that is able to acquire acceleration information and provide an analog signal to external devices such as oscilloscope or host computer. The frequency bandwidths are 4kHz for X, Y axes and 2.5kHz for Z axis [91].

To eliminate transients of high interference, power supply decoupling capacitors are required for this circuit. As a common design practice, the capacitors should be placed the nearest possible to the circuit to ensure high frequency noise to be kept away from the circuit [92]. A 100nF ceramic and 10µF aluminium electrolytic decoupling capacitors were chosen as recommended by the manufacturer of the LIS3LO2AS4 [91].

To obtain best results with the accelerometer output, the frequency bandwidth should be the smallest possible for a given application [91]. The maximum frequency of vibration generated by the miniature DC motor is 250 Hz, hence the cut-off frequencies (f_c) of the accelerometer outputs were chosen at 1 kHz. The cut-off frequencies were implemented by adding external capacitors ($C_{load(X,Y,Z)}$) at the output pins. These act as low pass filters for anti-aliasing and noise reduction for the circuit.

The values of the external capacitors could be obtained using the following general formula:

$$C_{load(X,Y,Z)} = \frac{1.45\mu F}{2\pi . f_c . R_{out}} \quad (8)$$

R_{out} represents the internal filtering resistor, which is 110 kΩ (with ±20% tolerance) according to the manufacturer's datasheet. The external capacitors were chosen as 1nF (the nearest value of available capacitors), which gives acceptable value of cut-off frequency within the ±20% tolerance of the internal resistor.

4.2 Calibration of the Accelerometer

To ensure the accelerometer is working in perfect condition, several characteristics of the accelerometer were tested against the manufacturers' datasheet. The characteristics include Self-Test, Zero-g level and Orientation.

4.2.1 Self-Test

This test is done to verify the movement of the seismic mass by the electrostatic test-force of the accelerometer [91]. For a given voltage in the self-test mode (V_{st}), the output voltage change, $V_{out(\Delta)}$, in relation to the movement of the seismic mass is defined by the following equation:

$$V_{out(\Delta)} = V_{out(Vst=Logic1)} - V_{out(Vst=Logic0)} \quad (9)$$

The self-test was done at the full-scale of ±6G. The results were compared with the accelerometer's datasheet to ensure that the self-test voltage output changes are within the typical values of the calibrated specification by the manufacturer.

4.2.2 Zero-g Level

The zero-g level corresponds to the output signal of the accelerometer without the presence of gravitational acceleration. On a horizontal surface, with the accelerometer pins pointing upwards, the sensor will measure zero-*g* in X and Y axes while +1*g* for Z axis. The accelerometer is factory calibrated at V_{dd} = 3.3V, hence the ideal voltage output, V_{out}, at zero-*g* is mid-way between 0 and 3.3V, i.e. V_{out} = V_{dd}/2=1.650 V. A

deviation greater than the V_{out} is considered as positive acceleration, while deviation lesser than V_{out} is considered as negative acceleration. These deviations from the zero-*g* level are known as zero-*g* offset [91].

For this application, the zero-g level of the accelerometer has been tested on a horizontal surface with the pins pointing downwards. The voltage outputs for all three axes with no presence of acceleration are as shown in Table 4-1. The obtained voltage outputs will be considered in calibrating the accelerometer according to its orientation.

Table 4-1: Voltage outputs for X, Y and Z axes without the presence of gravitational accelerations in the X and Y directions

Axes	***X***	***Y***	***Z***
Corresponding Acceleration (*g*)	0	0	-1
Voltage Output (V_{out}), V	1.664	1.705	1.114

4.2.3 Orientation Check

The orientation check is important to relate the *g* acceleration with the obtained output voltage. The output voltage are measured at 6 orientations of the accelerometer (+X, -X, +Y, -Y, +Z, -Z). These voltages correspond to the g acceleration at the chosen scale (±6G). By tilting the accelerometer by 90º about the three axes, any two of the readings would be 0g and the third would be either -1*g* or +1*g*.

A spirit level was used to ensure measurements were carried out on a level surface. To ensure a perfect 90º orientation, a protractor was placed on top of the scale, and the accelerometer was taped onto it.

By supplying an input voltage, V_{dd} of 3.3V to the accelerometer, the output voltages at 0º, +90º, 180º and 270º were measured. These values are important in obtaining the linear relationship between the output voltage and its corresponding g acceleration, as shown in Figure 4-1. Both plots and linear equations were obtained using Microsoft Excel.

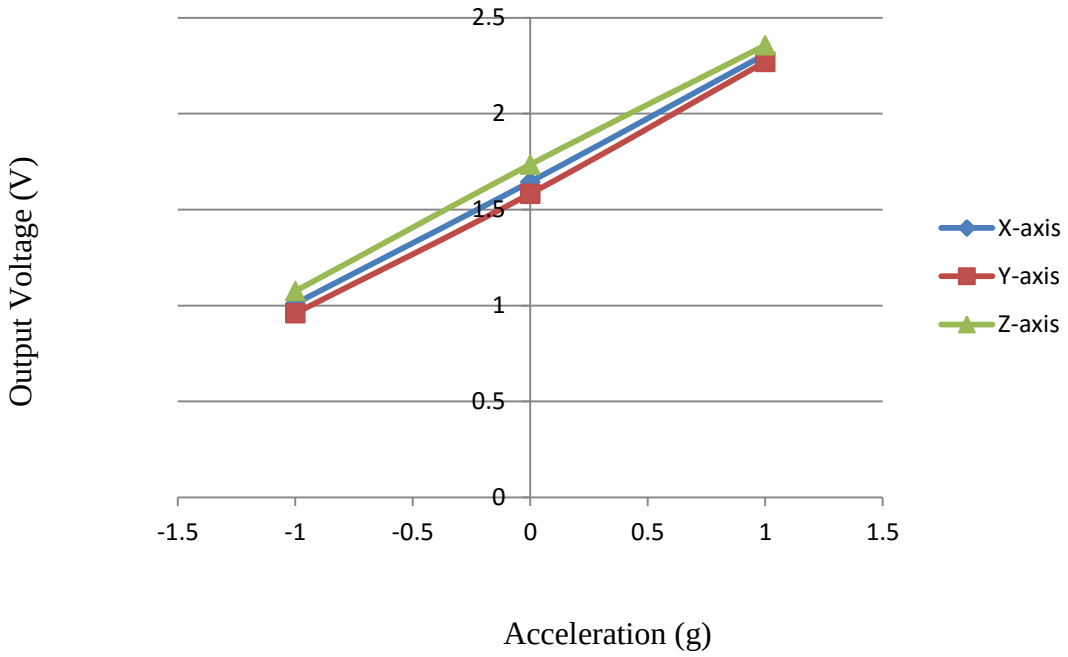

Figure 4-1 : Linear Relationship between Acceleration (g) and Output Voltage (V)

The linear relationships between the acceleration (G_X, G_Y, G_Z) and output voltage (V_X, V_Y, V_Z) for the 3 axes were obtained as follows:

$$V_X = 0.6495(G_X) + 1.6595 \quad (10)$$

$$V_Y = 0.655(G_Y) + 1.615 \quad (11)$$

$$V_Z = 0.6405(G_Z) + 1.7155 \quad (12)$$

Manipulating the equations, the accelerations (G_X, G_Y, G_Z) for the X, Y and Z axes become

$$G_X = \frac{V_X - 1.6595}{0.6495} \quad (13)$$

$$G_Y = \frac{V_Y - 1.615}{0.655} \quad (14)$$

$$G_Z = \frac{V_Z - 1.7155}{0.6405} + 1 \quad (15)$$

As the corresponding acceleration for the Z-axis at the initial condition (when no acceleration acting on the accelerometer) is -1g (as recorded in Table 5-1), +1g is added to the G_Z equation to set the measurements to begin at 0g.

4.3 Experimental Apparatus for Vibration Measurement

The miniature motor was securely positioned on top of the accelerometer using superglue to record the generated vibration when voltage is supplied to it. As a common practice, a 100 µF (non-polar ceramic) decoupling capacitor was included with the motor circuit design. The motor was allowed to freely rotate and measurements were taken when the motor reached steady-state. Two separate power sources were utilized to supply input voltages to the motor and accelerometer. Output data were measured using a 4-channel digital phosphor oscilloscope (Tektronix DPO3014). The experimental setup and the accelerometer/ motor circuit are as shown in Figure 4-2and Figure 4-3.

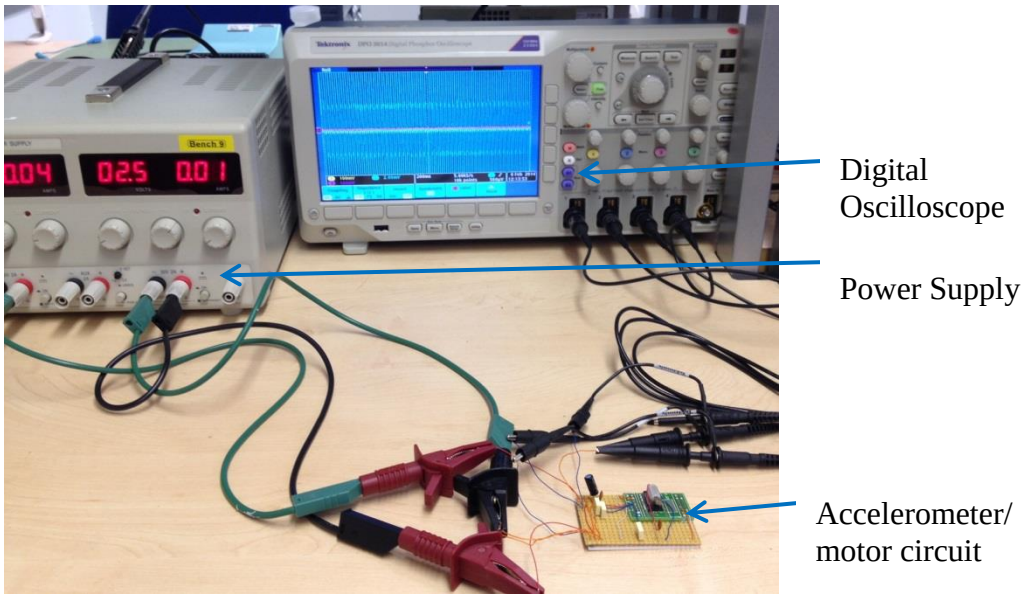

Figure 4-2: Experimental apparatus to obtain the vibration amplitude of the motor

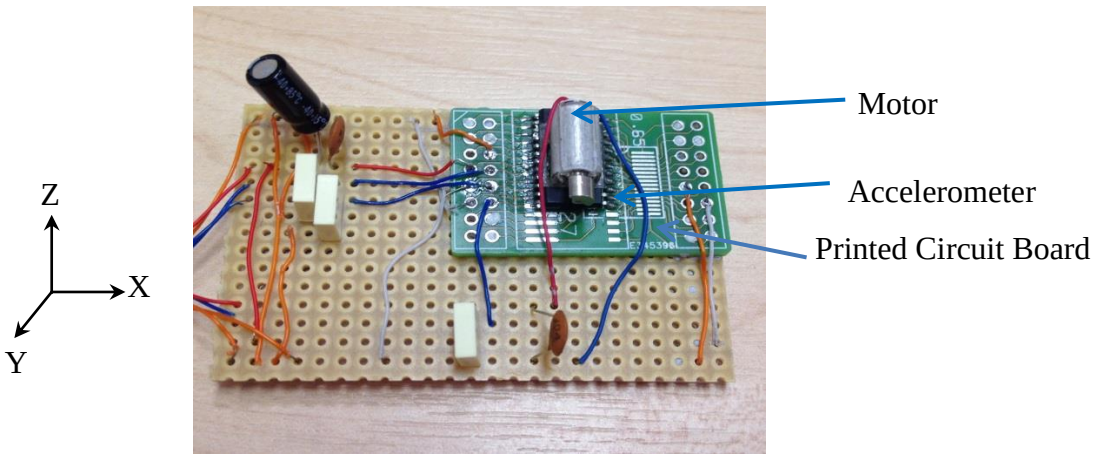

Figure 4-3: Accelerometer and motor circuit. The arrows on left show the vibration axes of the motor and the accelerometer

4.4 Experimental Results

4.4.1 Acceleration Outputs and Frequency Responses

The acceleration outputs were recorded in the X, Y and Z axes for input voltages to the motor that were varied from the 0.6 V (typical start voltage). Increments were made in 0.5 V steps to 3 V (rated voltage) and then to 3.6 V (maximum operating voltage of the motor).

The Fast Fourier Transform (FFT) Matlab® was used to examine the frequency response generated by the motor vibration. Figure 4-4 to Figure 4-7 show the accelerations and the FFT responses observed for 1V and 3.5V respectively.

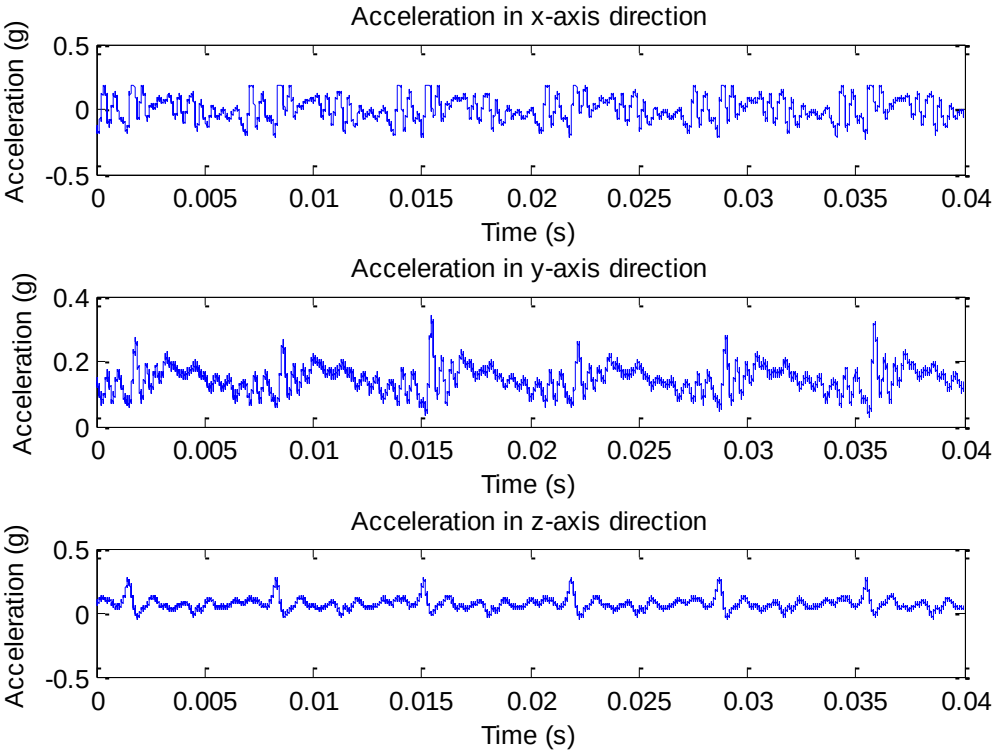

Figure 4-4: 1V supply – Acceleration Waveforms for the X, Y and Z axes.

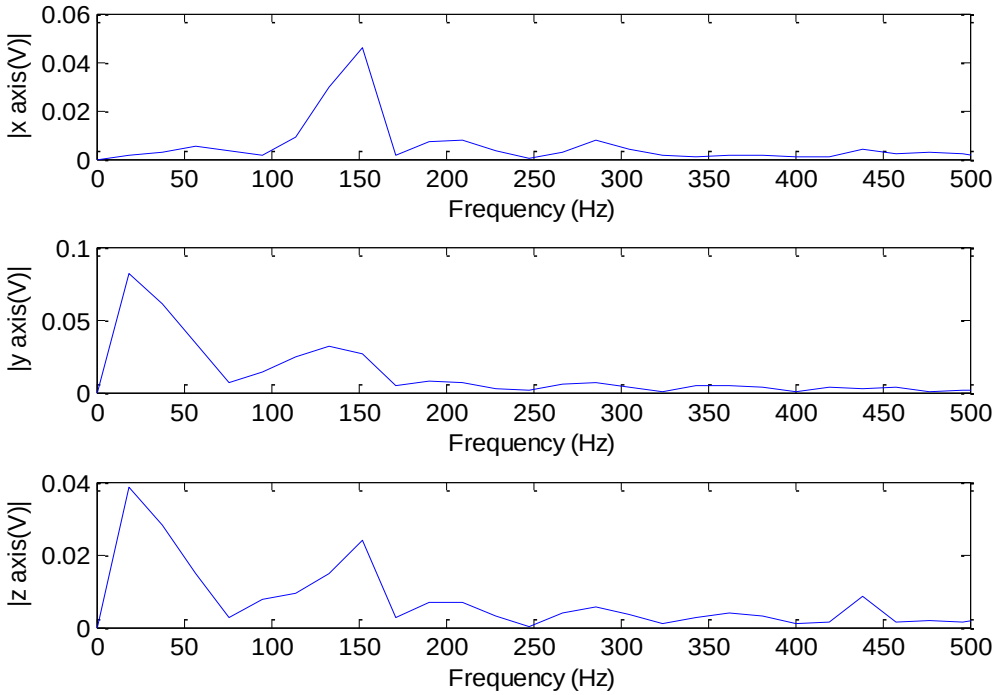

Figure 4-5: 1V frequency response observed in the X, Y and Z axes. Dominant frequencies (highest peaks) were observed at 152.6 Hz at X axis and 19.07 Hz at both Y and Z axes

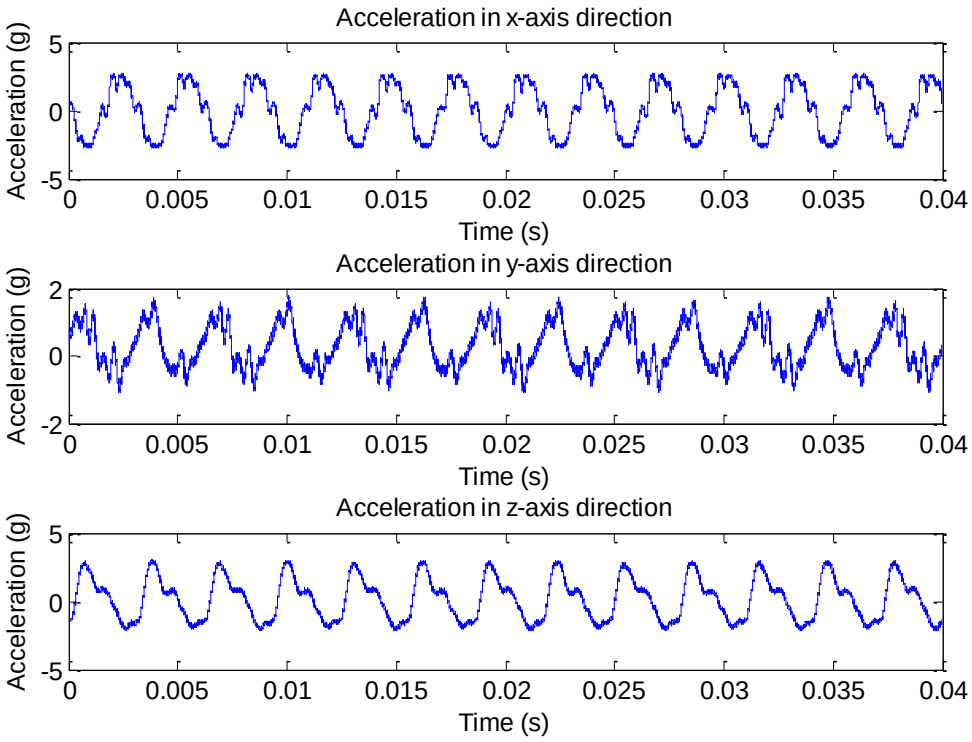

Figure 4-6: 3.5V supply – Acceleration Waveforms for the X, Y and Z axes.

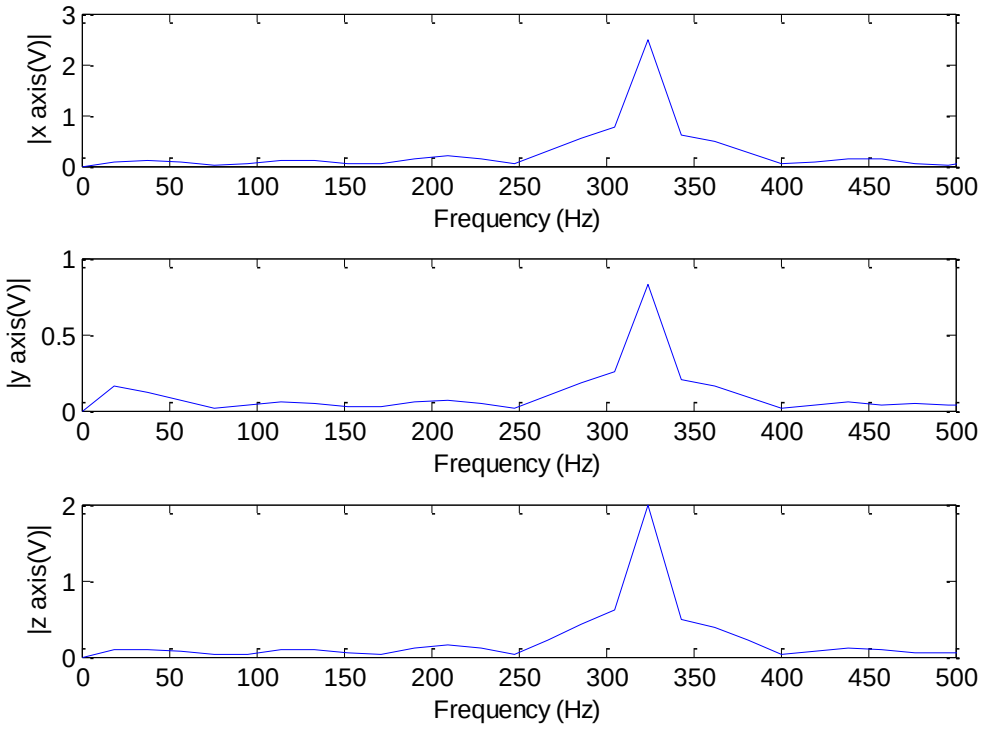

Figure 4-7: 3.5V frequency response observed in the X, Y and Z axes. Dominant frequencies (highest peaks) were observed at 324.2 Hz for all axes.

4.4.2 Vibration Amplitudes and Frequency Response vs. Voltage Input of the Motor

The measured data were tabulated to observe the effects of voltage supply of the motor to the vibration amplitudes and generated frequencies. (See Appendix C for the data). Figure 4-8 shows the relationship between vibration amplitudes (in root mean square), with the motor input voltage while Figure 4-9 highlights the relationship of generated frequencies to the motor input voltage.

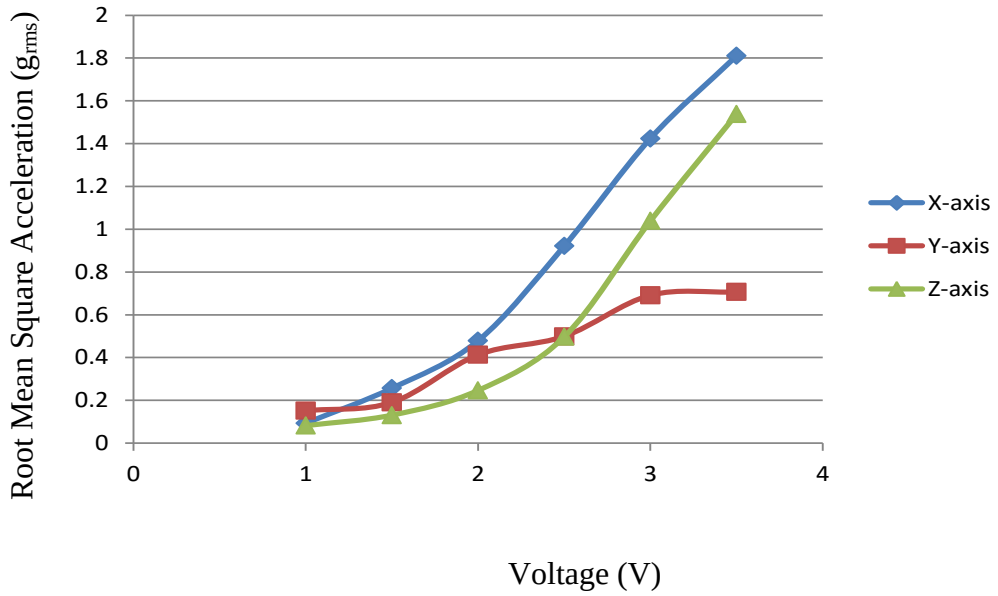

Figure 4-8: Acceleration (g) vs. Voltage (V)

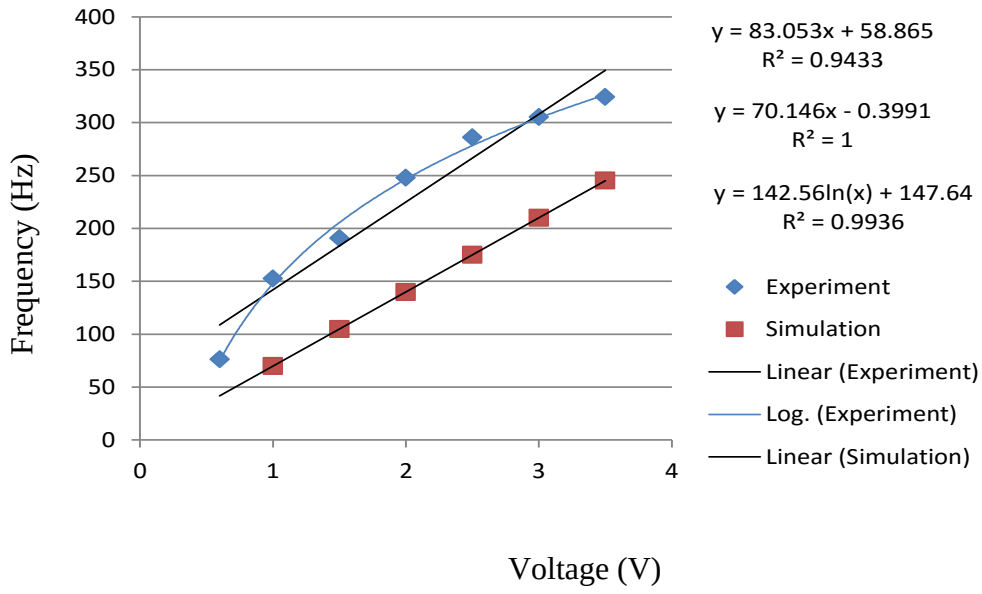

Figure 4-9: Vibration Frequency (Hz) vs. Voltage (V)

4.5 Discussions

From the experiment, the motor was struggling to rotate when voltage supply was less than 1V (Figure 4-4). It could be observed that at 1V, the highest peak acceleration were recorded at 0.25*g* for x and z axes and 0.5*g* for y axis. Dual peak frequency responses observed between the x and the y and z axes (Figure 4-5) also indicate that the vibration output of the motor is not consistent at a lower voltage.

From the experiment, as the voltage supply increases, the peak-to-peak acceleration of the motor picked-up and went up to 5.4*g* peak-to-peak at 3.6V (Figure 4-6) which is half of the simulated output. This is because the mass of the circuit board affects the vibration amplitude. Increasing the mass of the vibrated object reduces the net vibration acceleration. This in turn will decrease the chance of vibration being perceived. Therefore it would take higher input supply to generate vibration for a heavier test rig and vice-versa [81]. The simulated results only consider mass of the miniature motor which is 1.1 g while the circuit board consists of an accelerometer and extra wirings, with a total mass of 16.11 g.

For a given voltage supply, the motor will vibrate in two planes that are perpendicular to the body length of the motor [81]. For this application, the X and Z axes were perpendicular while the Y axis was in parallel to the body length of the motor (Figure 4-3). It could be observed from Figure 4-8 that the vibration experienced in the X and Z axes were much stronger as compared to the Y axis. When positioned on the skin surface, the vibrations in the X and Z axes will be felt as a slight stretching and indentation on the skin respectively. During the psychophysical investigation at the final stage of this project, the directionality of the haptic stimulation will be considered only at the axis where the strongest vibration is produced. This will ensure that the frequency of vibration of the motor could be controlled within the desired bandwidth. Further explanation in achieving the strongest vibration axis of the motor is described in Section 8.3.

To measure the effective vibration energy content, the measured peak-to-peak accelerations should be converted to the root mean square (RMS) accelerations [93], [94]. The outcome of the conversion is as shown in Figure 4-8 . It can be seen that the highest effective vibration content was recorded at 1.8 g_{rms} and 1.5 g_{rms} at the X-axis and Z-axis respectively, with voltage supply of 3.5V. The plot is useful as it gives information on the actual vibration to be felt by the users at varying voltage inputs.

The relationship between the frequency and voltage supply for both simulation and experiment is plotted in Figure 4-9. By adding the linear trend lines to the plot, it was observed that the experiment result (R^2=0.9433) is not as perfectly linear as compared to the simulations results (R^2=1). This result is expected, as the motor is subjected to external factors during experiment, such as the way it is mounted and the actual maximum frequency/vibration it could handle. Nevertheless the simulation results obtained previously provides a background idea on the behaviour the motor at different voltage supplies.

To further assess the relationship of the frequency of vibration to input voltage, a log trend line has been used. With the R^2 value of 0.9936, it gives reliable information in estimating the required voltage for a desired frequency of vibration.

It could be observed from Figure 4-9 that the motor generates vibration frequency between 76 Hz to 320 Hz depending on the input voltage. This frequency band falls within the frequency sensitivity of the hairy skin which is between 65 to 400 Hz [85]. The frequency of interest, which is 250 Hz, occurs when the motor is supplied with 2V. At this voltage, the accelerations (RMS) of the motor are 0.5 *g* and 0.2 *g* at the X and Z axes respectively, which are within the range of detection threshold of the skin at 50 Hz to 250 Hz frequency range [51] .

4.6 Summary

This chapter compared the simulation results with the actual setting by measuring the amplitude of the miniature motor vibration using a 3-axis linear accelerometer. The findings show that both simulation and experiments have similar trends, in which the vibration and frequency will increase as the voltage supply to the motor is increased. The plots obtained from the experiment give valuable information for manipulation of supply voltage in obtaining the desired frequency and vibration. External factors that affect the amplitude and frequency of vibration such as the mass and material of arm band strap to mount the motor have also been identified and will be considered as selection factors in the next stage of this research work. This part of research work has been presented and published at a conference technically co-sponsored by the IEEE Engineering in Medicine and Biology Society [95].

Chapter 5 Data Acquisition Strategies

The next stage of this research work was to acquire signals from the sensor when it was in contact with textured surface. A test rig by Muridan [96] has been used and modified for this purpose. The test rig consisted of a hollow aluminium sliding tube with attached linear encoder. This assembly was originally from an inkjet printer and is powered by a DC motor. The linear encoder attached to the printer sliding mechanism measures the position of the sliding tube relative to the aluminium base. The velocity of the block was varied by varying the voltage supplied to the DC motor. A finger link that holds the piezoelectric sensor was positioned at the middle of the sliding block. The voltage output in relation to the textured surface was recorded using a 200kS/s data acquisition device by National Instruments (NI DAQPad-6016). The test apparatus is shown in Figure 5-1.

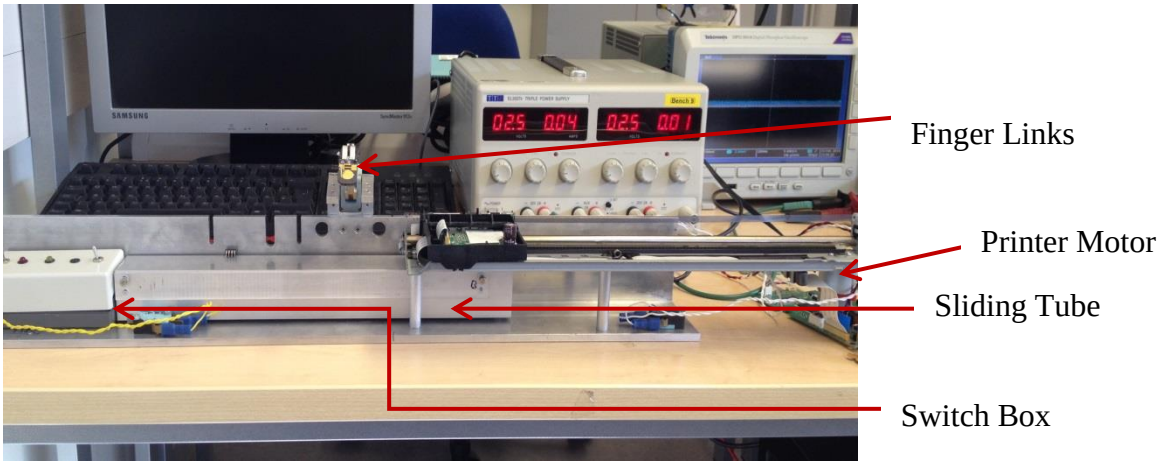

Figure 5-1: Test apparatus for data acquisition process

5.1 Movement mechanism of the test apparatus

A new movement mechanism has been included in the test apparatus to ensure the block only slides along the required length. This is to prevent it from sliding off the base and significantly distort the acquired signal. Furthermore some part of the circuits may get damaged when subjected to impact forces from the high momentum if it accidentally slid off the base track.

The movement mechanism was controlled by a Double Pole Double Throw (DPDT) ON-ON switch and two limit switches at both ends of the rig. The DPDT switch was used to rotate the motor in forward and reverse directions. The working voltage supply to run the motor was 6V, with a current supply of 500 mA. The limit switches disconnect the DC power supply when the sliding block reaches the ends of the track, so that the block stops moving further off the track. A Single Pole Double Throw (SPDT) switch was used to power up the entire circuit as well as to provide signals to a light emitting diode (LED) indicating the power state (on/off). To avoid friction during the movement, nylon bolts were fitted at the left and bottom sides of the tube. The circuitry for the movement mechanism is as shown in Appendix D.

5.2 Data Acquisition Device and Configurations

5.2.1 NIDAQPad-6016

To ensure a much higher resolution output than the previous work [96], the NIDAQPad-6016 (Figure 5-2) has been chosen to acquire signals from the sensor. The device consists of 16 single-ended / 8 differential input channels with 16 bits resolution at a maximum sampling rate of 200 kS/s. The NIDAQPad-6016 is a bus-powered multifunction system that only require power supplied through the Universal Serial Bus (USB) without external power supply [97].

Figure 5-2: NIDAQPad-6016 Data Acquisition Device (reproduced from [97])

Apart from its high resolution signal output, this device has 2 analog output channels, which made it capable in controlling the voltage output for the haptic actuator. With the aid of the LabView program, a signal acquired from the piezoelectric sensor was processed to produce associated on and off pulses to represent repetition of regular patterns of the surface texture. This signal was passed from the data acquisition device to a motor driver circuit to power the miniature DC motor of the haptic actuator.

5.2.2 Terminal Configurations and Rig Connections

Two inputs were acquired with the NI data acquisition device. One input was from the piezoelectric sensor and another from the encoder. In acquiring the signal generated during the sliding motion of the piezoelectric sensor on the surface texture, the INA118 instrumentation amplifier output was electrically connected to the analog input channel of the device. As the data acquisition system is a floating source, the ground reference output of the amplifier was connected to the common reference point terminal of device, and subsequently grounded.

The encoder was wired to the second analog input terminal of the acquisition device. A voltage divider has been constructed to scale down the range of the encoder output to 0.29V (initially at 3.2V) to match the sensor output signal which operated within the same voltage range. This was done so that the magnitudes of the two signals were similar and thereby ensured easier observation of both input signals at the control panel. The encoder signal is used to measure the position and velocity of the moving block.

The acquisitions for both signals were done simultaneously and continuously at the frequency rate of 75 kHz per channel, with -0.5V to 0.5V input range. The sampling rate was initially set at 100 kHz per channel but had to be reduced as it caused buffer overflow that freezes the data acquisition system.

5.3 Piezoelectric Sensor

A piezoelectric sensor has been used to acquire signals when it brushes against textured surface. This sensor is designed to mimic the human mechanoreceptors at the fingertips. The sensor is mounted at the end of the finger link and held secure with small bolts. The sensor and finger link system used for this work have been developed by Cranny [13], Cotton [16] and Light [98]. Figure 5-3 illustrates the sensor with its finger link system.

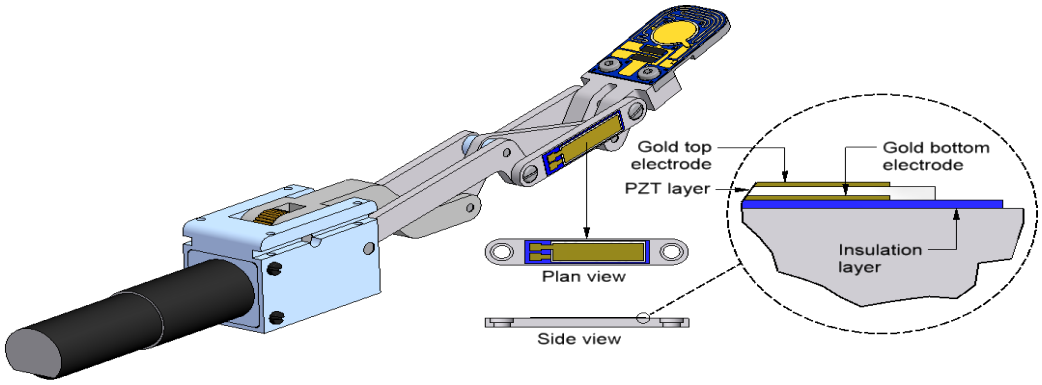

Figure 5-3: The finger link system (illustration credit to Dr. Andy Cranny, University of Southampton)

Referring to Figure 5-3, the yellow circular shape is the dynamic force sensor. This is the area of contact between the sensor and the textured surface. This part of sensor is made of four layers which are insulation layer, gold bottom electrode, PZT layer and gold top electrode. The positive and negative electrical charges generated by the PZT layer due to the contact with the surface will move to the gold top electrode and gold bottom electrode. The charge output from the sensor is converted to a voltage signal with a suitable amplifier. The sensing was performed through a layer of a silicone glove.

To conduct the experiment, the finger link was mounted to a bracket. This will put the finger in a stationary position while the block with the textured surface slid along the aluminium base.

5.4 Voltage Amplifier

The piezoelectric sensor will generate an electrical charge when a pressure is applied to it. When continuous, varying forces are exerted to the surface of the sensor, an AC voltage is observed across the device terminals [99]. An amplifier has been carefully designed to interface with the sensor. This amplifier was used to produce a voltage signal within the required frequency range and signal amplitude.

The INA118 instrumentation amplifier has been chosen due to its capability to achieve high input impedance and to produce less distortion to the original signal. This characteristic is important for this design as the piezoelectric sensor has large output impedance, and to minimize the loading effect, comparable input impedance is required [100].

A different amplifier configuration has been designed to replace the amplifier designed in the past work [96] to achieve a more reliable output. In previous work, a charge-mode amplifier has been interfaced with the sensor in obtaining voltage signals. The output voltage, V_{out}, as well as the cut-off frequency of the charge amplifier isdependent on the feedback capacitance, C_f, instead of the input capacitance, C_s. This configuration is suitable for use with normal operational amplifiers and especially useful when the sensor is remotely located from the amplifier [101]. As the amplifier was mounted in close proximity to the sensor, the voltage mode amplifier is appropriate [99] and has been designed for this application. In this mode, the amplifier output as well as the frequency passband is dependent on the capacitance close by the sensor, C_s [99]. With this configuration, the required frequency bandwidth for the data acquisition task could be obtained. The schematic design of the voltage amplifier is as shown in Appendix E.

Decoupling capacitors, C_d, have also been included in this circuit design. The capacitors were connected to positive and negative power supply pins and individually grounded. The purpose of including these capacitors was to overcome signal oscillations.

The wiring and connections within the circuit should also be short lengths, as longer wire and connectors will generate noise in the circuit (50 Hz mains pick-up) and significantly affect the output signals. The piezoelectric sensor and the charge amplifier were also positioned close to each other to overcome the unwanted noise in the signals.

5.5 Impulse Test on the Piezoelectric Sensor

To check the capability of the piezoelectric sensor in picking up the required signals, an impulse test has been conducted. This test was done by gently tapping the fingertip sensor using the back of a pen. At this stage, the data were acquired using a digital oscilloscope.

An impulse or a tap is the integral of a force with respect to the time. In this experiment, the force from the light tap will activate the charges in the piezoelectric sensor. The charges were then amplified by the charge amplifier, and its output in terms of voltage could be observed from the oscilloscope.

The outcome from the impulse test is as shown in Figure 5-4. It can be observed that without tapping the sensor, the waveform is 12 mV peak-to-peak due to external noise (50 Hz). When the tapping occurred, the signal shot up to 96 mV, an 87% increase from the initial condition. The 12 mV peak-to-peak noise has been reduced from 250 mV peak-to-peak obtained in the previous charge amplifier design. This observation showed that the amplifier is reliable is acquiring the input signal.

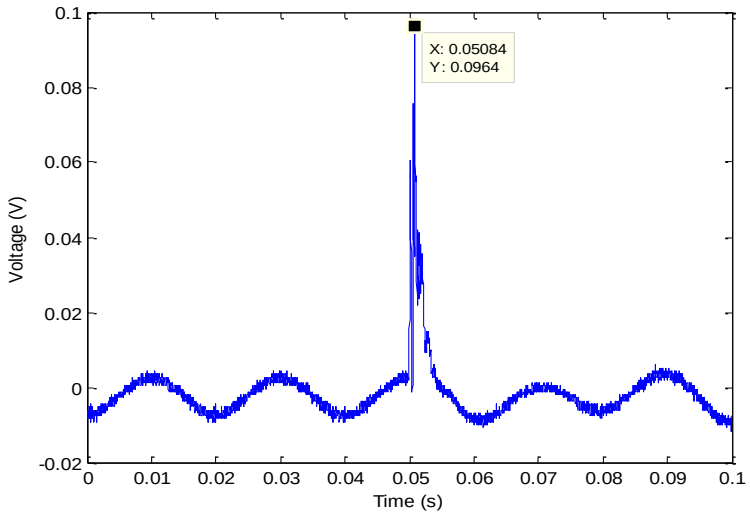

Figure 5-4: Voltage output when light tapping was done on the fingertip

5.6 Encoder

The signals from the linear encoder were also acquired in order to measure the velocity of the sliding block. At a given voltage signal, the block may accelerate, decelerate or remain at a constant velocity. Ideally, the block will accelerate during the

first few milliseconds of the experiment and remain at a constant velocity until it reaches the limit switch, which will stop the block. The friction between the contact surfaces, however, may decelerate the movement of the sliding block. To estimate the grating widths of the surface texture, the velocity should ideally remain constant to generate a peak in the FFT of the signal from the sensor.

The plastic encoder strip in the experiment rig consists of a series of black and transparent stripes (Figure 5-5). By determining the width of a pair of black and transparent stripes, the encoder velocity can be calculated. The widths were measured by gathering the data samples during the sliding motion of the block. These samples were acquired using the NI DAQPad-6016. The distance travelled by the block was measured using a digital Vernier calliper. Using MATLAB® program, the data length and the number of black and white stripes (in pairs) were obtained. By dividing the displacement of the block (in mm) with the number of pairs, the width of one black and transparent pair was determined. Five measurements were made and the mean of width was calculated. The width of one pair of the encoder stripes is 0.0865 mm. The measurement data is attached in Appendix F.

Figure 5-5: Linear encoder of the rig. W, the width of a pair, is 0.0865 mm.

5.7 Summary

This chapter described the test apparatus used to acquire signals from a textured surface. Modifications have been made to the original apparatus ensure much more accurate and reliable results were obtained, which include the movement mechanism of the sliding tube as well as the design of the charge amplifier. A new switching circuit has been constructed to ensure the block only slides along the required length of the aluminium tube without falling off track. The modified voltage amplifier has proven to provide a much crisper output than before with much less external noise. Also, the capture of data has been improved by replacing a digital oscilloscope with a data acquisition device from the National Instruments to ensure higher output resolution from 8 bits to 16 bits.

Chapter 6 Data Acquisition of Surface Textures

After testing the experimental apparatus to ensure that it performs reliably and the new design of the instrumentation amplifier has a high sensitivity, the next stage of this research work was to acquire signals from the piezoelectric sensor and encoder when the surface texture was in motion. The gathered signals will be used for calculations of the dimensions of the surface textures.

6.1 Surface textures

The surface textures from previous research were used in the experiments with the new amplifier [96] . The gratings were made in pairs on 310 mm acrylic strips. The length of a texture is 100 mm. The gratings were fabricated with different dimensions to represent a variety of surfaces for the sensor to detect.

Four surface textures (A, B, C and D) with different dimensions were investigated. A test on a smooth surface (Type A) was conducted for control purposes. Type B has repeating patterns, with similar widths of grooves and ridges. Type C consists of repeating patterns of different widths of ridges and grooves. Type D has a set of repeating patterns of increasing widths of grooves and constant widths of ridges. Figure 6-1 show the dimensions of the surface texture.

To confirm the accuracy of the surface dimensions, all surface textures were measured using a microscope (Motic B3 Professional Series). The microscope is equipped with image processing software to capture and transfer fine images to a computer for further analysis. The measurements of the surface texture are as attached in Appendix G.

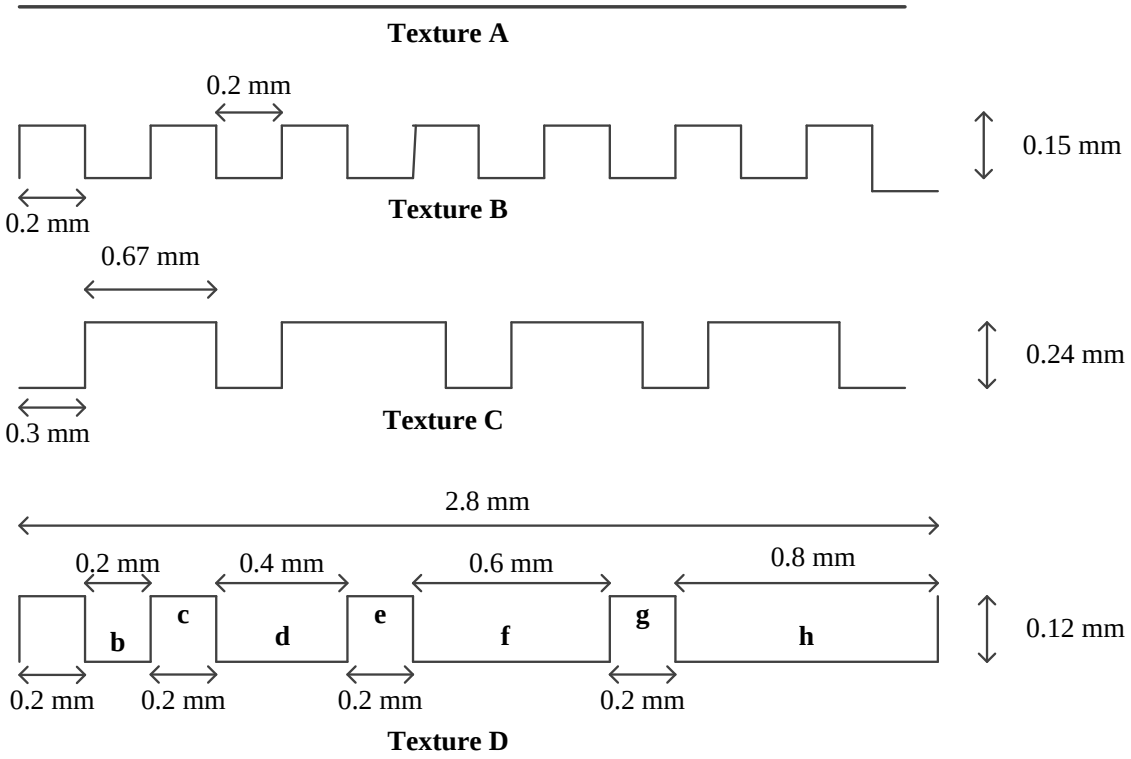

Figure 6-1: Dimensions of Surface Textures under Investigation (Texture A – smooth surface, Texture B – repeating every 0.4mm, Texture C – repeating every 0.97 mm, Texture D – repeating every 2.8 mm)

6.2 Experiments

The acrylic strip that consists of the fabricated surface texture was attached to the sliding block using screws at both ends of the strip. By having these removable strips, investigations on different types of surface texture could be conducted as these strips could be easily removed and reattached. The piezoelectric sensor, mounted on the fingertip and layered with some material from a silicone glove, was positioned on the vertical side of the surface texture. The contact force between the sensor and the surface was 60mN, which was approximately the mass of the fingertip [102]. This value was not measured or controlled, but to ensure that reliable signals could be detected by the sensor, there should be contact between both surfaces. On the other hand, the contact force should not be very high to avoid unnecessary friction that may in the extreme, result in the block not sliding.

The piezoelectric sensor could also be attached directly on the apparatus, but was mounted on the fingertip instead to demonstrate the capability of the prosthetic finger

in acquiring signals from surface textures. Figure 6-2 shows the top view illustration of the moving block and the piezoelectric sensor.

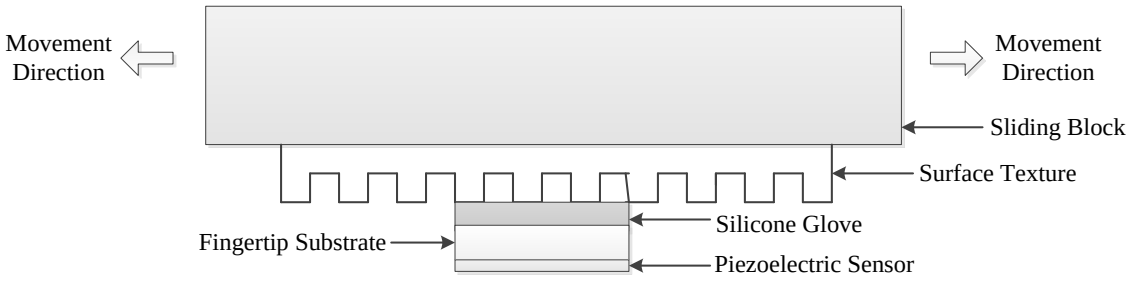

Figure 6-2: Top view illustration of the moving block and the piezoelectric sensor

The positioning of the sensor played an important role in delivering the output signal. The sensor will be more sensitive when positioned in full contact with the surface texture under investigation. Figure 6-3 shows how the sensor was mounted to obtain a reliable output signal.

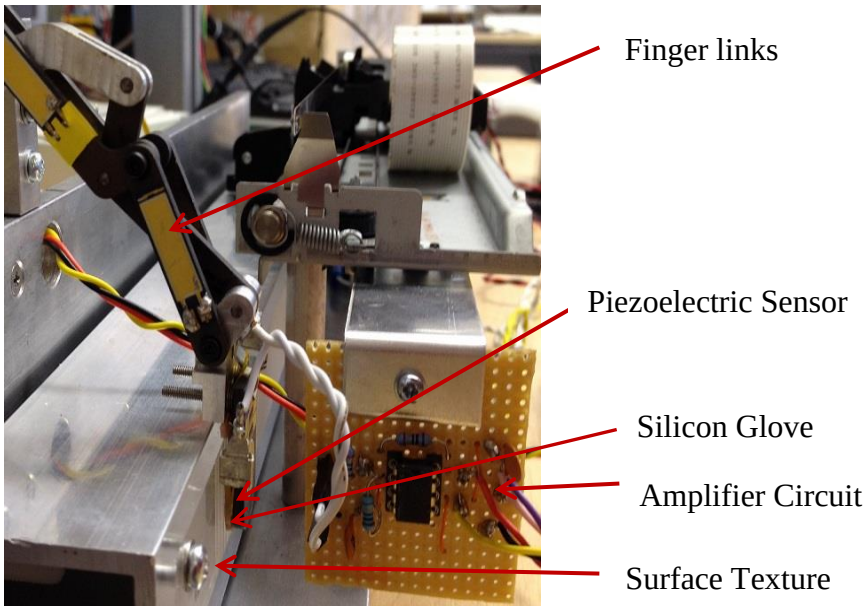

Figure 6-3: Positioning of the sensor and the surface texture to provide a more accurate reading of the signals

To acquire the signal generated by the sensor, a ±2.5 V voltage was supplied to the amplifier circuit and 5.5 V – 6.0 V was supplied to the test rig to move the block. Varying the supply voltage to the rig caused the velocity of the block to vary. The block would move past the stationary sensor in either the left or right direction. The information about the velocities and the output voltage from the sensor were gathered by the data acquisition device (NIDAQPad-6016) and saved in the Excel format for analysis. As the maximum frequency that could be detected by the tactile information-

processing system of a human is 1 kHz [19], the piezoelectric sensor and encoder signals were sampled at a higher rate of 75 kS/s throughout each test. This was to ensure all the signals were accurately reconstructed up until 35 kHz in discrete time without losing any important data. The LabView software was used to program the data acquisition and data saving tasks.

6.3 Output Signals

Two sets of data were gathered during the experiment, which were the encoder data to calculate the velocity of the sliding block, as well as the voltage signal generated by the piezoelectric sensor when in motion contact with the surface. The signals were saved in the technical data management streaming (TDMS) file format which is the data storage system of the LabView software. Data in this format were later converted into Excel format and exported to MATLAB for further analysis. The analyses in MATLAB were done in two stages. The first stage was to calculate the DC offset and to filter the piezoelectric sensor signals. The DC offset was calculated by subtracting each voltage output gathered by the piezoelectric sensor with the mean voltage.

A Kaiser window low pass filter, with a passband edge of 1.5 kHz and a stopband edge of 5 kHz, was chosen for this purpose. These filter specifications were selected as the sliding frequency of interest was 1 kHz and the transition frequency width could be limited to 5 kHz with low passband and stopband ripples.

The second stage of this post-processing task was to calculate the velocities, FFT outputs as well as the corresponding surface grating widths. The velocities were calculated from signals gathered from the encoder. This was done by selecting the equally sized encoder pulses within a data length. The equal sized encoder pulses were indicators that the velocity of the block was constant. An example of an encoder signal with a constant velocity could be observed in Figure 6-4.

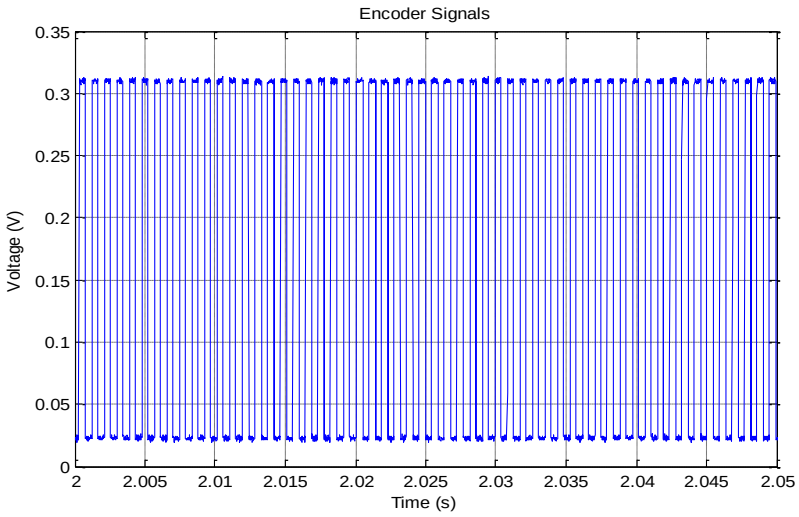

Figure 6-4: Encoder signal with constant velocity

The equally sized encoder pulses were visually selected from the produced MATLAB plots. Using the same software, the selected samples of the encoder signals were then verified by calculating the period for every pulse. The mean and standard deviation for the period of the pulses were then obtained. A deviation of less than 10% from the mean value of the period of encoder pulses indicates that the pulses were consistent and that the velocity of the block of the selected sample length was constant.

The total number of pulses and the period of the selected sample were determined. The velocity was then calculated by multiplying the total number of pulses with the measured width of the encoder stripe (as described in the previous chapter) and divided it with the period of the selected sample.

The surface grating widths were calculated by dividing the computed velocity with the FFT outputs generated in MATLAB. The calculated widths were then compared with the measured widths (previously obtained using microscope) to assess the accuracy of the system in acquiring the surface texture information. Ideally the differences between the calculated and the measured widths should be very low. For this work, differences of less than 10% were considered acceptable. These post-processes tasks were performed for all four surface textures.

6.3.1 Texture A (Smooth Surface)

This texture is a part of the control data, in which the purpose was to identify existing signals so that it would not be mistaken as signals generated by the fabricated surface gratings. For this texture, the supply voltages were varied to achieve speeds

between 70 mm/s to 120 mm/s. The experiments were repeated at least five times to confirm the repeatability of the generated output signals. The original and filtered piezoelectric signal waveforms for a sample are shown in Figure 6-5.

The total time it took for the block to move to the end of the track was 1.07 seconds. This period excludes the time before the block started moving (the first 0.59 seconds) and after the block reached the end of the track (the last 0.89 seconds). At the instance when the motor to move the block was switched on, there was a large spike in the signal, which was possibly due to the switching sound made by the toggle switch, or transient in the motor circuit or sudden movement of the block against the finger. The block also experienced an impact when it reached the end of the track. This is shown by the second spike in the figure. By having both stationary and moving signals in one plot, the signal-to-noise ratio (SNR) of the system could be obtained. For this smooth surface, the SNR recorded was 3.6 dB.

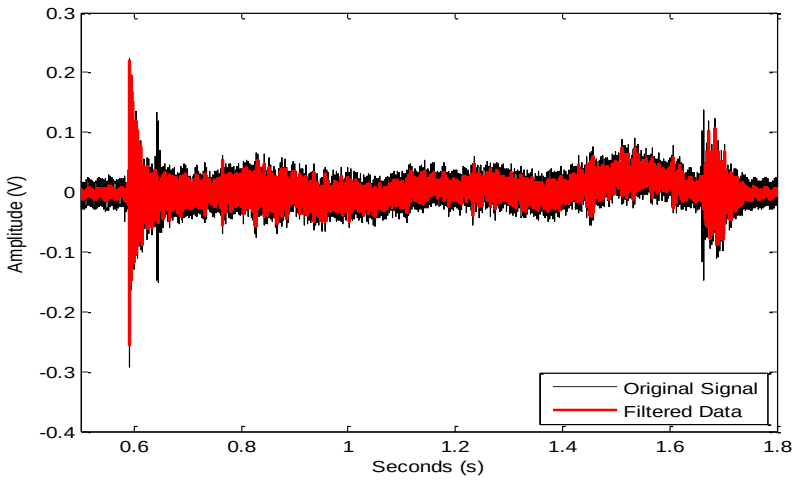

Figure 6-5: Smooth surface – Original and Filtered Signals for a whole length of data

The next part of the analysis was to obtain the FFT signals when velocity was constant. This could be determined by checking the evenly distributed pulse widths of the encoder signals. A MATLAB code was created to confirm that the velocity was at its constant state. The selected sample signals (at 1.1 s to 1.2 s) for both encoder and piezoelectric sensor, moving at 77.2 mm/s are as shown in Figure 6-6. In this sample, the mean width of the encoder pulse was 0.71 millisecond, with a standard deviation of 0.04 millisecond. The low standard deviation (5.4% from the mean value of the encoder pulse width) gave indication that the encoder pulses were equally sized and that the block was moving in a constant velocity.

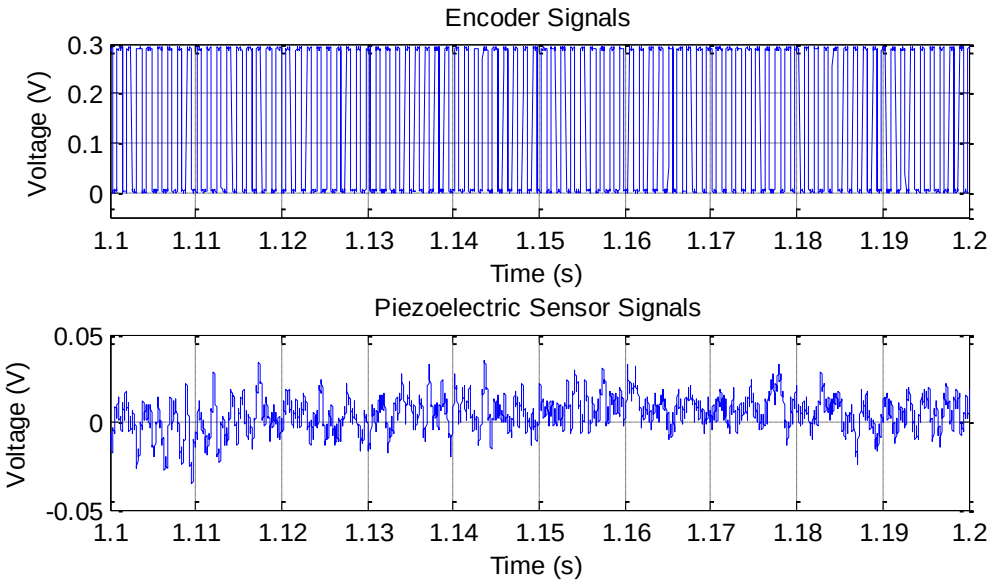

Figure 6-6: Smooth Surface – Encoder and Piezoelectric Signals at selected sample length

From the selected length of the signals, the FFT output could be obtained as shown in Figure 6-7. A component frequency was observed at 4.589 Hz, which may be due to external factors such as low hum generated by infrastructure in the building. This frequency component was filtered out in determining the widths of the ridges and grooves of the surface textures.

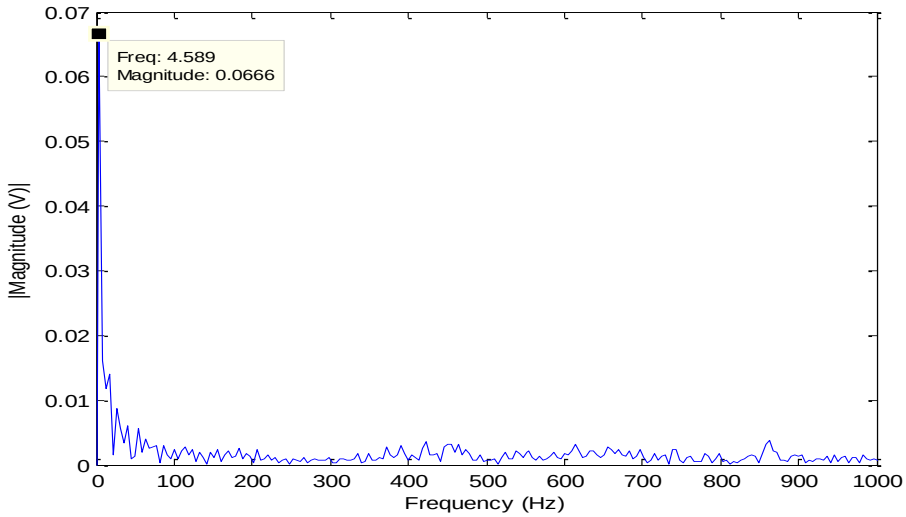

Figure 6-7: Smooth Surface - FFT Output

6.3.2 Texture B (Repeating patterns of similar widths of grooves and ridges)

For this surface texture, velocities were varied between 20 mm/s to 135 mm/s. At different velocities, components of the signals from an FFT analysis corresponded to the widths of the surface gratings. The clearest outputs however, were achieved when the velocity of the block moved at more than 90 mm/s. At these velocities, the FFT components were the dominant frequencies. At velocities less than 90 mm/s, the frequencies corresponding to the widths could be also detected, but these were not the dominant frequencies. The following Figure 6-8 shows the output waveform for one sample for Texture B.

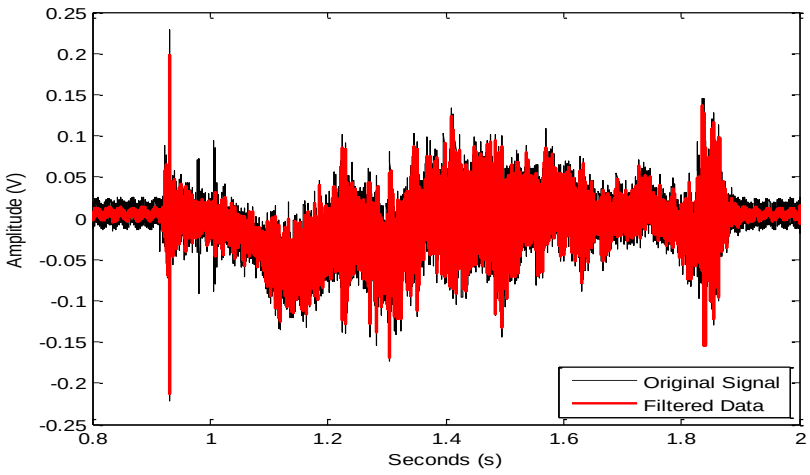

Figure 6-8: Texture B– Original and Filtered Signals for a whole length of data

At this velocity, the total time it took for the block to move to the end of the track was 0.76 seconds, excluding the first 0.92 seconds, and the last 1.90 seconds (as shown from the signal spikes). It could be observed that at the first few milliseconds (0.28 seconds) when the block started to move, the signal deviated a little to the negative side before going constant between ±0.1V. This was the transition signal detected by the sensor as there is a 1 cm of smooth texture before the beginning of the repeating surface patterns. It was therefore important to screen and select the appropriate signal output to ensure that only the part that consists the textured gratings were analysed. The selected data sample (from 1.3s to 1.4s), moving at 95.6 mm/s is as shown in Figure 6-9. In this sample, the period of the encoder pulses were recorded at 0.45 ± 0.009 millisecond (mean ± standard deviation), which was a 2.06% deviation from the mean value).

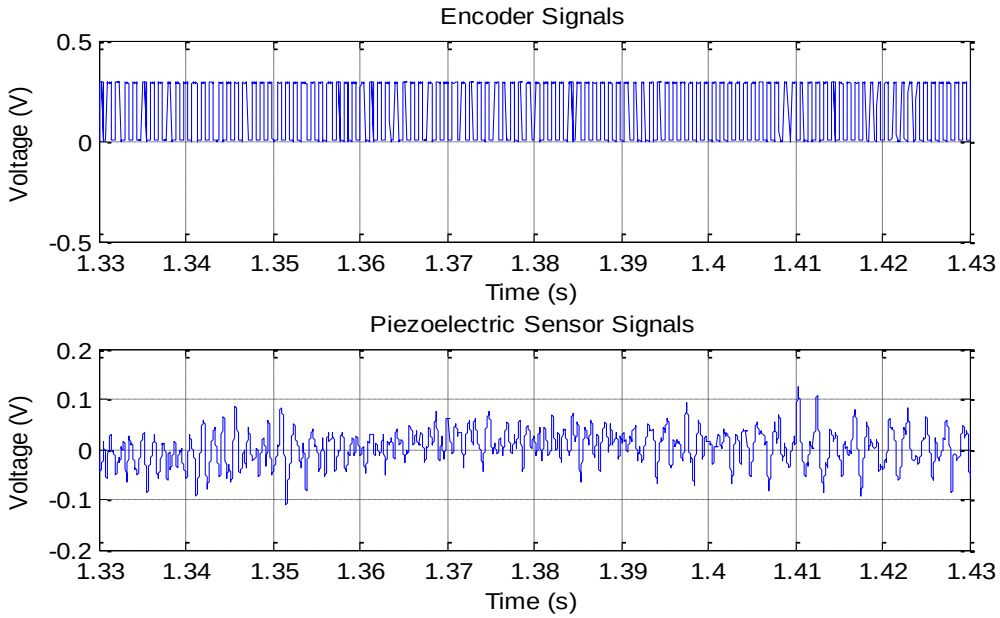

Figure 6-9: Texture B - Encoder and Piezoelectric Signals at selected sample length

A dominant frequency of 468.1 Hz was detected for the selected sample length, as shown Figure 6-10. From this frequency and the measured velocity, the widths, w of the ridge/groove could be calculated by dividing the frequency, f, with the velocity, v, which is equivalent to 0.204 mm. The accurate measurements from microscope are 0.2001 mm for the ridge and 0.1926 mm for the groove. This indicated 2.05% and 6.03% differences between the calculated and measured widths of ridge and groove respectively.

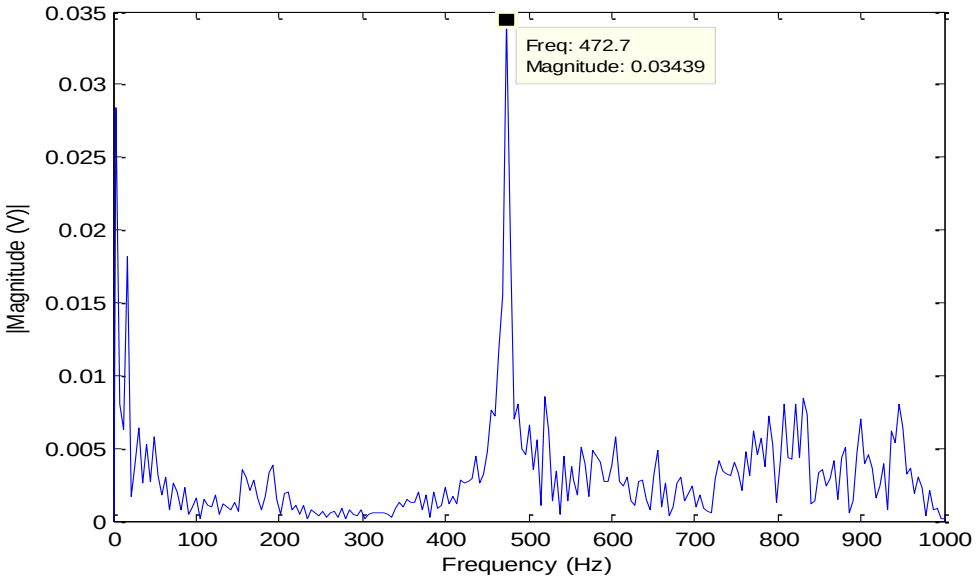

Figure 6-10 : Texture B – FFT Output

It could be observed that there is only one dominant FFT output for this particular texture. This was because the texture has a repeating groove and ridge at similar widths. A slightly less magnitude component at a very low frequency was also detected in the plot. This was the same as have been observed from the smooth texture surface. The summary for this observation is as shown in Table 6-1.

Table 6-1: Summary for one data sample of Texture B

Velocity (mm/s)	*Calculated FFT frequency (Hz)*	*Calculated width (mm)*	*Measured width (mm)*	*Percentage Difference (%)*
95.6	468.1	0.204	0.2001 (ridge) 0.1926 (groove)	2.05 (ridge) 6.03% (groove)

Experiments with this texture were repeated at varying velocities. The generated FFT outputs and their corresponding surface widths show the capability and reliability of the sensor to detect the dimensions of the surface texture. Figure 6-11 shows the differences between calculated widths and the measured widths for velocities varying from 20 mm/s to 135 mm/s. The highest percentage difference of 4.92% for ridge and 9.02% for groove were recorded when velocity was at 134.89 mm/s while the lowest percentage difference were 0.74% for ridge and 4.68% for groove when velocity was at 22.19 mm/s. At this low velocity, however, the generated FFT signal was not the dominant frequency. The dominant frequencies corresponding to the surface widths were achieved when velocities were above 90 mm/s. In all velocity conditions, it could be inferred that the data acquisition system was capable to gather reliable information of this surface texture as the percentage differences between the calculated and measured grating widths were within target (less than 10% difference).

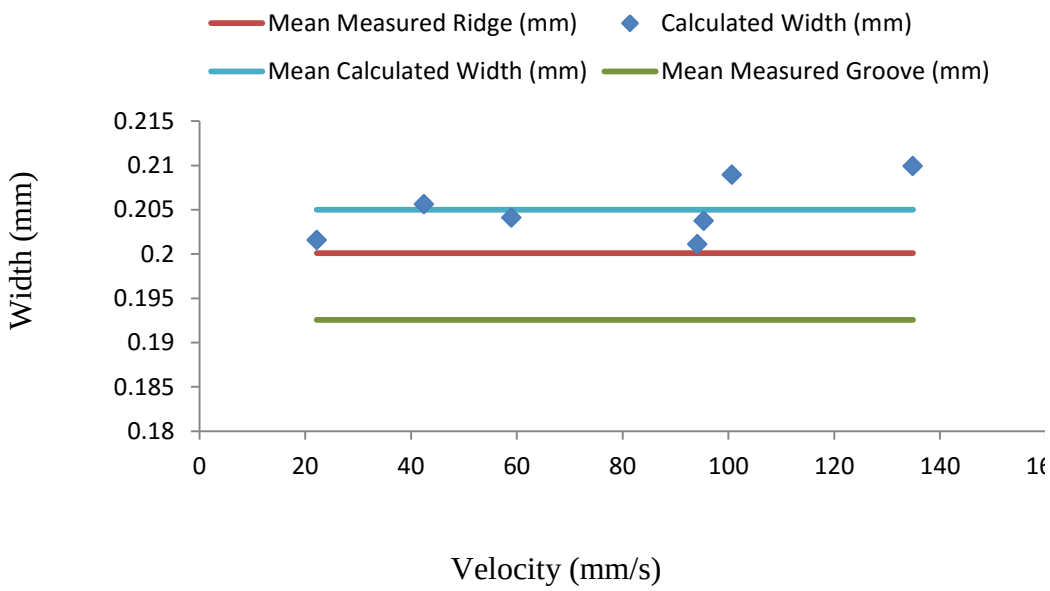

Figure 6-11: Texture B - Calculated grating widths (obtained from MATLAB) as compared to the measured widths (measured with microscope) at varying velocities. The red and green lines represent the mean measured widths of ridges and grooves, as shown in Appendix G.

The differences between the calculated width with the mean measured widths of ridges and grooves were 0.0049 mm (2.55%) and 0.0124 (6.46%) respectively. These low variabilities may be due to slight discrepancies during the measurement with the microscope, or possibly due to the effect of the varying velocities during the experiment.

6.3.3 Texture C (Repeating patterns of different widths of ridges and grooves)

Data were gathered when the sliding block was moving between 80 – 140 mm/s. The output waveforms for Texture C are as shown in Figure 6-12 to Figure 6-14.

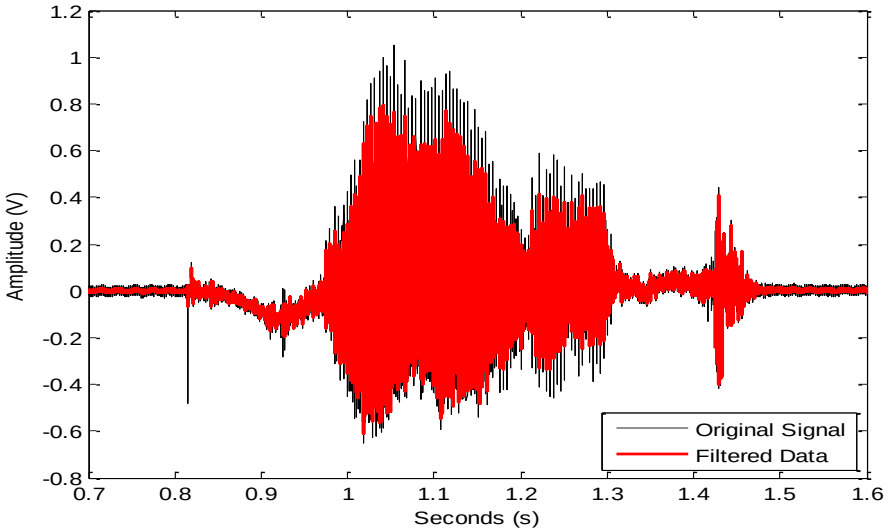

Figure 6-12: Texture C - Original and Filtered Signals for a whole length of data

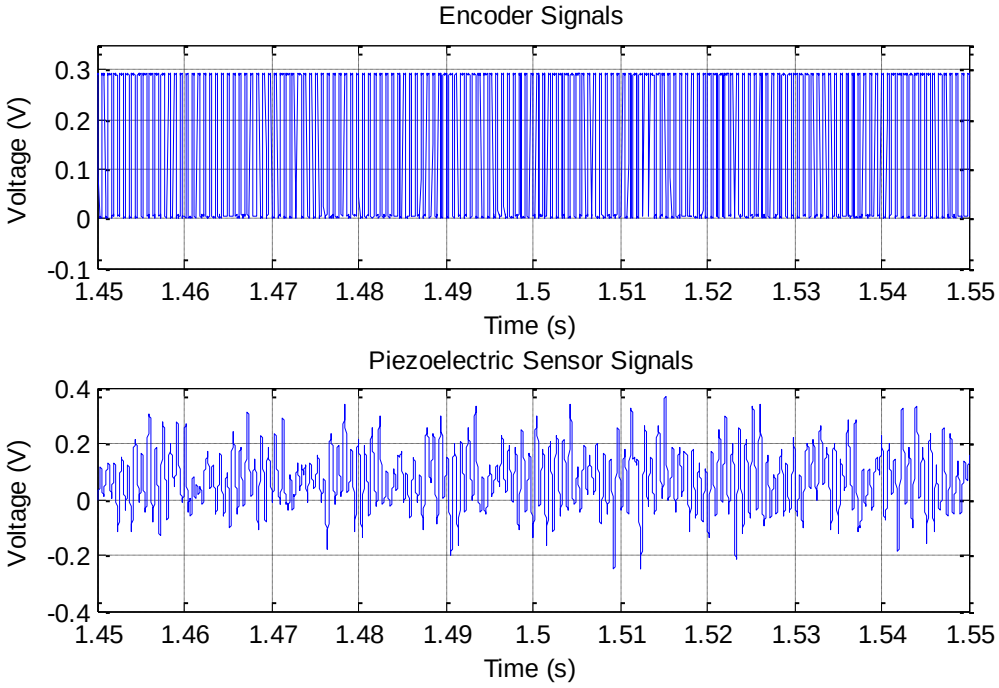

Figure 6-13: Texture C - Encoder and Piezoelectric Signals at selected sample length

Similar to Texture B, data were selected where velocity was constant. For Figure 6-13, the velocity was recorded as 116.7 mm/s. The period of one encoder pulse in this sample length was 0.37 ± 0.03 millisecond (mean ± standard deviation). The 8.2% deviation from the mean value show that the period of the encoder pulses were consistent.

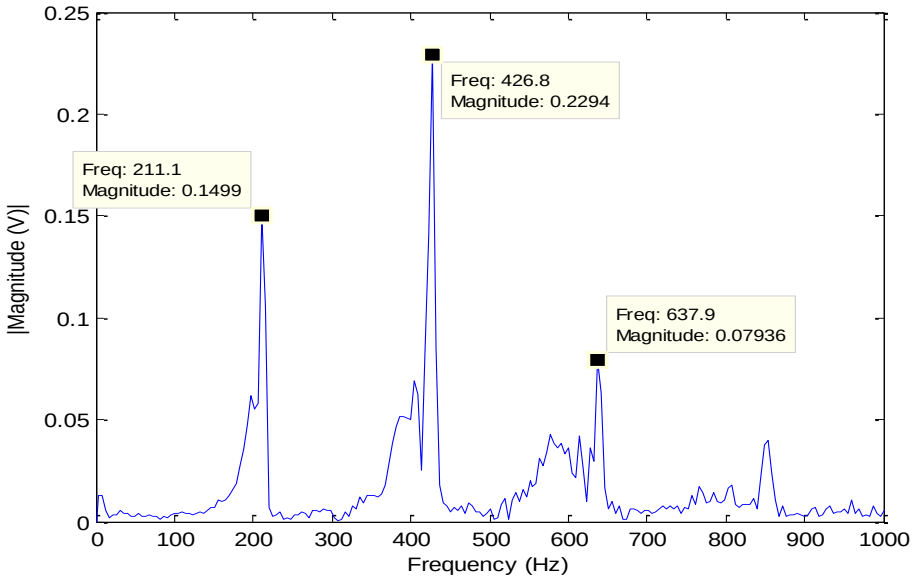

Figure 6-14: Texture C – FFT Output

As Texture C consists of two different widths, the FFT outputs should show two dominant frequencies corresponding to the widths. However, the plot also showed occurrence of a third frequency at a lower magnitude. As this third frequency has the lowest magnitude as compared to the first two frequencies, this frequency was not considered when calculating the dimensions of the surface textures. The observations for Texture C, recorded at velocity of 116.7 mm/s are as tabulated in Table 6-2.

Table 6-2: Summary for one data sample of Texture C

Velocity (mm/s)	*Calculated FFT frequency (Hz)*	*Calculated width (mm)*	*Measured width (mm)*	*Percentage Difference (%)*
116.7	426.8	0.273 (groove)	0.302 (groove)	10.3 (groove)
	211.1	0.553 (ridge)	0.676 (ridge)	22.3 (ridge)

Figure 6-15 shows the differences between the measured and calculated widths of ridges and grooves for velocities between 80 mm/s to 125 mm/s. It could be observed that in all velocity conditions, the percentage difference between the measured and calculated widths of ridge were much higher than the groove. The lowest percentage difference between the ridges was 19.13% when the block travelled at 119.79 mm/s while lowest between the grooves was 6.53% at velocity of 80.58 mm/s.

At velocities lower than 80 mm/s, the widths of the ridges and grooves could be detected but the FFT signals associated with the widths were not the dominant frequencies. The percentage differences between the calculated and measured widths for this texture were unfortunately higher than the allowable 10% difference. This matter will be discussed further in the discussions section.

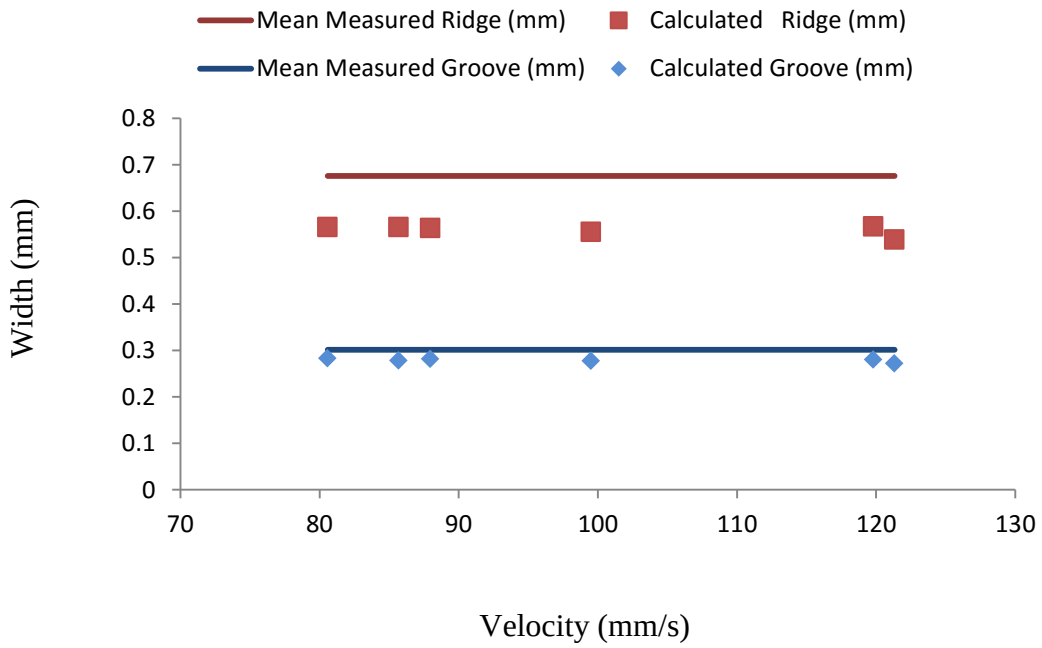

Figure 6-15: Texture C - Calculated grating widths (associated to the dominant frequencies obtained from MATLAB) as compared to the measured widths (measured with microscope) at varying velocities. The red and blue lines represent the mean measured widths of ridges and grooves, as shown in Appendix G.

6.3.4 Texture D (Repeating patterns of increasing widths of grooves and constant widths of ridges)

Surface texture D has a slightly complicated surface grating as compared to the other surface textures as it consisted of increasing widths of grooves. Therefore it was expected that there would be a lot of frequency components in the FFT plot. Data gathered for texture D are as shown in Figure 6-16 to Figure 6-18 for a constant velocity of 127.01 mm/s. In this sample of data, the recorded pulse width was 0.34 ± 0.03 millisecond (mean ± standard deviation), which was a 9.5% deviation from the

mean value of the pulse width. The consistencies of the pulse widths gave indication that the block was moving in a constant velocity.

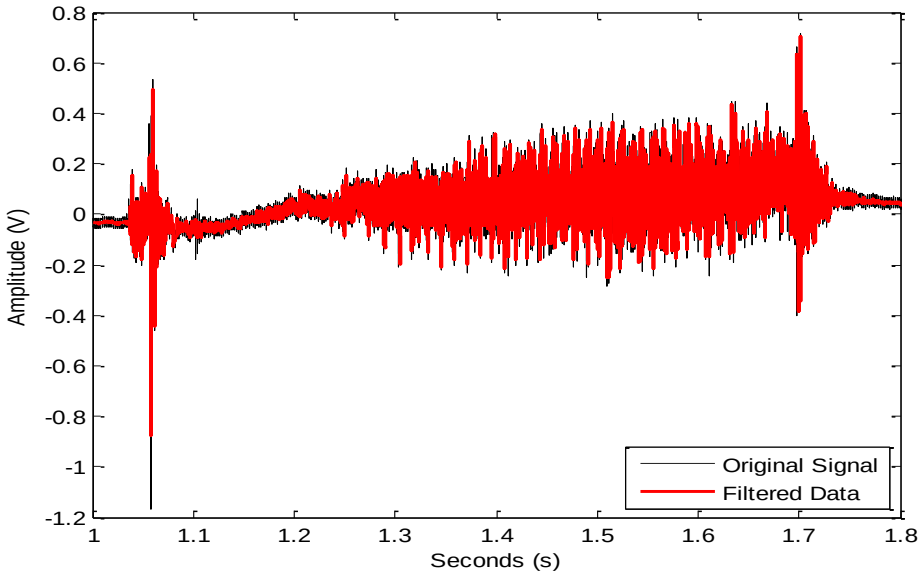

Figure 6-16: Texture D - Original and Filtered Signals for a whole length of data

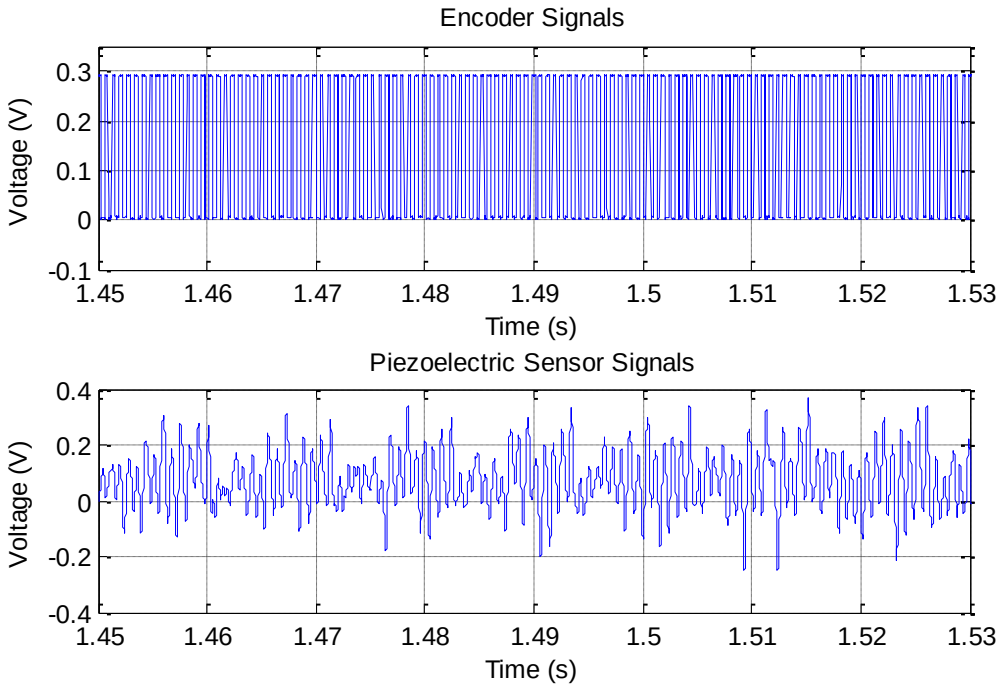

Figure 6-17: Texture D - Encoder and Piezoelectric Signals at selected sample length

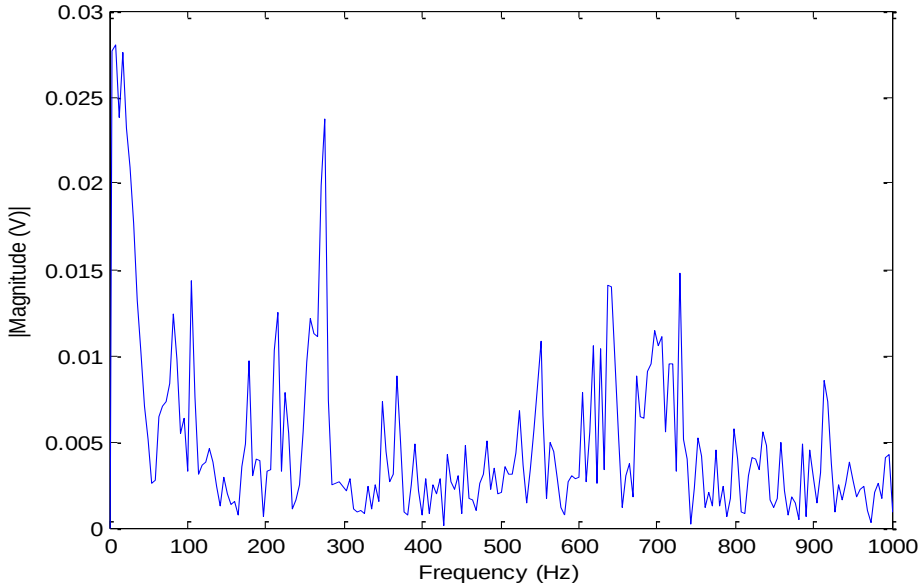

Figure 6-18: Texture D – FFT Output

For this texture, the expected frequencies were calculated first by dividing the measured widths with the measured velocity. With reference to the calculated expected frequencies, the obtained frequencies in the FFT plot were then selected to calculate the widths of the grooves and ridges. The observations for Texture D, recorded at velocity of 127.01 mm/s are as shown in Table 6-3 and Figure 6-19. For this sample of data, it was observed that the lowest and highest percentage differences were 0.221% and 8.721% respectively, which were considerably good as the percentage differences were less than 10%.

Table 6-3: Summary for one data sample of Texture D

	Measured Width (mm)	*Measured Velocity (mm/s)*	*Expected Frequency (Hz)*	*Obtained Frequency (Hz)*	*Calculated Width (mm)*	*Percentage difference (%)*
Ridge 1	0.180	127.01	702.7	697.5	0.1821	0.743
Groove 1	0.210	127.01	604.3	605.8	0.210	0.250
Ridge 2	0.194	127.01	654.4	637.9	0.199	2.590
Groove 2	0.412	127.01	308.2	307.5	0.413	0.221
Ridge 3	0.208	127.01	609.4	619.5	0.205	1.631
Groove 3	0.595	127.01	213.6	215.7	0.589	0.971
Ridge 4	0.212	127.01	600.4	605.8	0.210	0.895
Groove 4	0.777	127.01	163.3	179	0.710	8.721

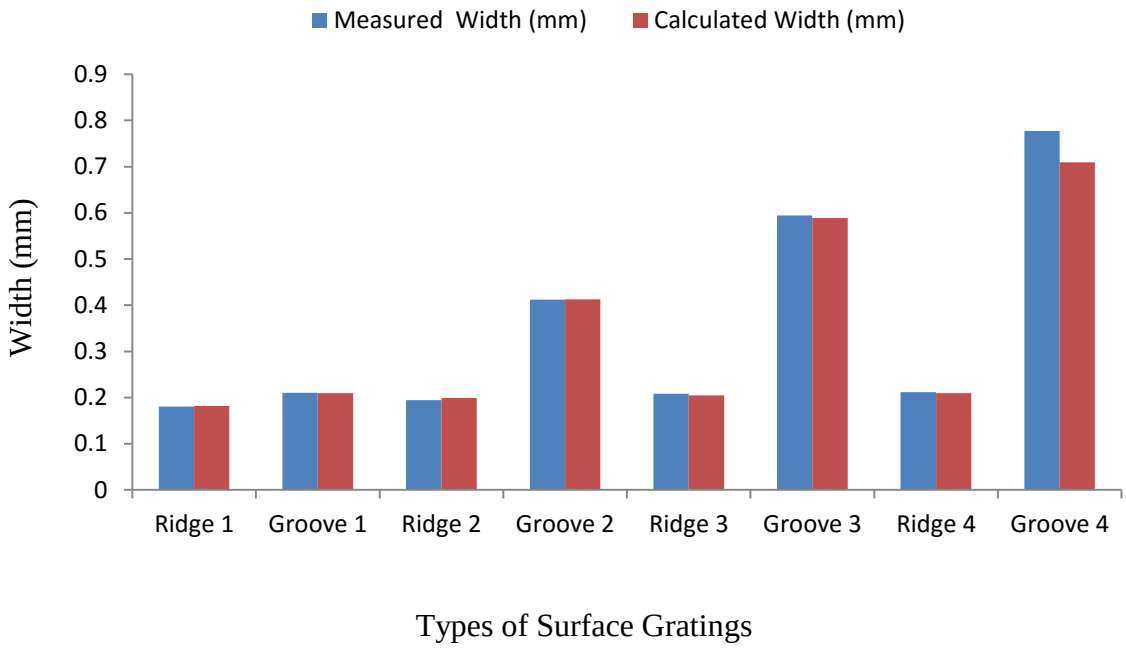

Figure 6-19: Grating widths differences between measured and calculated values

6.4 Data Processing in LabView

The data processing tasks have also been programmed in the LabView environment as well as Matlab® to enable the output vibration signals to be produced in real-time. Ideally, the prosthetic finger would gather signals from the surface textures, processes them to obtain information about the dominant frequencies and dimensions of the textures and translate this information into vibration signals that will be supplied to the residual arm. The MATLAB codes in filtering the input signals and calculating the FFT output as well as the corresponding gratings widths were transferred as a 'Mathscript' module in LabView from the Matlab® programs.

In the LabView environment, the voltage and encoder data previously gathered by the data acquisition board (NIDAQPad-6016) were fed into the Mathscript window. To reduce the processing time, the range of data was selected according to the time when the tube was moving at a constant speed. From the constant speed data, dominant frequencies were obtained and dimensions of the gratings were accurately calculated.

A graphical user interface (GUI) has also been designed to monitor the data processing tasks. This GUI allow users to select which data to be processed and can observe the output in terms of sampling frequency, velocity, FFT plots as well as the

calculated grating widths. The advantage of this GUI as compared to the previously obtained MATLAB output is that it could automatically and accurately pinpoint the peak values of the FFT by using the peak detector virtual instrument (VI) that is available in LabView. A threshold level was specified so that only peaks detected above the threshold level will be considered for grating widths calculation. Apart from that, the 'width' feature in the peak detector VI was utilized to restrict the number of consecutive data points to use in the quadratic least square fit. Ideally the 'width' should be the smallest possible so that only the highest peak within the neighbouring peaks is considered for the peak detection. For this application, the threshold level was set to be 70% of the highest detected peak with 'width' value of 3.

As the peaks could be automatically pinpointed, the grating widths of the surface textures also could be automatically displayed rather than having to manually locate the peak FFT values and calculate the grating widths. The GUI is applicable for different types of surface textures. Figure 6-20 shows the GUI for the acquisition and processing tasks of one sample for surface texture C.

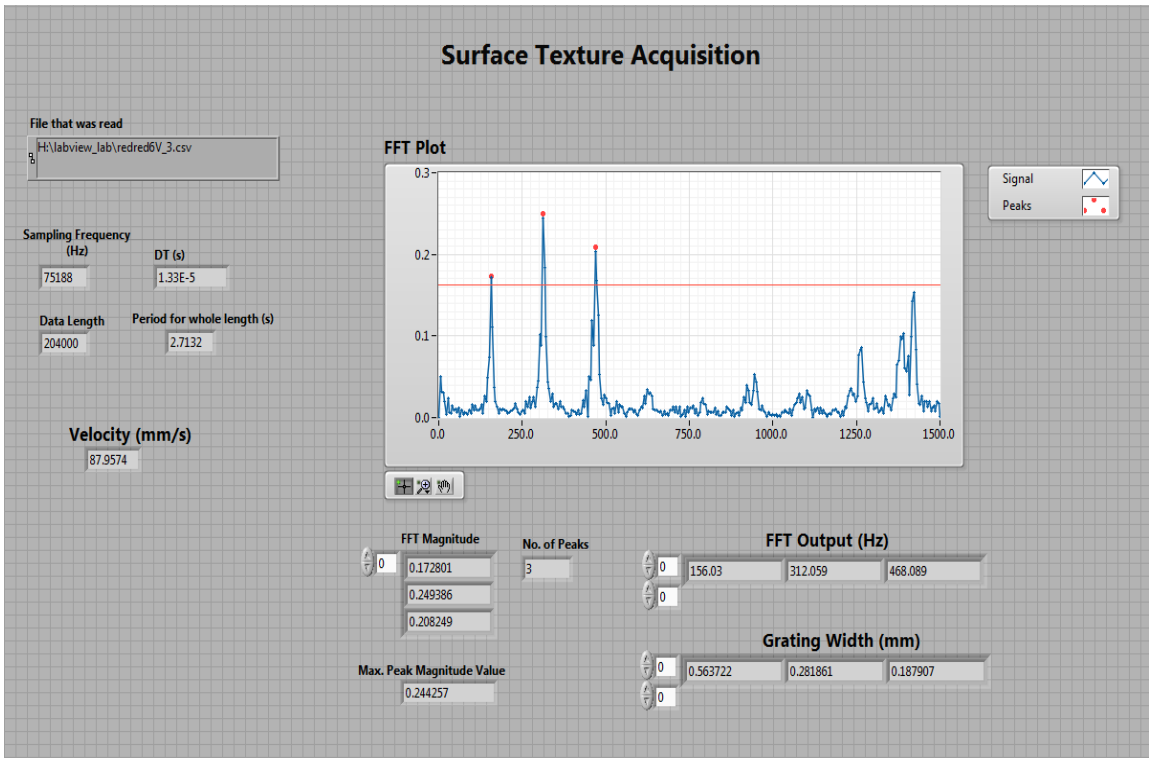

Figure 6-20: Graphical User Interface (GUI) for the surface texture acquisition and processing tasks

6.5 Discussion

This part of experiment has shown a significant improvement in sensing surface textures. In previous work [96], the capability of the artificial finger was limited to detecting the combination width of a ridge and a groove of the surface. By modifying the amplifier circuit configuration (as deliberated in the previous chapter), the sensitivity of the piezoelectric sensor has improved tremendously. At velocities ranging from very low to very high, the widths of every ridge and groove were repeatedly and successfully identified.

In most findings, it has been observed that the frequencies corresponding to the groove widths were more dominant (higher) than the frequencies corresponding to the widths of ridges. This implies that the piezoelectric sensor is more sensitive in detecting grooves than in detecting ridges. Physically, the contours in the surface gratings triggered the piezoelectric sensor to vibrate. A contour is detected at the instance when there is a change between the levels of the surface texture (between the ridge and the groove). This observation matches with the capability of human mechanoreceptors at the fingertips that could perceive roughness much better at a groove of a surface rather than at the ridge [20]. Psychophysics investigation by Lederman [103] showed that as the widths of a ridge is increased, the estimation of roughness becomes lower. This characteristic is observed with Texture C in which the percentage difference between the actual and measured width is larger as compared to other surface textures with narrower ridge widths.

As the frequencies obtained for the grooves were more dominant than the ridges, it made it feasible for surface with complex textures to be discriminated. Using the highest detected frequency peak as a reference point, a threshold value could be set so that frequency peaks detected above the threshold value will be deciphered as grooves. In Texture D for instance, the threshold level was set to be 80% of the highest detected peak. Therefore peaks detected below this level will be deciphered as ridges.

The occurrences of harmonics have been observed in Texture C when the experiment was repeated at other different velocities. This behaviour was very repeatable and the generated FFT plots produced exactly the same output patterns at different constant velocities. As shown in Figure 6-21, there were existences of second and third order harmonics for all four samples.

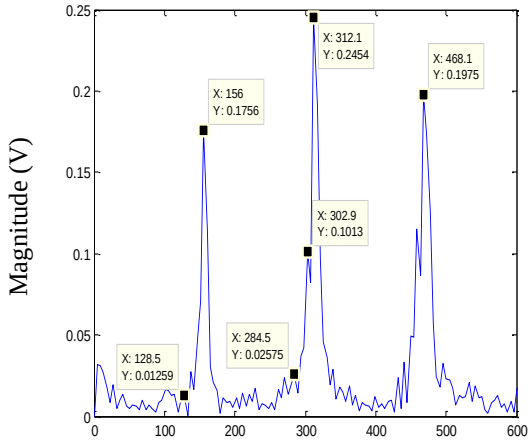

Sample 1: Velocity 87.63 mm/s

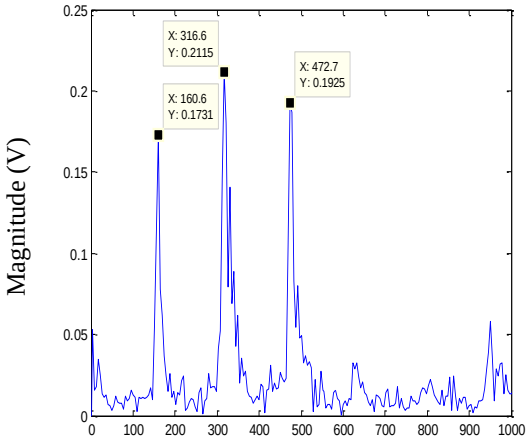

Sample 2: Velocity 90.53 mm/s

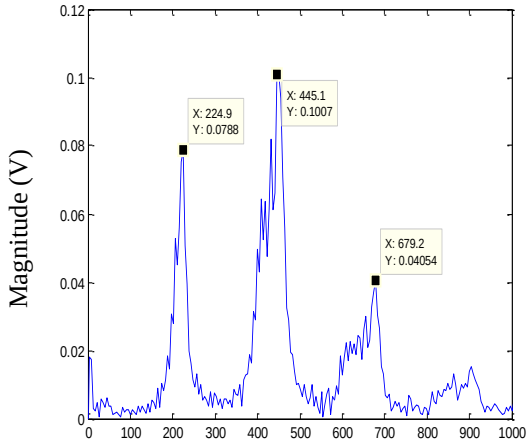

Sample 3: Velocity 121.32 mm/s

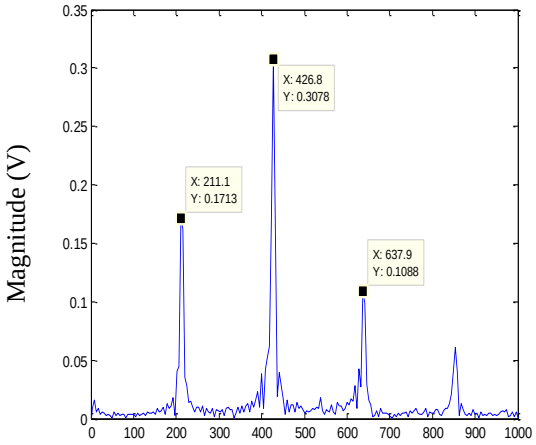

Sample 4: Velocity 119.8 mm/s

Figure 6-21: FFT Plots for four other different samples for Texture C. The X and Y labels on the plots indicate the values for frequencies and their magnitudes respectively.

As shown in Table 6-4, the ratio of the third frequency to the first frequency is 3, while the ratio of the third frequency to the second frequency is 2. The frequencies that are associated with the widths of grooves and ridges of Texture C were also identified; however these frequencies were not the dominant frequencies. The exact same patterns produced at different velocities is a distinct indicator of Texture C, however further investigation is required to establish the findings about the occurrences of the harmonic frequencies. At this stage, although the percentage difference between the measured

and calculated widths, particularly for the ridge is considerably large, it is believed that the texture has been represented by the FFT output. Therefore the obtained information has been carried forward in generating vibration pattern associated with this texture which will be explained in the next chapter.

Table 6-4: Surface Texture C – Frequency ratios

	Frequency 1, f_1 (Hz)	*Frequency 2, f_2 (Hz)*	*Frequency 3, f_3 (Hz)*	*f3/f1*	*f2/f1*
Sample 1	156	312.1	468.1	3.0006	2.0006
Sample 2	160.6	316.6	472.7	2.9433	1.9714
Sample 3	224.9	445.1	679.1	3.020	1.980
Sample 4	211.1	426.8	637.9	3.022	2.022

Although the grating widths could be detected at different ranges of velocity, the artificial finger gave the clearest output when the velocity was between 90 mm/s to 130 mm/s. This was when the generated FFT frequencies corresponding to the grating widths were the dominant frequencies. This may be due to the condition of the track that causes lesser surface contact between the texture and the sensor when the sliding block was at lower velocities. This could also possibly be the optimum velocity range for the piezoelectric sensor, which is also well within the capability range of a human finger. A person can still discriminate surface texture at a speed of up to 207.3 mm/s for grating widths greater than 500 μm [104]. This finding is also similar as with the previous work [96] in which dominant frequencies associated to the grating widths were observed at velocities above 90 mm/s.

The existence of a low frequency component (4.589 Hz) in every surface, including the smooth surface, was possibly due to external factors. The cause of a low frequency ‘noise’ could be many and varied, such as a low hum generated by plant in the infrastructure of a building. This low frequency noise may also likely due to the noise produced by the moving block. This identified low frequency component has been filtered out and not considered in calculating the dimensions of the surface textures.

To ensure that the sensor system provided acceptable output signals, it was highly important that the sliding block moved at a constant velocity. The dominant frequency signals from the FFT analysis could be observed much more clearly when the block was moving in a constant speed rather than during acceleration or deceleration (as shown in Figure 6-22). The widths of the ridges and grooves of the texture were then calculated with the calculated dominant frequency signals at the constant velocity. Apart from that, if the velocity is varying slowly, rather than a spike in the FFT plot, there would other frequency components spread around the dominant frequency.

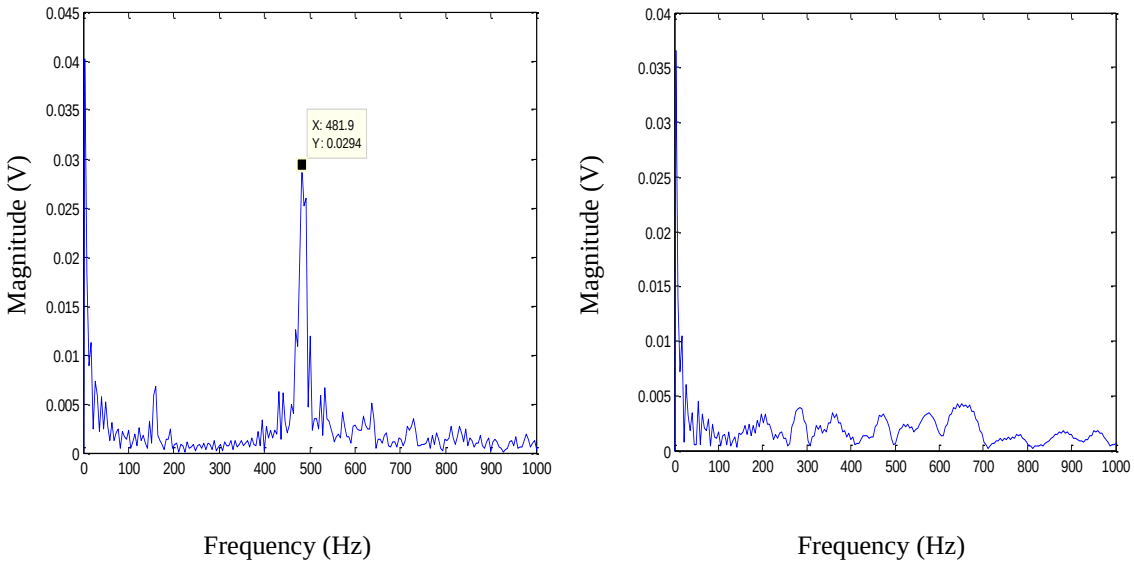

Figure 6-22: FFT outputs when the block moving in constant velocity (left) and during varying velocity (right) for the same surface texture (Texture B)

The information about the velocity of the block was gathered from the encoder signals and further analysed in MATLAB to identify the regions of constant velocity. As the sensor data during the time the velocity is constant had to be selected manually, it hindered further processing of the data to be analysed in the real-time environment. The 'Producer – Consumer Virtual Instrument (VI)' in LabView could be utilized in selecting the constant velocity data automatically, however this increased the processing time as the whole length of the signals (up to 200 000 samples) had to be analysed before being able to locate the constant velocity.

One way to ensure the block moves at a constant velocity was to minimize the friction at every part of the rig that has direct influence in moving the block. The previously fitted nylon bolts at the left and bottom sides of the sliding block were

checked and replaced. The top of the block were also be tightly anchored to avoid instability. The unstable block will slightly shift the block away from its designated track that will result in inconsistency in velocity. Furthermore this will also lead to less surface contact between the sensor and the texture under investigation and drastically affect the signal readings.

Although these measures have been implemented, the block still experienced variation in velocities and require post-processing analysis in MATLAB/LabView to locate the constant velocity. Therefore to overcome this selection complexity, the test rig may be further modified to achieve a constant sliding speed throughout the acquisition process. A PID controller may be utilized to drive the block to the targeted velocity and maintain its speed before it stops [105].

In a practical point of view, it may not be feasible for a prosthetic hand user to maintain a constant speed when exploring a surface texture. A way to address this situation is by training the users to slide the prosthetic finger at a constant speed. This may make the device to feel less natural at first. However, as with other types of prosthetic devices, after a lot of practices, the users will learn the process and the task should become easier and feels more natural.

Another way to tackle this issue is by using a different calculation method that does not rely on FFT analysis to identify the surface textures. This is because the dominant frequency obtained from the FFT analysis could only be achieved at constant velocities. Works by Song showed that surface textures could be classified using its friction properties when the artificial finger was moving at a low acceleration [54]. The technique however, is beyond the scope of this research, and could be considered as a recommendation for future work.

6.6 Summary

This chapter showed that the artificial fingertip is able to accurately determine the widths of every groove and ridge of a surface texture at different velocities. Voltage signals were gathered and analysed from four different surface textures. The dominant frequencies from the FFT analysis as well as the velocity information obtained from the encoder signal were used in calculating the dimensions of the surface texture. These findings are a stepping stone in providing supplementary sensations to the human residual arm, which will be the highlight of the next chapter. This part of research work

has been presented and published at a conference technically co-sponsored by the IEEE Engineering in Medicine and Biology Society [106]. Some part of this paper also has been produced in the IET Journal of Science, Measurement & Technology [102].

Chapter 7 Integration of Surface Texture with Haptic Actuator

This part of research work concentrated on interfacing the information gathered from the piezoelectric sensor of the artificial hand and the surface texture to create a vibration sensation to be felt on the residual arm. This was done by processing the gathered information in the LabView environment and outputting signals to hardware that could generate the associated vibration stimuli.

The overall experimental set up for this integration stage is as shown in the following block diagram (Figure 7-1). Selected post-processed data from MATLAB that have shown reliable outputs in associating the FFT dominant frequency with the widths of surface gratings were fed into LabView. The ‘on’ and ‘off’ pulses were then generated in the LabView environment to represent the surface textures. The signals were later channelled to a data acquisition board, a high voltage isolator and a buffer circuit before becoming input signals to the haptic actuator (motor). The motor will rotate according to the ‘on’ and ‘off’ signals and produce the associated vibration patterns.

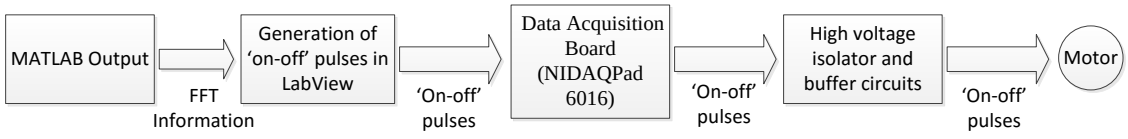

Figure 7-1: Block diagram for the integration stage

7.1 Signal Manipulation

As the surface textures under investigation were repetition of regular patterns, ‘on’ and ‘off’ signal pulses were used to closely represent the textures. ‘On’ pulses meant that a steady voltage signal was supplied to the vibration motor to mimic the ridge of the surface while the ‘off’ pulses meant that the voltage signal was cut off (or paused), to represent the groove of the surface texture. The on-off pulses are an effective method in perceiving “smooth” or “rough” sensations. A constant speed of vibration is associated to a “smooth” sensation, while short pulses is associated with “rough” sensations [25].

The voltage to be supplied to the haptic device should provide a vibration frequency of 250 Hz as this is the optimum frequency for mechanoreceptors in the residual arm [45]. From the previous findings, the motor was able to provide a 250 Hz frequency of vibration when the voltage supplied to the motor was 2V (Figure 4-9). Therefore input signals were manipulated to provide a constant 2V supply for ‘on’ pulses and 0V for ‘off’ pulses.

The durations of the ‘on-off’ pulses were calculated by taking the reciprocal of the dominant frequencies, F, which have been verified to estimate the width of grooves and ridges of the surface texture. The calculated values of the duration were scaled according to the transient response of the motor. The duration should be within the capability of the motor as a very short duration will not allow ample time for the motor to be fully in rotation or in braking mode. According to the motor datasheet (Appendix A), the typical lag, rise and stop time for the motor are 16 milliseconds, 28 milliseconds and 36 milliseconds respectively. Therefore an additional 80 milliseconds is required per one haptic event, or per ‘on’ and ‘off’ pulses. The durations of the ‘on-off’ pulses should also not be too long as it may cause discomfort to the users. As reported by Kaaresoja [50], stimuli longer than 200 milliseconds is considered as annoying.

7.1.1 Texture A (Smooth surface)

A smooth sensation could be created by using constant vibration [25] [66]. Therefore to mimic the sensation felt by a bare finger when exploring a smooth surface, a continuous voltage supply of 2 V was utilized to generate the vibration. To match with the duration it takes for other types of texture (for the psychophysical

investigation, which will be explained in the next chapter), the period for the smooth vibration sensation was set as 2000 milliseconds.

7.1.2 Texture B (Repeating patterns of similar widths of grooves and ridges)

The FFT analysis for texture B showed only one dominant frequency (Figure 6-10). This is because the texture has grooves and ridges of the same widths. To recreate the sensation of this texture, the same dominant frequency was used to represent both ridges and grooves. A constant 2 V voltage supply was set for of 500 milliseconds to represent the ridge of the surface and the supply voltage will be cut off for another 500 milliseconds to represent the groove of the surface. The ‘on’ and 'off' pulses can be repeated in a user-defined number of cycles.

7.1.3 Texture C (Repeating patterns of different widths of ridges and grooves)

The two most dominant frequencies (Figure 6-14) were manipulated in representing this texture. From previous findings in Chapter 7, the frequencies associated with the width of the groove were more dominant than the frequency associated with the width of ridges. Therefore the most dominant frequency between the two was selected to represent the groove while the less dominant, to represent the ridge. The approximated durations were 1000 milliseconds and 500 milliseconds for the ridge and groove respectively. This meant that 2 V input voltage will be supplied for 1000 milliseconds to represent the ridge and will be paused for 500 milliseconds to represent the groove.

7.1.4 Texture D (Repeating patterns of increasing widths of grooves and constant widths of ridges)

Texture D has patterns of grooves increasing in width in 0.2 mm step sizes up until 0.8 mm (four-fold) (Figure 6-1). The FFT analysis for this texture gave multiple dominant frequencies (Figure 6-18). With reference to the previous findings, the highest four dominant frequencies were associated with the grooves while the lower four frequencies as the ridges. The approximate duration for the on and off pulses to represent the widths of grooves and ridges are as tabulated in Table 7-1.

Table 7-1: Descriptions of the vibration patterns and their associated surface textures

Vibration Pattern	Descriptions	Associated Texture
Pattern A	Continuous vibration (2000 millisecond)	Texture A
Pattern B	Repeated 500 millisecond* pulses with 500 millisecond* pauses in between	Texture B
Pattern C	Repeated 1000 millisecond* pulses with 500 millisecond* pauses in between	Texture C
Pattern D	Repeated 250 millisecond* pulses with 250 millisecond* pause in between, then 250 millisecond* pulses with 500 millisecond pause in between, then 250 millisecond* pulses with 750 millisecond* pauses in between, and finally 250 millisecond* pulses with 1000 millisecond* pauses in between	Texture D

*Approximate duration

7.2 Configuration with LabView and Data Acquisition Board

The durations, sequence and the number of cycles of the 'on' and 'off' pulses for all four surface textures were programmed in LabView. For ease of psychophysical investigation at the later stage, the LabView programs for all four surface textures were done in separate block diagrams. The programs were done according to a generic flow chart, as shown in Figure 7-2.

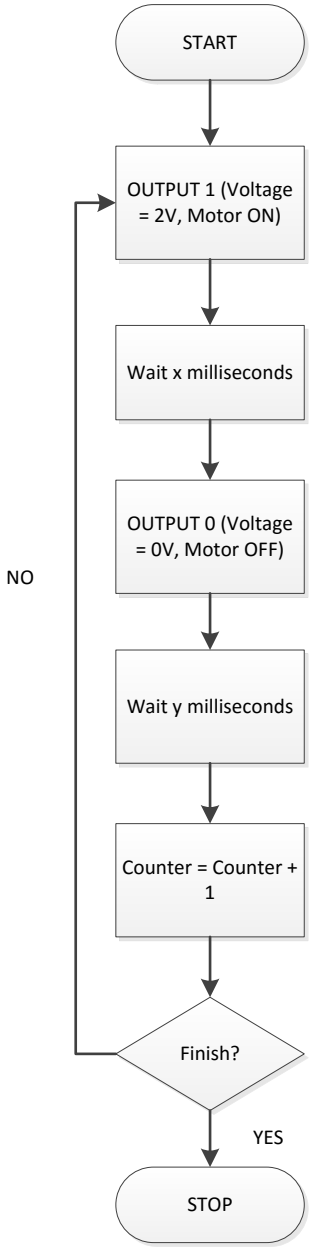

Figure 7-2: Generic flowchart for on and off states in LabView

The programs started when the 'Run' button was pressed. The data acquisition tasks were configured and provided 2 V input to the motor. The motor will continue to run at the defined amount of time (x milliseconds). Once the period has lapsed, the voltage will be switched to 0 V, which will turn the motor off. This condition remained until the next predefined amount of time (y milliseconds). The counter value will be increased and proceed to repeat the process if it has not reached the user defined number of cycles. The program will stop its execution once the counter has reached its defined value or when a stop button is activated.

As two states (ON and OFF) were involved, the state machine virtual instrument was utilized in this program. The duration for the on and off states were dependent on

the dominant frequencies while the repetitions of the vibration patterns were implemented using a counter. The number of cycles was user defined and could be controlled at the front panel of the LabView. An example of front panel and block diagram for Pattern B are as shown in Figure 7-3 and Figure 7-4 respectively. The blocks in the flow chart of the LabView front panel will blink according to the stages of the process.

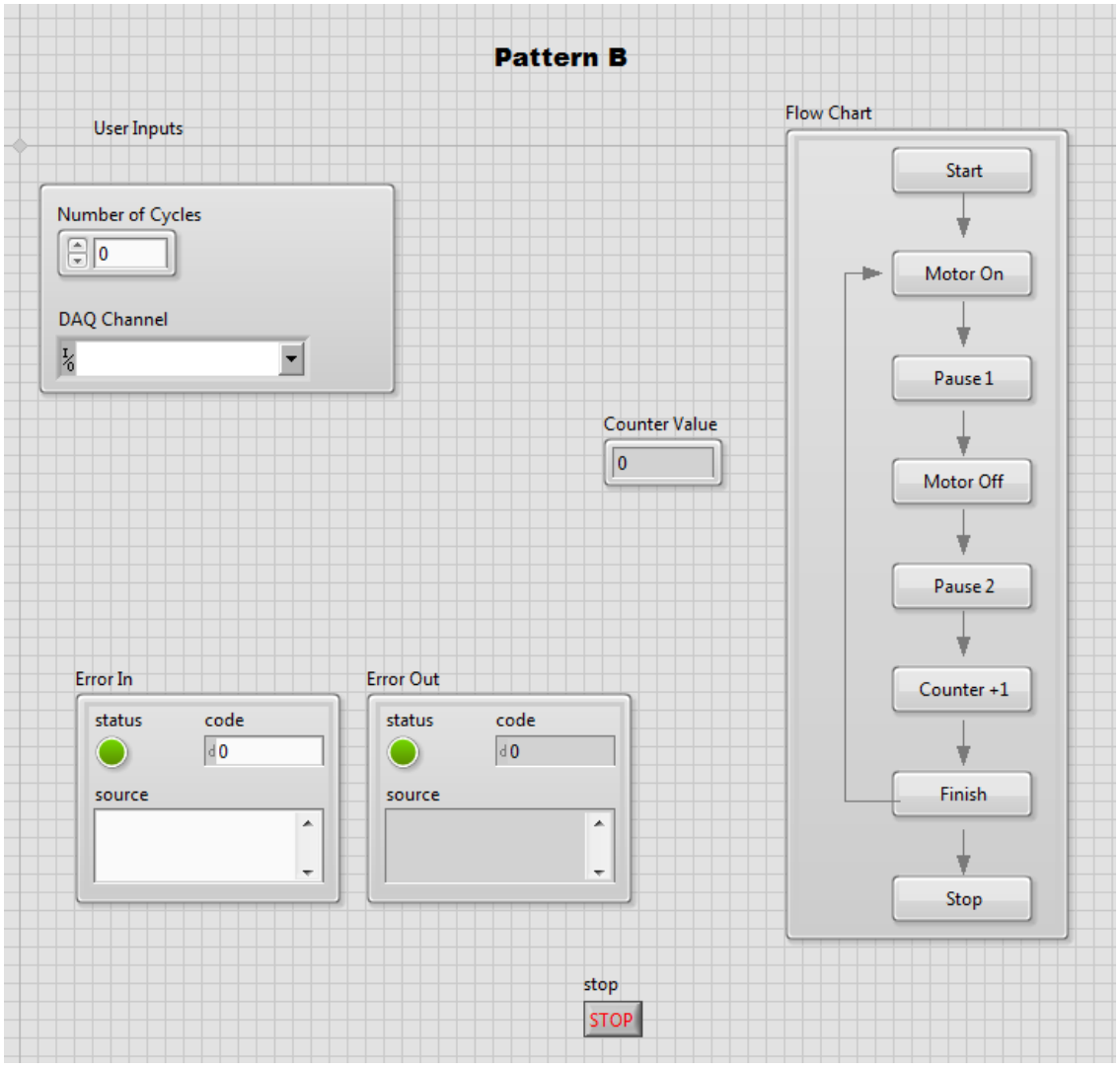

Figure 7-3: Example of a LabView front panel (Pattern B)

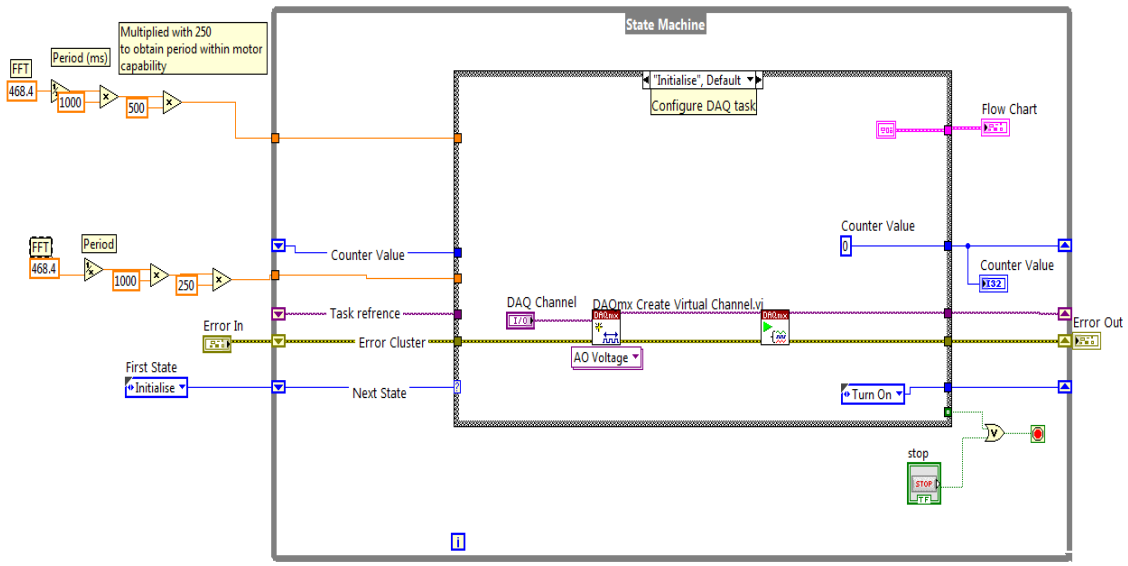

Figure 7-4: Example of a LabView block diagram (Pattern B)

A data acquisition board (NIDAQPad-6016) was used to channel the pulses out to the motor in generating the associated vibration patterns. To execute the LabView program, the output terminals of the data acquisition board (AO 0 and AO GND) have to be wired accordingly. For observation purposes, both terminals were first wired to the input and ground probes of an oscilloscope.

To interface between the software (programming) and the hardware (motor circuitry), a virtual channel had to be defined in the LabView environment. The virtual channel specified the output terminals that have been wired. To ensure a more flexible control of the output, the DAQmx virtual instruments were used instead of the DAQ Assistant which was used during the previous data acquisition (to gather information about the surface texture). The DAQmx virtual instruments include the 'DAQmx Create Virtual Channel' and 'DAQmx Start Task' for initialization purpose, 'DAQmx Write' to save data during the on and off states and 'DAQmx Stop Task' and 'DAQmx Clear Task' to halt the process and clear data.

7.3 Hardware Configuration

The output pulses from LabView became the input signals to the motor circuitry in generating vibration output. The voltage output that could be supplied from the data acquisition board was ±10 V with a ±5 mA maximum current drive [97]. The voltage requirement to obtain the 250 Hz frequency of vibration from the motor was 2 V which

was within the supply range of the data acquisition board. However the output current was not sufficient as the typical operating current of the motor needed is 50 mA. Furthermore, for a precautionary measure, the data acquisition board needed to be protected from any reverse currents that may damage the board. Also, as the motor will be attached on human arm, it was pertinent that the device should be isolated from the mains supply. Therefore a circuit was specifically built to amplify the current supply, protect the data acquisition board and isolate the motor from the mains supply.

7.3.1 Buffer circuit

This circuit was built as a buffer between the motor circuitry and the data acquisition board. The output current supply from the data acquisition board was also amplified at this stage. The circuit is as shown in Figure 7-5.

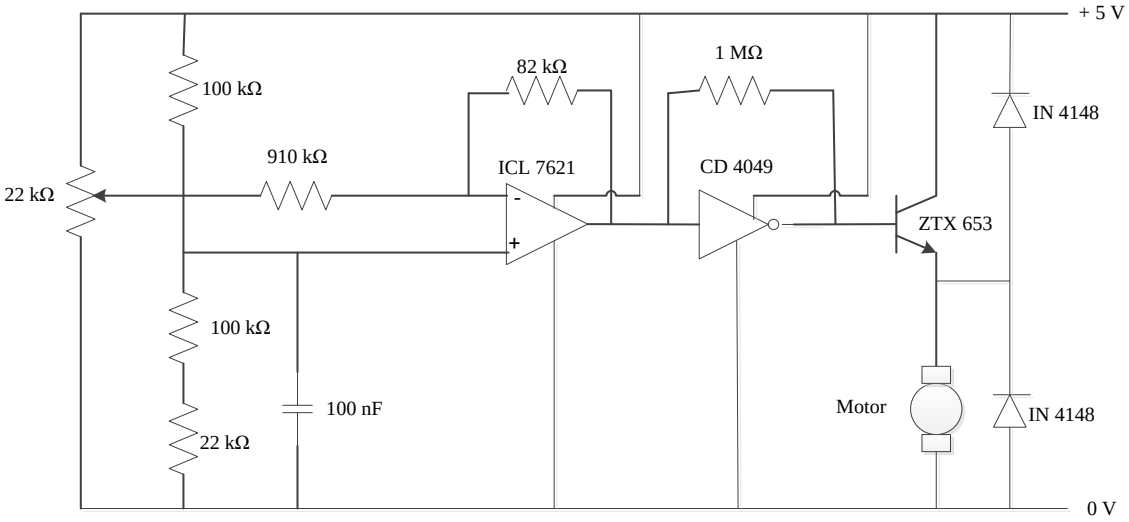

Figure 7-5: Buffer circuit between the DAQ board and the motor circuitry

In the initial construction and testing of the buffer circuit, the motor was represented by three 100 Ω resistors, positioned in parallel, at the emitter junction of the transistor. This was done to avoid the possibility of damage to the motor during testing. The parallel resistor resulted in 33.3 Ω across the output, which was the typical maximum terminal resistance of the motor.

A 22 kΩ potentiometer was used to adjust the input voltage from 0V to 5V. The input voltage and the voltage across the parallel resistors were measured and the relationship equation between both variables was obtained. This was done to determine the right input voltage in order to output 2 V across the motor, which could generate the desired 250 Hz frequency of vibration.

The gain of the inverting op-amp was set to attenuate the signal (in this case, 0.09) to minimize the sensitivity of the output voltage with respect to the changes in the input voltage. The values of the bias resistors (100kΩ) set the operating point of the amplifier at half of the supply voltage. This was done to enable a single supply rail to be utilised between 0 to 5 V, with a midpoint at 2.5 V. A 100 nF decoupling capacitor was included to reduce any noise that may present from the power supply.

The inverting buffer (CD 4049) was set in its linear region using a 1MΩ feedback resistor to act as a simple high input linear amplifier. Diodes were added in the circuit to provide a return path for the motor current during turn off to protect the motor and transistor from over voltage The plot between the input voltage (voltage across potentiometer to ground) and the output voltage (voltage across the parallel resistors / motor) is shown in Figure 7-6.

Over the full voltage range the circuit has a nonlinear characteristic. However it has a linear part in the mid-range of input voltages. The position of the linear region can be adjusted by changing the voltage at the non-inverting input to the op-amp. The 22 kΩ resistor was inserted to slightly increase the voltage at the op-amp input. Increasing this voltage has the effect of moving the linear region to the left in the plot.

From an analysis of the data in this centre region, the input voltage to the buffer circuit required to obtain a 2 V output is 2.45 V.

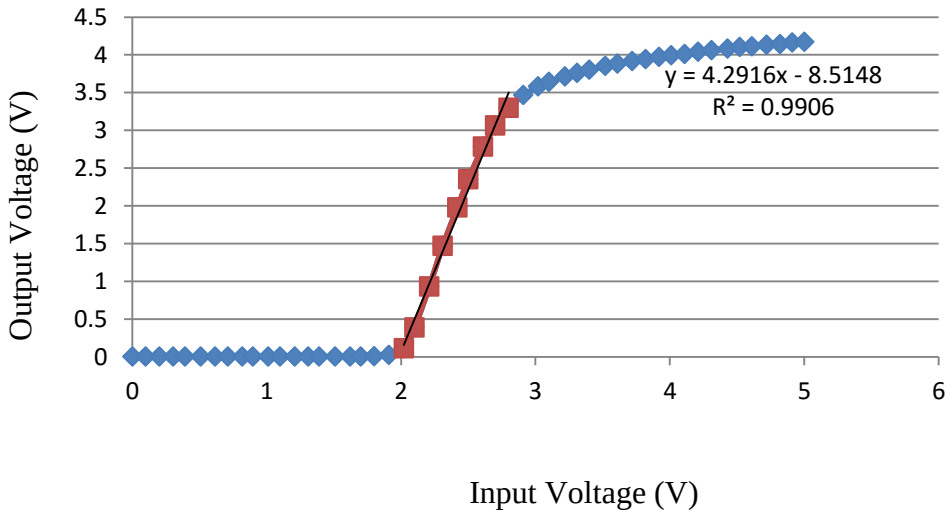

Figure 7-6: Transfer characteristic between the input and output voltages in the centre region of the characteristic

7.3.2 High voltage isolator and battery operated circuit

A 9V PP3 battery with a capacity of 550 mAh was chosen to power the system. To ensure that the supply voltage to the circuit maintained at 5V, a 5V voltage regulator was added into the circuit. A low current LED was also used to indicate when the battery switch was on or off. Figure 7-7 show the integration between the DAQ board with the high voltage isolator, battery, regulator and the buffer circuit. The output from the buffer circuit will be the input to the motor.

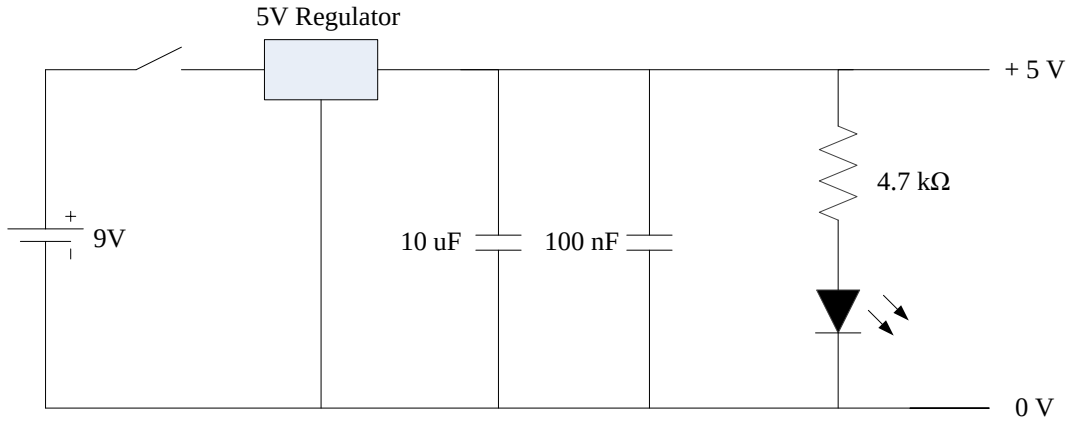

Figure 7-7: Battery and regulator circuit

As the vibration motor will be mounted on a human arm, it was an essential measure that the circuit that powers the motor is isolated from the mains supply. Therefore apart from having the vibration circuit battery operated, signals from the data acquisition board should be provided to the motor using an optically coupled isolator, instead of normal wiring. The selected high voltage isolator for this circuit was OPI1268 which consists of a photodiode that optically detects incoming input and converts it to a proportionate current This device has a 16kV isolation voltage and in the data sheet from the manufacture it is stated that one of its applications is for “medical equipment power isolation”.

Figure 7-8 shows the connection between the DAQ board to the isolator and the buffer circuit. The input pulses from the DAQ will be fed into the isolator circuit. To avoid reverse currents that could potentially damage the DAQ board, a diode was also included at the input to the circuit. The output from the isolator was connected to the input of an inverter and then to the 22 kΩ potentiometer of the buffer circuit which will in turn power the motor.

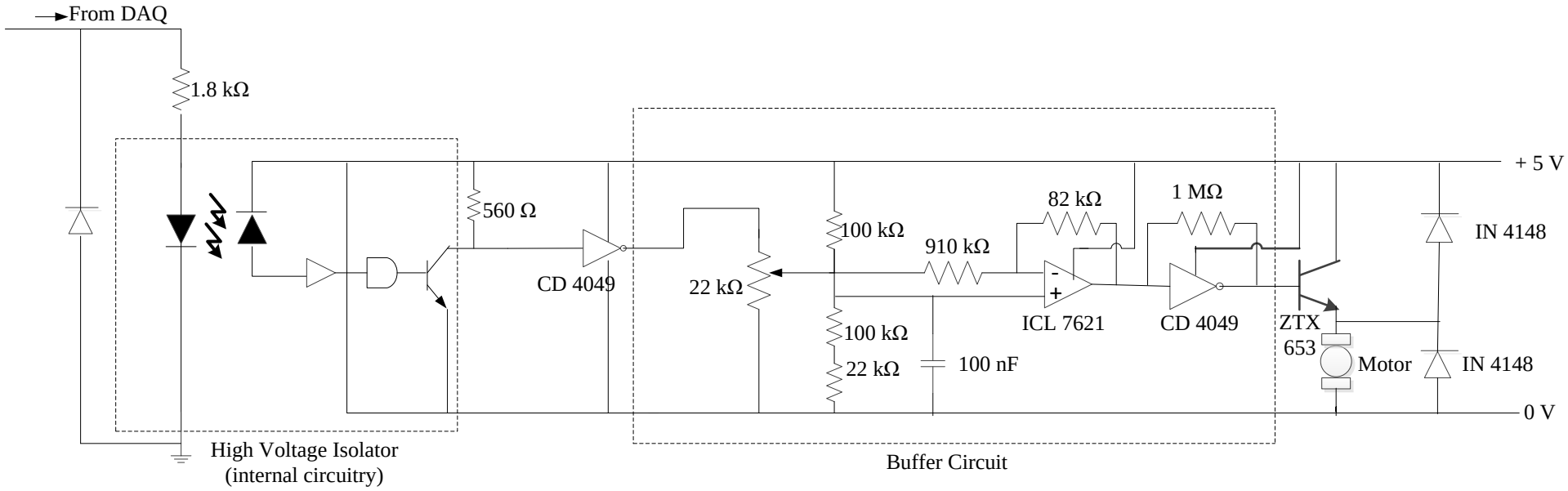

Figure 7-8: Connection between the DAQ, high voltage isolator and the buffer circuit

7.3.3 Output signals

The input signals from the DAQ board were tested to see its capability in producing similar signals as programmed in the LabView environment. The signals were the four vibration patterns designed according to the acquired information of the surface textures. A digital oscilloscope was used to measure the signals received from the DAQ board through the interface circuit. This was done by connecting the oscilloscope probes across the parallel resistors that represents the motor. The output plots for all four vibration patterns are as shown in Figure 7-9.

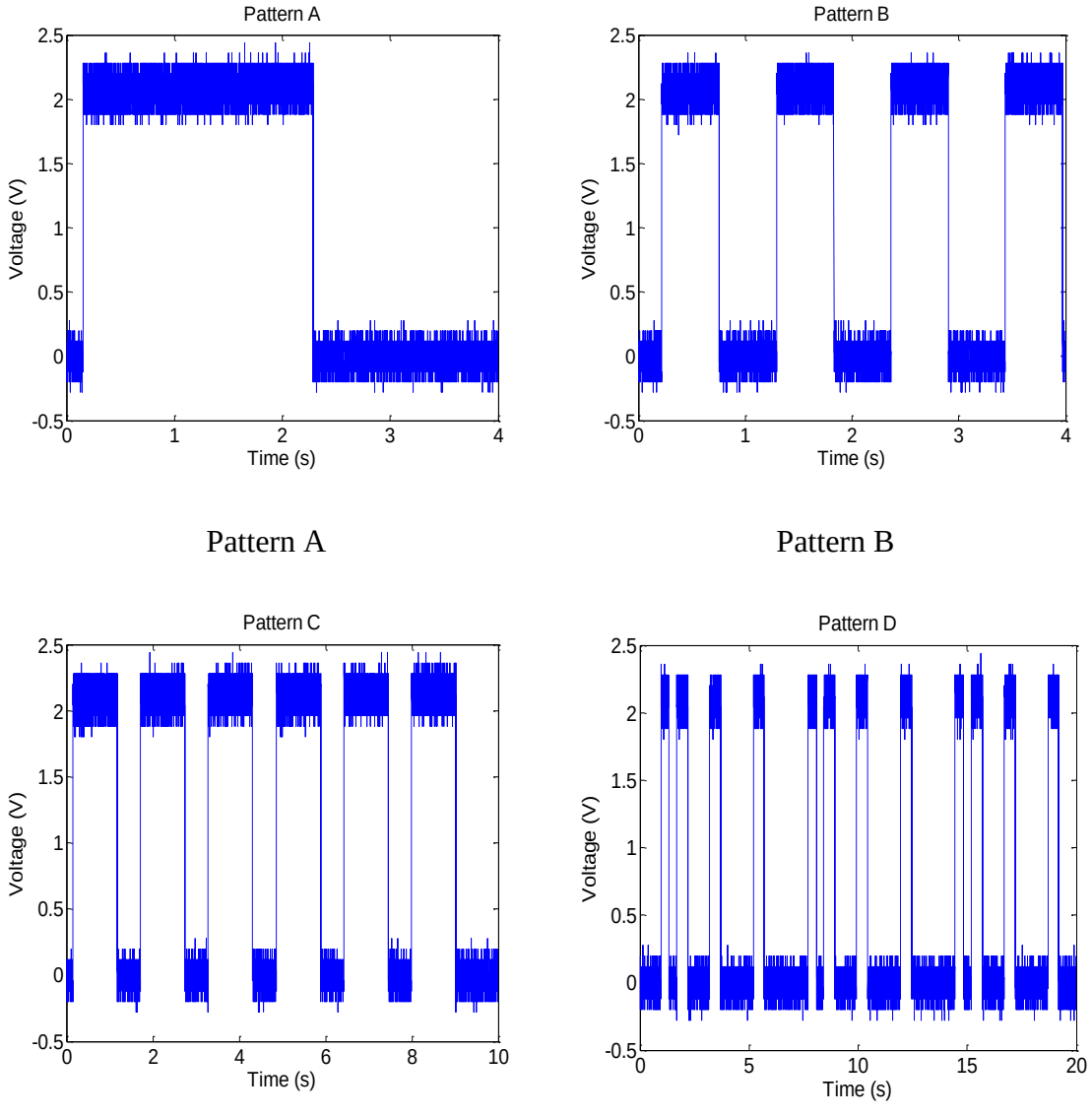

Figure 7-9: Output plots for the vibration patterns A, B, C and D measured across the parallel resistors

The vibration patterns shown in Figure 7-9 were on-off pulses without connection to the motor. 2 V input was set to create the 'on' pulses while 0 V was fixed for the 'off' pulses. Pattern A represents the smooth surface texture (Texture A). The constant 2 V input was set for a duration of 2 seconds (2000 milliseconds) before being switched off to provide a sensation when sliding a finger across a smooth surface. Pattern B showed the DAQ output in representing repeating textures (four cycles) of similar groove and ridge widths (Texture B). The period for both 'on' and 'off' pulses were set to be equal, which was 0.5 seconds (500 milliseconds). The output plot observed for Pattern C show the 'on' (1000 milliseconds) and 'off' (500 milliseconds) pulses repeated for six cycles in representing Texture C. Pattern D showed a repetition of three cycles of Texture D, which consisted of repeating patterns of increasing widths of grooves and constant widths of ridges.

The expanded version of the output plot across the parallel resistors is shown in Figure 7-10. From the plot, the occurrences of high frequency noise which may be due to external factors could be observed. The solid red line represents the mean of the voltage signal level at 2.07 V. No attempt was done to smooth the signal. The averaging was done to verify that the software was able to produce the 'on' and 'off' signals at a given voltage set by the potentiometer. The observed high frequency noise across the dummy resistors will not be picked up by the DC motor.

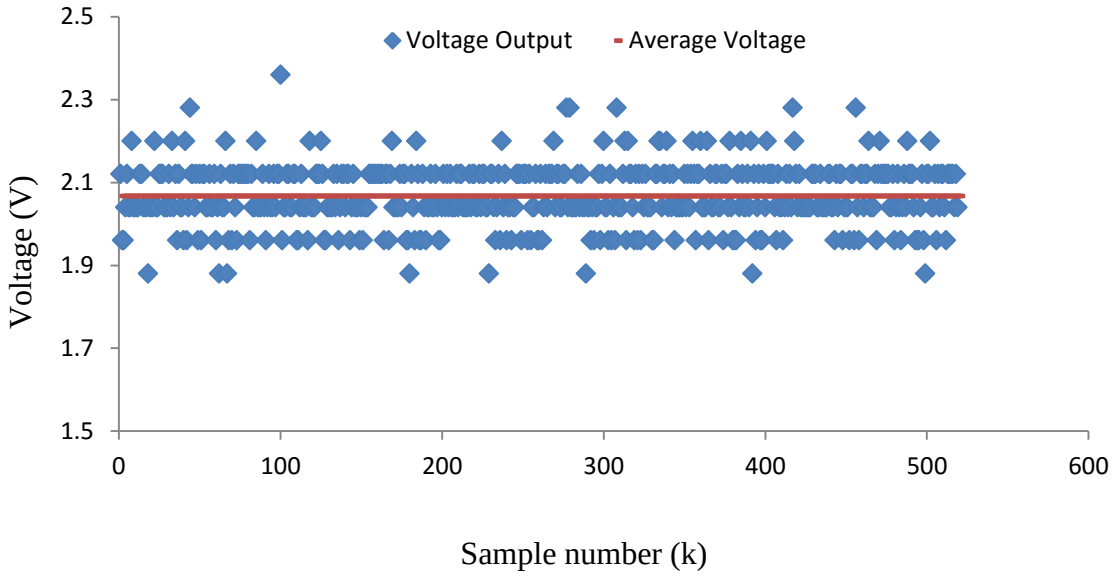

Figure 7-10: Expanded version of the DAQ signals through the interface circuit

As Figure 7-9 shows that the DAQ board can supply the output signals according to the ones programmed in the LabView environment, the vibration motor was

integrated with the complete circuit. From previous findings, the input to the buffer circuit was set at 2.45 V by adjusting the 22 kΩ potentiometer to rotate the motor at 2 V, which should achieve the 250 Hz frequency of vibration. The motor was mounted on an accelerometer, and the accelerations as well as the dominant frequencies were measured for all four vibration patterns. The output plots for the x-axis for all four patterns are shown in Figure 7-11. The overall output plots (more than one cycle in x,y and z-axis) are in Appendix H.

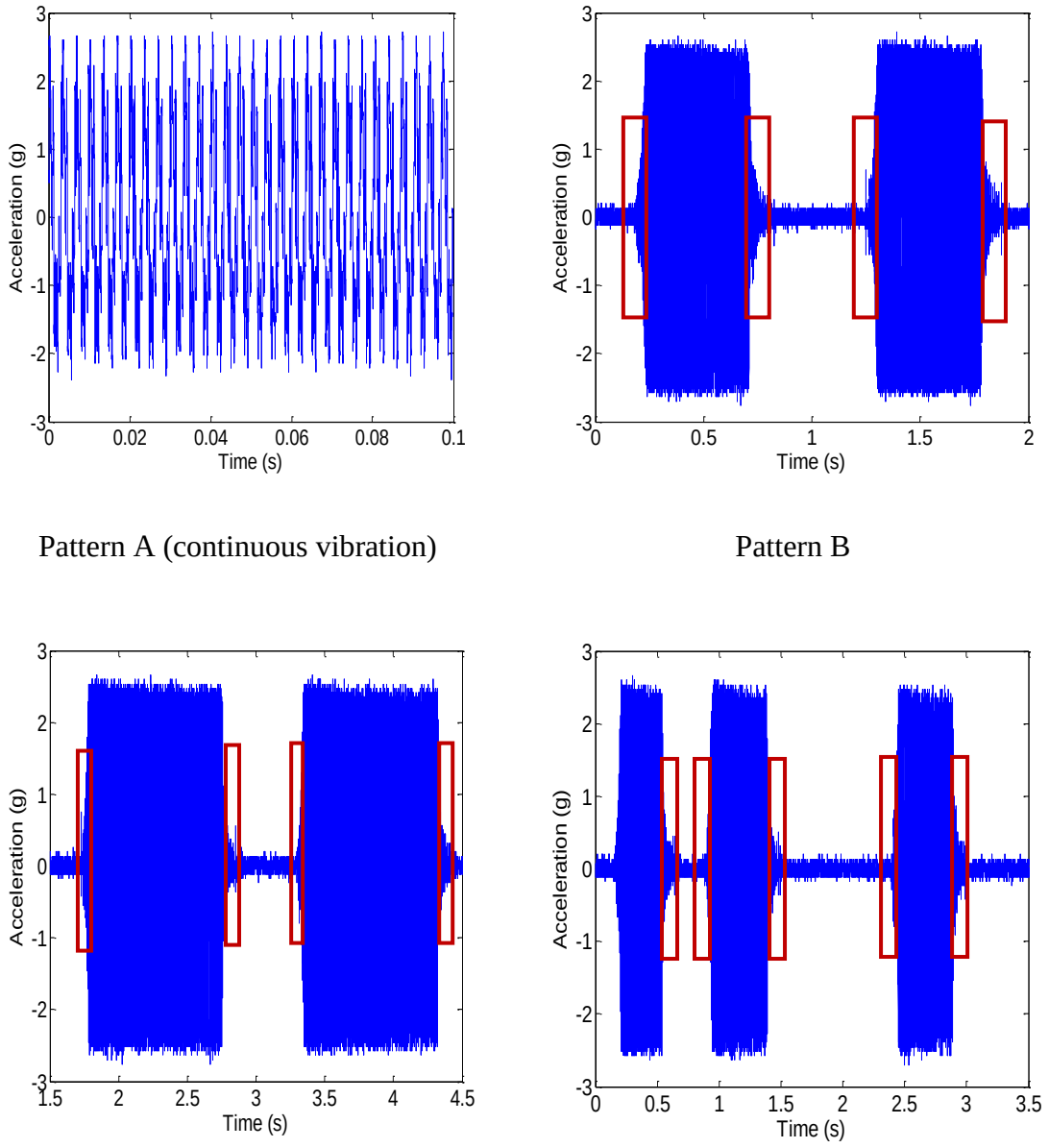

Pattern A (continuous vibration)

Pattern B

Pattern C

Pattern D

Figure 7-11: Acceleration in x-axis direction for all four patterns. The red boxes show the rise and stop period when the motor was running according to the 'on' and 'off' pulses

The plots in Figure 7-11 showed that the vibration patterns could be generated according to the 'on-off' pulses from the LabView. A further analysis was done to check the transient responses of the motor when subjected to the 'on-off' pulses (shown in Figure 7-13 and Figure 7-13). From the motor datasheet, the typical time it took for the motor to reach steady state from no rotation moment to full speed was 40 milliseconds. The typical stop time for the motor is 36 milliseconds. Table 7-2 show the mean transient response for the vibration patterns. These transient responses, due to the starting and braking of the motor have been anticipated. Therefore to ensure sufficient vibration could be perceived at the upper arm, 80 milliseconds were added for every duration of the 'on' and 'off' pulses to counter the time losses during the state transitions.

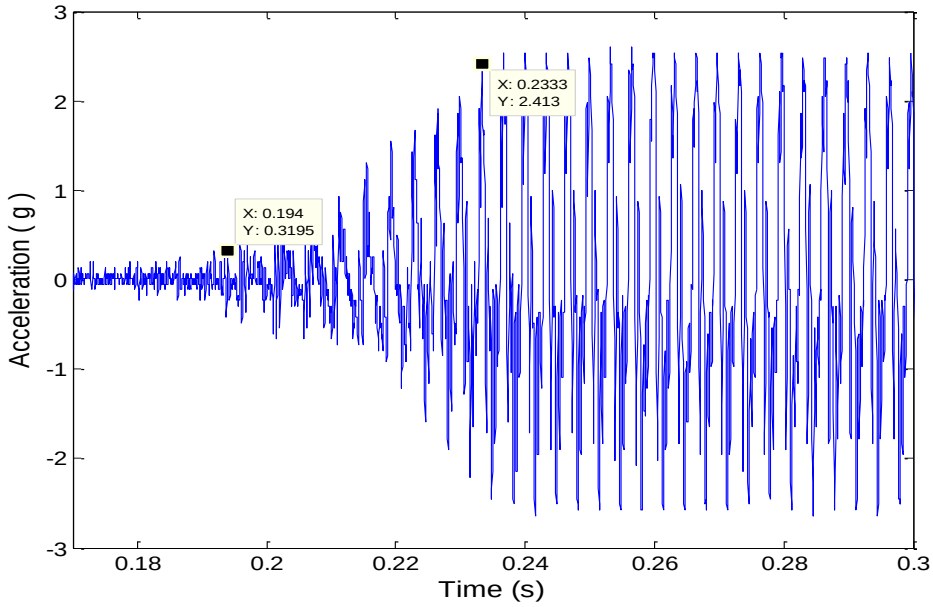

Figure 7-12: Typical rise time for the motor during the 'on' pulses

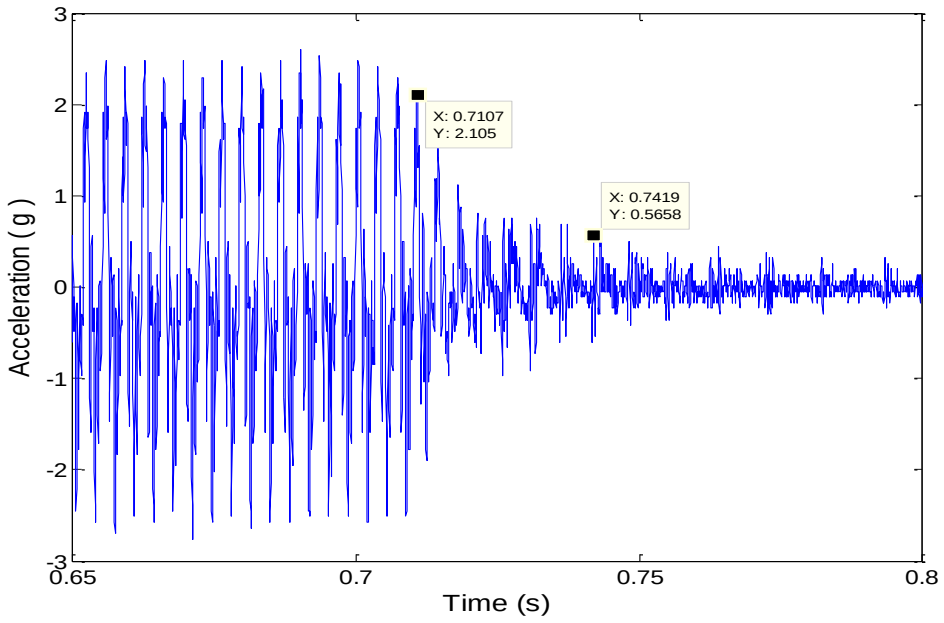

Figure 7-13: Typical stop time (bottom) for the motor during the 'off' pulses

Table 7-2: Mean transient responses for the generated vibration patterns

	Rise Time (millisecond)	***Stop Time (millisecond)***	***Total (millisecond)***
Pattern A	Continuous	Continuous	Continuous
Pattern B	41.5	31.7	73.2
Pattern C	41.5	35.5	77.0
Pattern D	41.4	37.5	78.9

Another observation with the output signals was that the frequency of vibration tended to vary although the input signal to the motor was constant. This variation was due to how the motor was mounted. When the motor was held stationary on top of the table, the desired 250 ± 10 Hz frequency of vibration could be achieved. However when the motor was held loosely on top of different surfaces, the frequency varied greatly. As the motor will be later attached on the upper arm, there was a high possibility that the frequency of vibration may not be within the desired range. A frequency measurement and control method has been added to confirm and maintain the frequency. This method is explained in the next section.

7.4 Frequency Measurement of the Vibration Motor

The final stage of this research work was to conduct investigations on healthy participants in associating the generated vibration patterns with the surface texture. To ensure the vibration patterns could be effectively perceived, the frequency of vibration of the motor should be 250 Hz. This is the peak frequency for the characteristics of the mechanoreceptors underneath the skin of the upper arm in detecting vibration.

In previous experiments, the vibration frequencies were measured using an accelerometer. For an accelerometer to work, it needs to be connected to power supply. Unless it is properly isolated from the mains supply, this device is not suitable to be used during the psychophysical investigation. Furthermore to measure the vibration, the motor needs to be mounted on top of the accelerometer. This in turn will block the direct vibration sensation to the upper arm. Therefore a different approach was used in measuring the vibration frequency when the motor was in motion.

The vibration frequencies were determined through FFT analysis of the motor terminal voltage. The motor consisted of three poles; hence the commutation points were three times for each revolution. To measure the frequency of vibration per revolution, the positive and negative terminals of the motor were connected to the probes of a digital oscilloscope. The motor was supplied with voltage from the DAQ board through the buffer and isolator circuits, and this input voltage was observed at the oscilloscope (Figure 7-14 (a)). For this measurement shown in Figure 7-14 (a), the input voltage of the motor was adjusted to 1.3 V.

The FFT function of the oscilloscope was utilized to obtain the frequency content for one revolution of the motor. As shown in Figure 7-14 (b), this was done by focusing the FFT calculation at the 100 mV ac of the input signal, which was the periodic variation produced by the rotation of the motor. To ensure only vibration from the rotating mass was measured, the body of the motor was held stationary on top of a table during the measurement using a finger.

In one revolution, the motor should ideally produce 250 Hz of vibration frequency. From Figure 7-14 (b), it could be estimated that the frequency for one motor revolution was 285 Hz. Therefore, the input voltage to the motor needed to be further adjusted to achieve to the desired frequency. As the oscilloscope provided a real time measurement from the motor, the dominant frequency could be monitored and

controlled. The dominant frequency could be easily changed by adjusting the potentiometer of the buffer circuit.

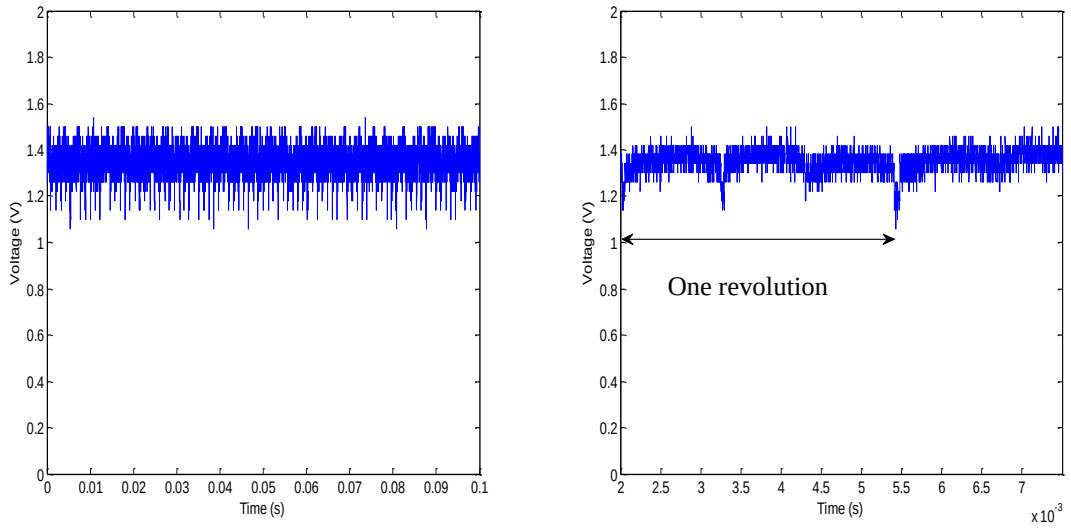

(a) (b)

Figure 7-14: Input voltage to the motor (left) and a zoomed in figure of the same input voltage to highlight one revolution of the motor (right)

Ten frequency measurements were carried out with these adjusted settings (Table 7-3). From the measurements, the vibration frequency of the motor was 255.7 Hz ± 7.8 Hz (mean ± standard deviation). The low standard deviation (below 5% of the mean) indicated that the motor produced consistent frequencies of vibration with the same input settings. An FFT plot from an analysis of the motor voltage is shown in Figure 7-15.

Table 7-3: Observed Dominant Frequencies of the Vibration Motor

Sample	*Observed Frequency (Hz)*
1	250
2	251
3	246
4	266
5	263
6	246
7	263
8	265
9	254
10	253
Mean	255.7
Standard Deviation	7.83

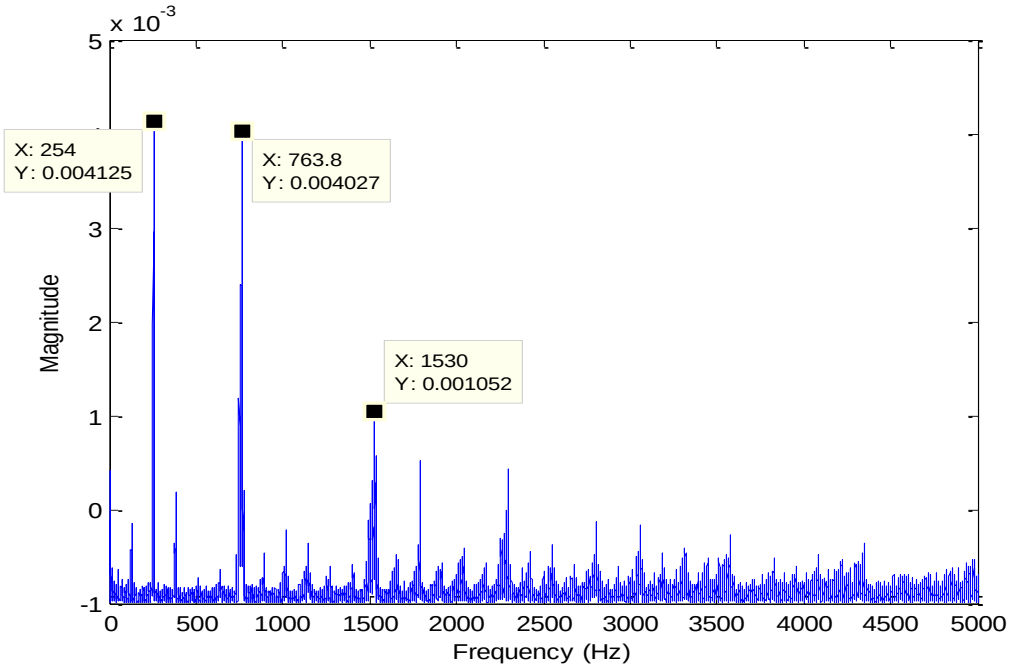

Figure 7-15: Direct FFT measurement of the vibration motor

The plot in Figure 7-15 showed dominant frequencies at 254 Hz, 763.8 Hz and 1530 Hz, with 254 Hz, within the desired range of frequency, being the most dominant. The subsequent dominant frequencies were multiples of 3 of the first dominant frequency. This was a result of the construction of the motor which consisted of three poles. The multiples of 3 of the dominant frequencies (3 x 245 Hz = 762 Hz, 6 x 254 Hz = 1524 Hz) confirmed that the motor was working accordingly and that the frequency could be manipulated according to the desired values.

7.5 Discussion

The transition of the information obtained from the surface texture to generation of vibration pattern was done in a straightforward approach. The ‘on’ and ‘off’ pulses were used to represent the ridge and groove of the surface textures. The periods of the pulses were the reciprocal of the frequency obtained from the texture, and scaled accordingly to be within the transient responses of the vibration motor.

The occurrence of delays during the switching of states (from ‘off’ to ‘on’, and vice-versa) has been expected. While it is not possible to completely eliminate the transient time, the duration for the rise time and stop time could be reduced by driving the motor in both forward and reverse directions (bi-directional) rather than in one direction. A motor driver with a PWM input could be utilised to achieve this. By setting the PWM duty cycle to 100%, the motor will rotate in forward direction at its maximum operating speed. At another extent, setting the duty cycle to 0% will result in motor rotating with the highest operating speed in the reverse direction. The motor will not rotate at 50% duty cycle [107]. By forcing the motor to rotate in the reverse direction will result in faster motor braking, which subsequently reduce the length of the vibration tails.

This method however, requires a more sophisticated circuit. As all that was required to produce the vibration patterns were the ‘on’ and ‘off’ signals [25], the 40 millisecond transient time from the current ‘on’ and ‘off’ pulses method were deemed acceptable and could be used in supplying sufficient amount of sensation to the human arm.

Unlike patterns A, B and C that could be automatically programmed in LabView, pattern D was manually coded. This was due to the complexity of the texture itself. Pattern A was a smooth surface which could be represented by a constant velocity of

motor. Pattern B and C were regular patterns of just up to two different widths of groove and ridge. Pattern D, however, consisted of grooves of multiple widths, and although the widths could be calculated from the obtained dominant frequencies, the sequence of the groove widths could not be determined. Therefore in this current work, pattern D was manually coded in LabView according to the known sequence of the surface texture. A further investigation will be needed to automatically ascertain the sequences of the grooves and ridges.

In this work, the patterns were generated from the saved data previously gathered from the surface texture. The selected data has been post-processed in MATLAB and had shown repeatable accurate outputs in relating the dominant frequency of FFT analysis with the widths of the textures. Therefore by using the analysed data, the chances of the generated vibration patterns to represent the surface textures is high.

Ideally the vibration patterns were to be generated in real time. The LabView is capable to analyse the FFT during the sliding motion of the artificial finger across the textured surface. However as the sliding speed of the block was not constant, the obtained FFT outputs were not the accurate representation of the surface texture. To address this situation, a controller may be designed to ensure a constant velocity of the sliding block without having it to be manually searched.

Another observation in producing the associated vibration frequency was the lengthy processing time. With the selected data during the constant velocity, the time it took for both MATLAB and LabView to obtain the FFT results was more than one minute. This was due to the high sampling frequency set at the data acquisition board which was 75 kS/s. One way to reduce the processing time would be to reduce the sampling frequency. The trade off with this option may be a poor signal reconstruction, and this in turn will result in losing important signals that are critical in determining the dimensions of the surface textures.

The frequency measurement procedure was also included in this part of research work. It is a good practice to always check the frequency of operation of the motor. This is because although the voltage input provided to the vibration motor is the same throughout the investigation, the vibration output may differ greatly. This is due to the type of surface the motor is mounted on. A soft surface will result in lower frequency of vibration as it absorbs more vibration as compared to the hard surface. Over time, the working condition of the motor may also deteriorate. On top of that, the inertia of the motor mounting platform will also affect the frequency of vibration. Therefore it

should be carefully designed to ensure a stable output. This is explained in the next chapter.

Thus by implementing the frequency measurement procedure, not only the frequency could be monitored and instantly adjusted to the desired value, the condition of the motor could also be verified from the FFT output as it could show the dominant frequencies according to the number of poles of the motor. This proven method added more value to the selected ERM motor in providing vibration sensation to the upper arm as it is only applicable for ERM type vibration motors due to its physical characteristics.

In this work, the frequency of the motor was adjusted by manually changing the input voltage to the motor in producing the desired frequency. This system could be further upgraded to work automatically in a closed-loop system. One possible way to do this is by adding a PI controller to the system. This controller will adjust the input voltage to the motor according to the output feedback produced by the motor. By setting the desired frequency value (in this case, 250 Hz) as a set-point value, the input voltage to the motor will be continually adjusted and maintained at the voltage that produces the 250 Hz frequency. The LabView software and the National Instruments data acquisition device could be used in implementing this automatic closed-loop system.

7.6 Summary

This chapter described how the signals obtained from the surface texture were processed to generate associate vibration patterns. The signals were transformed to ‘on’ and ‘off’ pulses in the LabView environment and forwarded to the data acquisition board (NI DAQPad-6016) to give high and low voltage signals to the motor. A buffer and amplifier were added to protect the data acquisition board from potential damage and to amplify the supply current to the motor. A high voltage isolator was also added as the motor will be later mounted onto human upper arm. The motor is battery operated and regulated at 5 V. A frequency measurement procedure was also implemented to ensure the desired frequency is achieved every time the motor is mounted on the upper arm.

Chapter 8 Psychophysics Evaluation

According to the Oxford English Dictionary, psychophysics is “The interaction between mental states and physical events and processes; (also) the branch of science that deals with these” [108]. Psychophysics evaluation is a scientific study that measures the relationship between the sensations felt by the human organ (psychological domain) with the properties that causes the sensation (physical domain) [109]. The purpose of this investigation is to associate the vibrations perceived on the posterior upper arm with the sensation felt when sliding a finger across a fabricated textured surface. The vibration patterns were generated from the information gathered from textured surfaces. It was therefore conjectured that the sensation perceived on the index finger when touching a textured surface would have close similarity to the sensation felt at the upper arm. This evaluation was carried out to see whether people are able to discriminate and match both sensations together. This study has been reviewed and approved by the Ethics Committee of the University of Southampton (Ethics ID: ERGO/FPSE/15290). The ethics documentation is attached in Appendix I.

8.1 Method

8.1.1 Subject

Fifteen participants, twelve female and three male, over the age of 18 years, took part in this psychophysics investigation. All participants were undergraduate and postgraduate students of University of Southampton. The participants should be medically stable and able to tolerate the sensations transcutaneous of haptic vibrations

applied to the skin surface of the upper arm in order to be recruited for this test. Exclusion criteria such as pacemaker users, or people with poorly controlled epilepsy, on long term medication and with history of upper motor neuron (UMN) condition were also applied. None have participated in psychophysical experiments before. All have given written consent prior to starting the test.

8.1.2 Stimuli

Two types of stimuli were present in this test; the surface textures and vibration patterns. The surface textures were fabricated on four 310 mm acrylic strips, each with different dimensions. The detailed dimensions of all four strips have been described in the previous chapter. For ease of identification by the participants, all four surface textures were labelled and colour-coded, as shown in Figure 8-1 below.

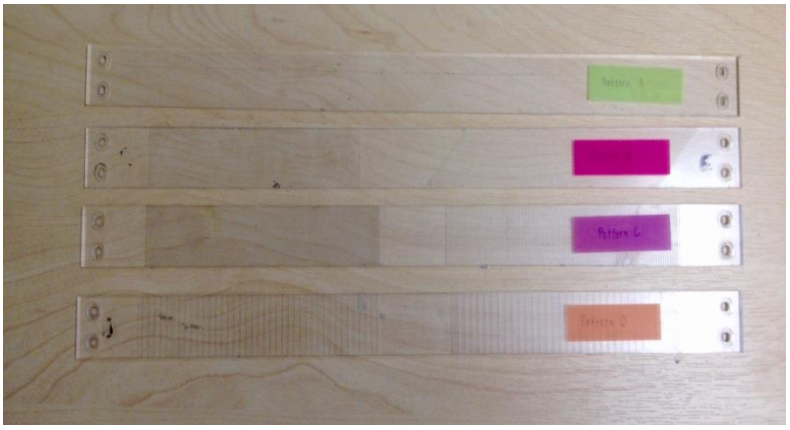

Figure 8-1: Acrylic strips of the fabricated surface textures (Yellow - Texture A, Pink - Texture B, Purple – Texture C and Orange – Texture D)

Four different types of vibration, each randomly repeated for five times, have been generated and applied to the upper arm of every participant. Hence the total number of sample, N was 300 (4 types of vibration x 5 repetitions x 15 participants). To minimize the duration of vibration to the participants, the vibration pulses were slightly shorter than during the initial test (Table 7-1). This was done to avoid discomfort to the users as stimuli longer than 200 milliseconds could be perceived as annoying [50]. The revised description of the four vibration patterns and their associated surface textures are as listed in Table 8-1.

The vibrations were provided by an 11 mm long miniature motor with a maximum supply of 2V, 50 mA (vibration frequency of 250 Hz). This is the same motor that has been tested in the previous chapters. The vibration patterns were

selected by the investigator (according to the predetermined random sequence) from the graphical user interface (GUI) programmed in LabView. The input signals from the GUI were translated to vibration output through a buffer circuit.

Table 8-1: Descriptions of the vibration patterns and their associated surface textures

Vibration Pattern	***Descriptions***	***Associated Texture***
Pattern A	Continuous vibration (1500 millisecond – 1 cycle)	Texture A
Pattern B	Repeated 250 millisecond* pulses with 250 millisecond* pauses in between (5 cycles)	Texture B
Pattern C	Repeated 500 millisecond* pulses with 250 millisecond* pauses in between (3 cycles)	Texture C
Pattern D	Repeated 250 millisecond* pulses with 250 millisecond* pause in between, then 250 millisecond* pulses with 500 millisecond pause in between, then 250 millisecond* pulses with 750 millisecond* pauses in between, and finally 250 millisecond* pulses with 1000 millisecond* pauses in between (1 cycle)	Texture D

*Approximate duration

The motor was battery powered and opto-electronically coupled to provide isolation with the mains power supply. To ensure that the motor will consistently produce 250 Hz of vibration frequency throughout the test, it was mounted on a specially fabricated brass clip that provides higher mass at both sides of the motor. The leads of the motor were mechanically secured to avoid metal fatigue that may break the wires. This was done by adding plastic terminals with thicker wires attached. A velcroband was then weaved into the designed slots of the terminals and clips. It was then strapped onto the participants' upper arms during a test. The complete vibration haptic device is shown in Figure 8-2.

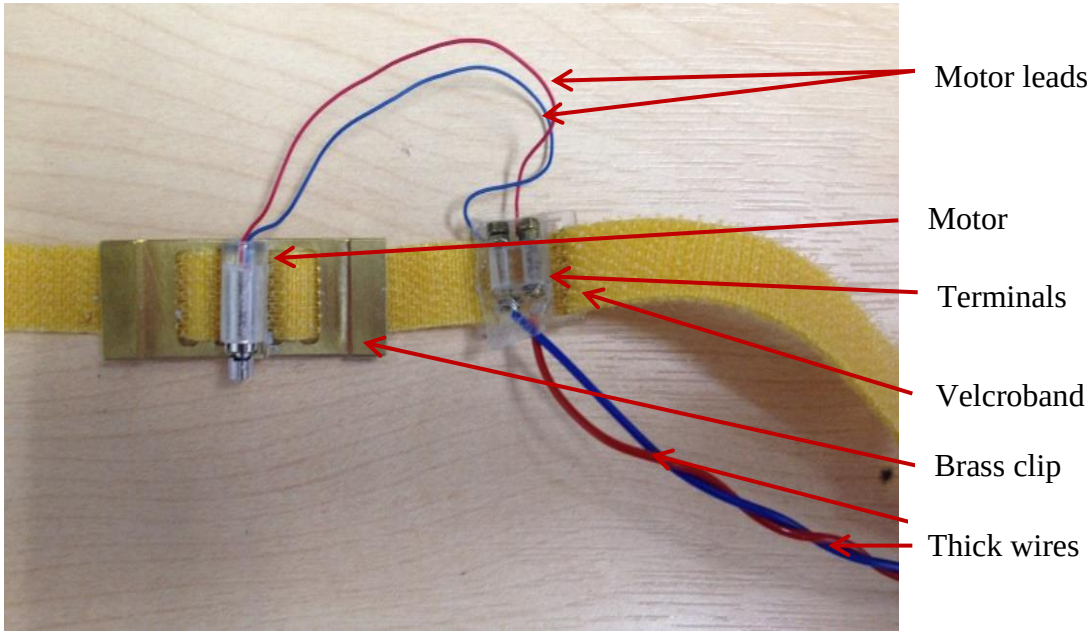

Figure 8-2: Vibration device

The frequency of the vibration stimuli during operation were checked using the frequency measurement method described in the previous chapter. The FFT results should show a dominant frequency of 250 Hz. These measurements gave confidence that the frequency supplied by the vibration stimuli was at the set frequency. The frequency checks were done before and after every psychophysical test to ensure that there was no variation (or very minimal variations) in the set vibration frequency that may affect the perceived sensations.

Figure 8-3 shows one of the FFT outputs produced by the vibration stimuli. The dominant frequency was observed at 245.5 Hz. The subsequent dominant frequency was 736.2 Hz, which was due to the motor commutation points that were 3 times per rotation.

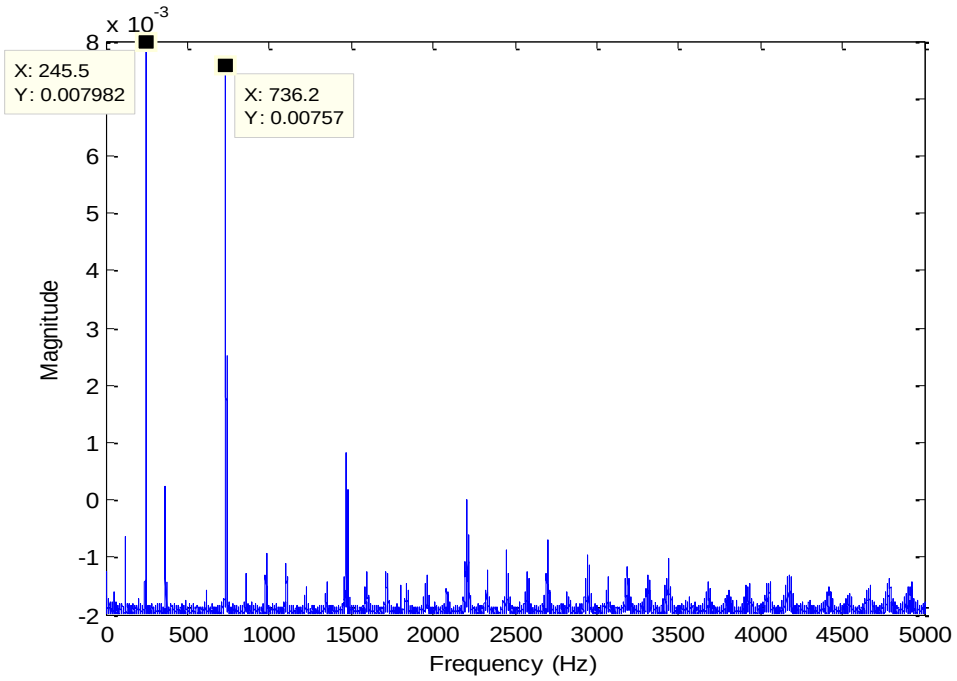

Figure 8-3: FFT Output of the vibration stimuli

8.1.3 Procedure

The psychophysical test was performed to one individual participant at a time. During the test, the following procedures were conducted:

1. Upon arrival at the venue of the test, the participant was welcomed and seated in a chair. A brief introduction about the research was given and the participant was given opportunity to ask questions about the research and the procedures of the test. The participant was also informed that they may stop the test at any time should they feel uncomfortable with the vibration stimuli.
2. The participant was then asked to slide his/her index finger on the four textured surfaces (labelled as Texture A, Texture B, Texture C and Texture D), already prepared on a table. This was done to ensure that participant is familiar with the surface textures.
3. Next the participant was requested to put his/her arms by his/her sides. The length of the dominant upper arm (between the tip of shoulder (scapular acromion) and the elbow (humeral coronid fossa)) of the participant was measured using a measuring tape. The vibration stimuli

were then strapped on the posterior of the upper arm at ¼ of the total length from the participant's tip of shoulder.

4. He/she was then introduced to the four different types of vibration patterns (Pattern A, Pattern B, Pattern C and Pattern D) to become familiar before the test began. The participant may request for the stimuli to be repeated before starting the test.
5. Once the participant was ready for the test, twenty vibrations (four patterns, randomly repeated five times) were provided one at a time. Participants will be asked to associate the provided surface textures with the generated vibration. For each vibration patterns perceived at the upper arm, the participants will verbally state the type of textures closely represented by the vibration.
6. The information was gathered by the investigator using a specially prepared data collection form (named as data collection plan in the ethics documentation in Appendix I).
7. When all information has been gathered for the twenty vibration patterns, the participant will be thanked for his/her contribution and invited to contact the investigator if they have further questions about the study.

The skin surface of each participant was vibrated twenty times and each stimulus was given one at a time (four patterns, randomly repeated five times). All participants received the same sequence of stimulation, pre-set in a random order. In this work, the random order means that vibration A is not necessarily followed by vibration B, or vibration C is not necessarily stimulated before vibration D. The sequence was done according to the data collection plan sheet attached in the ethics documentation in Appendix I. The sequence in the data collection plan was designed to ensure that the judgements on the perceived vibrations were not influenced by the preceding vibration patterns.

The maximum duration of the vibration was five seconds per pattern and it took about twenty minutes in total to complete the test. Figure 8-4 shows how the haptic device was mounted on a person's arm, the position of the surface texture and apparatus in conducting the psychophysical test.

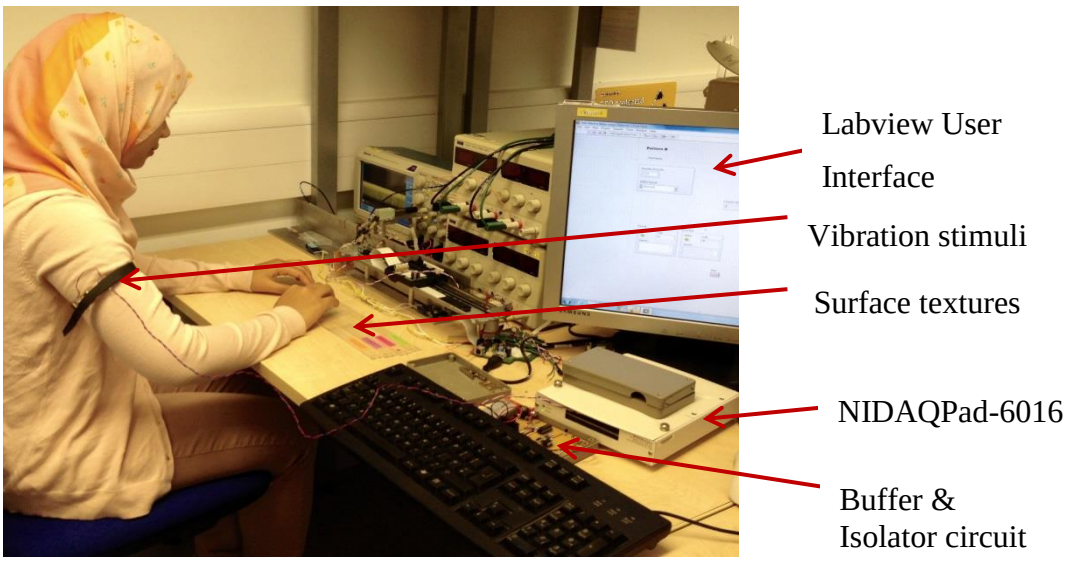

Figure 8-4: Positions of the vibration stimuli, surface textures and other test apparatus for the psychophysical test

8.2 Results

To test whether there is a relationship between the vibration patterns and the surface textures, a chi-squared ($\chi 2$) test of independence with $\alpha = 0.01$ as criterion for significance has been conducted on the gathered data. This analysis was carried out using IBM SPSS Statistics (Version 22) software. The results from the analysis are as shown in Figure 8-5 and Table 8-2 to Table 8-4.

The histogram in Figure 8-5 showed the frequency (observed count) of a texture being selected for a given vibration pattern. The observed counts show whether there is an association between a surface texture and a vibration pattern. Ideally, texture A should have the highest count for vibration A. Similarly textures B, C and D should have the highest count for vibration patterns B, C and D. In this test, it was noted that textures A and D have the highest count for vibration patterns A and D respectively. This gave early indication that there is association between these two properties.

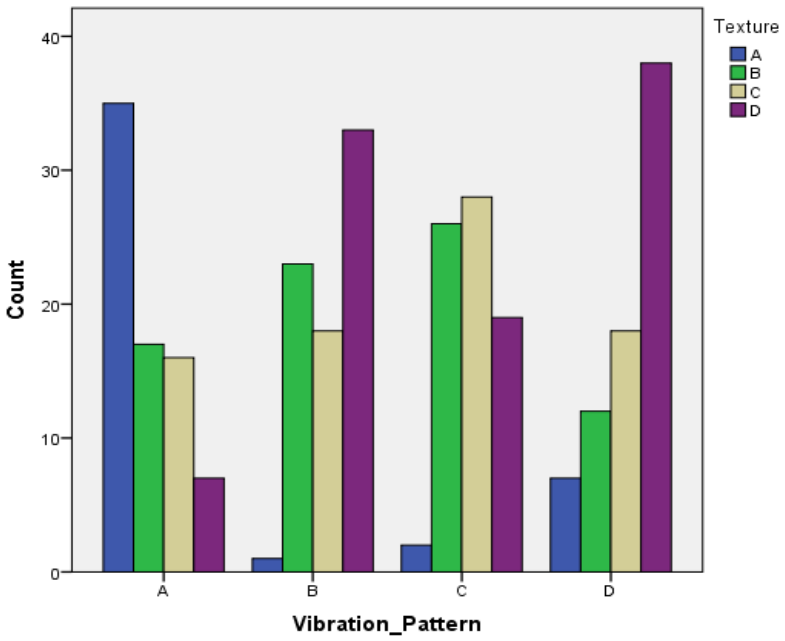

Figure 8-5: Histogram of selected surface textures with supplied vibration patterns

Table 8-2: Contingency table of the Vibration Pattern and Surface Texture

			Texture				
			A	B	C	D	Total
Vibration Pattern	A	Count	35	17	16	7	75
		Expected Count	11.3	19.5	20.0	24.3	75.0
	B	Count	1	23	18	33	75
		Expected Count	11.3	19.5	20.0	24.3	75.0
	C	Count	2	26	28	19	75
		Expected Count	11.3	19.5	20.0	24.3	75.0
	D	Count	7	12	18	38	75
		Expected Count	11.3	19.5	20.0	24.3	75.0
Total		Count	45	78	80	97	300
		Expected Count	45.0	78.0	80.0	97.0	300.0

Table 8-2 is the contingency table of the vibration patterns and the surface textures, generated using the SPSS software. There were 300 number of samples altogether with 75 samples for each vibration patterns. The term ‘count’ refers to the frequency a texture being selected for a given vibration pattern. The ‘expected count’ is the projected frequency if there is no association between the two variables (surface texture and vibration pattern). In theory, if there is no association between the two variables, the expected count should be almost equal with the observed count. From the table it could be seen that there are large differences between the observed and

expected count for vibration patterns A and D with textures A and D respectively, as compared to vibration patterns / surface textures B and C.

Table 8-3 shows the results from the χ^2 test of independence. It could be concluded that there was a statistically significant relationship between the vibration patterns and the perceived texture, χ^2 (9, N = 300) = 103.450, p <0.001, as shown by the Pearson Chi-Square value. The Cramer's V value obtained from this association was 0.339 (Table 8-4).This is the strength of the association between the vibration pattern and the surface texture. This value indicates that there was a moderate association between the two variables [110].

Table 8-3: χ^2 Test Statistic, degrees of freedom and P-Value

	Value	df	Asymp. Sig. (2-sided)
Pearson Chi-Square	103.450[a]	9	.000
N of Valid Cases	300		

Table 8-4: Size of effect between the Vibration Pattern and the Surface Texture

		Value	Approx. Sig.
Nominal by Nominal	Phi	.587	.000
	Cramer's V	.339	.000
N of Valid Cases		300	

It could be observed from the histogram in Figure 8-5 that Vibration A and Texture A as well as Vibration D and Texture D give the most contribution in associating the vibration patterns and their corresponding surface textures. A follow-up analysis has been done to verify this, shown in Figure 8-6, Table 8-5 and Table 8-6. The Bonferoni correction has been performed in this follow up test to ensure the chances of Type I error (false-positive result) is reduced [111]. As four comparisons were made in this follow-up test (vibration pattern A with texture A, vibration pattern A with texture D, vibration pattern D with texture A and vibration pattern D with texture D), the criterion for significance became $\alpha/4 = 0.01/4 = 0.0025$. The p-value has also been adjusted using the SPSS software.

The result from the χ^2 test of independence shows that the association between both vibration patterns and the surface textures was significant, χ^2 (1, N = 87) = 39.966,

p <0.001, with the effect value, φ = 0.678. This is a strong association, as has been outlined in [110].

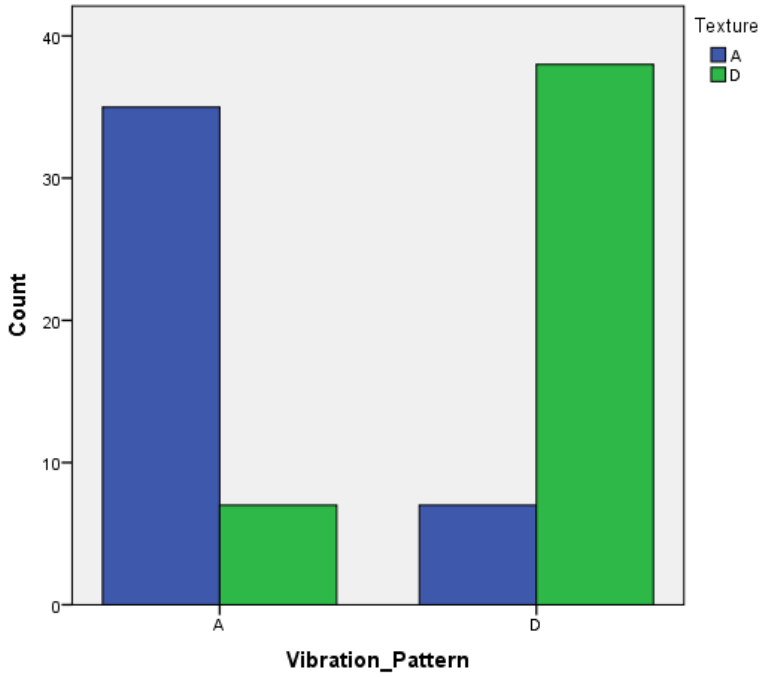

Figure 8-6: Histogram of the follow-up analysis for the surface textures and vibration patterns A & D

Table 8-5: χ^2 Test Statistic, degrees of freedom and P-Value for the follow-up analysis of Vibrations Patterns and Surface Textures (A & D)

	Value	df	Asymp. Sig. (2-sided)
Pearson Chi-Square	39.966	1	.000
N of Valid Cases	87		

Table 8-6: Size of effect between the Vibration Pattern and the Surface Texture (A & D)

		Value	Approx. Sig.
Nominal by Nominal	Phi	.678	.000
	Cramer's V	.678	.000
N of Valid Cases		87	

It is therefore could be inferred that given a vibration pattern, people are more likely to select the same surface texture that has been used to produce signals in generating that particular vibration pattern. The odds that people will likely to select

texture A when given vibration A are 8.5 times higher than the odds of selecting texture A when given vibration D. Similarly, the odds that people that will tend to select texture D when given vibration D is 9.98 higher than selecting texture D when given vibration A.

Another follow-up analysis was done to see the weakest association between the two variables. From Table 8-2, the observed and expected counts for vibration patterns B and C with textures B and C were almost equal. This gave indication that the association between the variables were very low. Similar to the follow-up analysis for vibration patterns A and D with textures A and D, the criterion of significance was reduced to 0.0025. The p-value for this test has been adjusted according to the Bonferoni corrections using the SPSS software.

The results from the χ^2 test of independence (Table 8-7) showed that there was no statistically significant association between Vibration B with Texture B and Vibration C with Texture C, χ^2 (1, N = 95) = 0.590, p=0.443. The Phi value, φ = 0.078, confirmed that the strength of association between the selected vibration and textures were very weak (Table 8-8).

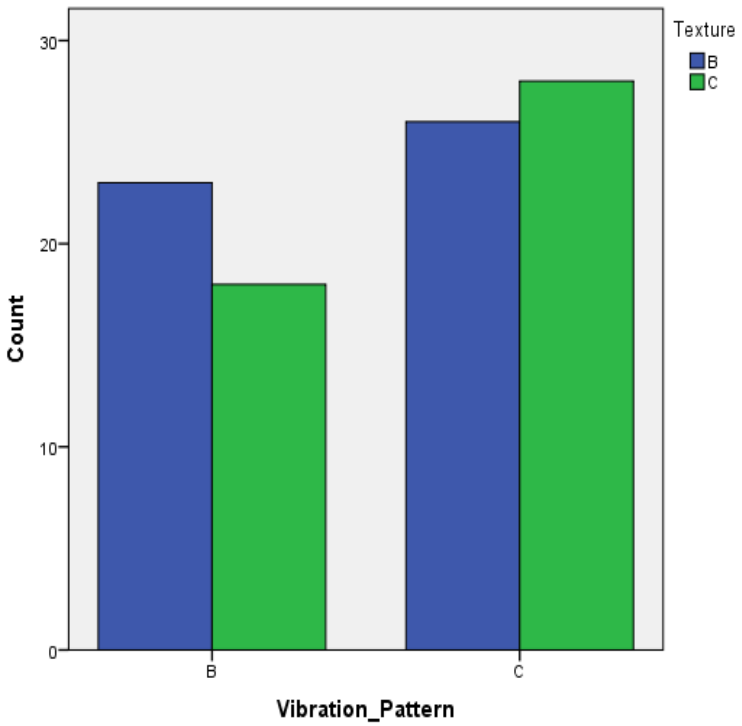

Figure 8-7: Histogram of the follow-up analysis for the surface textures and vibration patterns B & C

Table 8-7: χ^2 Test Statistic, degrees of freedom and P-Value for the follow-up analysis of Vibrations Patterns and Surface Textures (B & C)

	Value	df	Asymp. Sig. (2-sided)
Pearson Chi-Square	.590	1	.443
N of Valid Cases	95		

Table 8-8: Size of effect between the Vibration Pattern and the Surface Texture (B & C)

		Value	Approx. Sig.
Nominal by Nominal	Phi	.079	.443
	Cramer's V	.079	.443
N of Valid Cases		95	

The histogram in Figure 8-7 showed the selection tendency of the people when supplied with vibrations patterns B and C. A higher frequency count was observed for texture B when supplied with vibration B. Similarly, a higher frequency count was observed for texture C when supplied with vibration C. It is thus could be inferred that although the association between the selected variables were weak, people were still able to match the vibration patterns with the surface texture.

8.3 Discussion

The psychophysical test has been designed specifically to enable observations about the association between the generated vibration patterns with the surface textures. These observations were done using the Chi-square test for independence (also known as Pearson's chi-square test), which is a statistical procedure in discovering if there is a relationship between two categorical variables [112]. In this study, '*vibration patterns and surface textures are independent*', was the null hypothesis, $H_{0,}$ while '*vibration patterns and surface textures are not independent*' was the alternative hypothesis, H_a. The H_0 will be rejected if the p-value is less than the chosen significance value of 0.01 ($p<.01$). The strength of association between both variables was obtained by checking the Pearson's Chi (for 2-by-2 contingency tables) or Cramer's V (for contingency table with size of more than 2-by-2). As the sampling method was random and the variables were categorical, this test was deemed as appropriate [113].

The vibration frequency of interest for this test was 250 Hz as this is the optimum frequency of Pacinian Corpuscle mechanoreceptor located at the upper arm [45]. When glued and tested on a flat and hard surface like a table, the vibration stimuli were able to produce repeatable 250 Hz vibration frequencies at a predetermined input voltage. However when the stimuli was strapped and tested on the upper arm, the frequency range swayed between 250 Hz ± 20 Hz which was unacceptable. This may cause varying levels of perceived sensations that would cloud participants' judgement on the associated surface textures. The variability was due to the instability caused by the rotation of the motor as the motor was not strongly and properly anchored as well as compliance of skin surface.

A solid platform made of brass; measured 40 mm x 16 mm x 1 mm in length, width and thickness, weighing 6.9 g was specially fabricated to produce stable vibration output from the motor. The thicknesses at 5 mm from both ends of the platform were 3 mm, which made both ends of the platform having greater mass. As the higher mass was concentrated further away from the middle of the platform, the rotational inertia due to the rotation from the motor mounted at the middle of the platform increased, which made the platform more stable. Furthermore, the z-axis of the platform became properly anchored hence vibration could only be perceived from the strongest vibration axis of the motor, which was the x-axis (y-axis had the lowest vibration strength). Ultimately the frequency of vibration could be controlled to be within the desired range.

Another important criterion in designing the motor platform was its mass. The mass should not be too low as it would cause instability in the vibration. At another extreme, the mass should not too high as it would result in negligible vibration to be perceived. Different mass ratios between the fabricated platforms to the motor have been designed and tested until the desired output was achieved. The mass ratio of this brass platform (mass: 6.91g) to the mass of the motor (mass: 1.1g) was 6.28. Figure 8-8 illustrates the fabricated brass platform. The dimensions of the platform are attached in Appendix J. By anchoring the motor to the brass platform, the range of motor vibration frequency became 249.6 Hz ± 6.62 Hz (mean ± standard deviation, N = 10), which was desirable for this psychophysics investigation (Table 8-9).

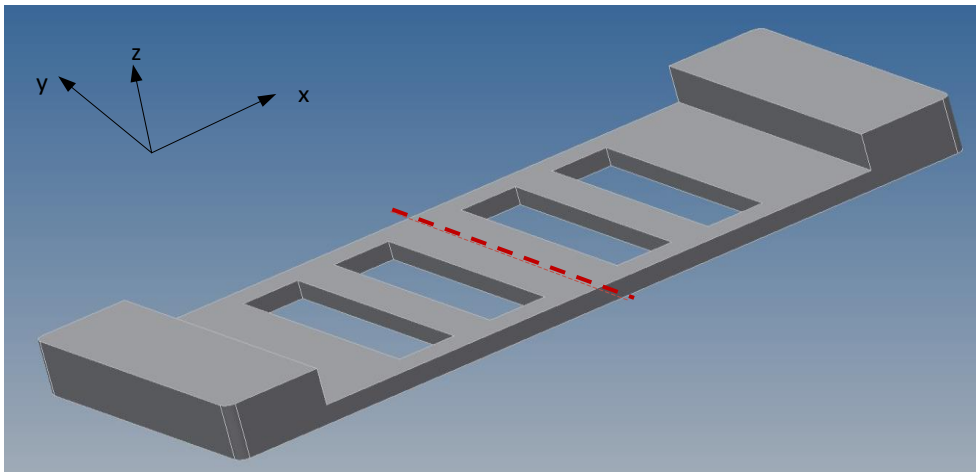

Figure 8-8: Brass platform as a mechanical mounting for the vibration motor. Dashed red line is the middle area of the platform where the motor was glued. A higher mass was concentrated at both end sides of the platform, and are thicker than the rest of the platform. The velcroband was weaved between the four slots.

Table 8-9: Observed Frequencies of the Vibration Motor with the Brass Platform

Sample	*Observed Frequency (Hz)*
1	243
2	240
3	248
4	243
5	250
6	262
7	255
8	255
9	250
10	250
Mean	249.6
Standard Deviation	6.62

The number of cycle during each vibration pattern was set so that the duration it took for every stimulation test were almost the same for all four patterns. Referring to Table 8-1, Patterns A, B, C and D were set to 1, 5, 3 and 1 cycle(s) per stimulation test to ensure that the durations were within 1.5 – 2.5 s. This will avoid participants from making simplified guesses that short pulses were for simple textures and longer pulses for more complicated textures without concentrating on the sensations felt from the vibration patterns.

In this psychophysics test, the ratio of female to the male participants was 4:1. As the mechanoreceptors that detect the sensation from vibration stimulation on the skin surface are located deep beneath the skin layers [45], the results of the investigation was believed to be unaffected with respect to gender imbalance. Based on this information, it was deduced that regardless of gender and the physical attributes, the same stimulation could be felt similarly for every participant. Further investigations may also be performed at a later stage to confirm about the perception of the stimulations for different genders.

Before the test began, the participants were required to touch and explore the surface texture. The vibration patterns were then presented to them in random order without informing the types of patterns (whether A, B, C or D). This method was applied to avoid any 'learning' effects or deduction based from memory. In order to see whether the participants were able to associate the vibration patterns with surface textures, their judgement about patterns should be from the sensation they felt rather than relying on a priori information.

Some participants, however, preferred that they should be informed or trained about the types of vibration patterns. This was because they felt that they tend to make false assumptions in associating the patterns and textures from the initial encounter, and will continually make the same false assumptions throughout the test. An example for such case could be seen from the histogram in Figure 8-5. A lot of people made the assumption that vibration pattern B should be associated with texture D. The assumption remained throughout the entire test that resulted in selections of texture D were 13.3% higher than the selection of texture B when given vibration pattern B.

It would have been possible to prepare another test with another set of data with people being informed about the types of vibration patterns. Although it will likely to give higher accuracy in matching both variables, it may be irrelevant to the study objective. Furthermore, in an ideal situation, the prosthetic finger should be able to

gather various types of texture surface information and translate it to signals for the motor to provide associated vibration patterns in real-time. Therefore judgement of vibration patterns based on previously known patterns was deemed unnecessary and may lead to inaccurate findings. However, this work could be extended for applications that involve discriminating surface textures of various objects used in daily life. For this purpose, training the users with a learning phase would be beneficial to them as they will easily recognize and appropriately respond to the objects. It was noted from this investigation that patterns with distinct features achieved high matching scores whereas the ones with less distinct features produced low matching scores. The participants could easily associate a constant vibration from the motor (pattern A) with a smooth texture (texture A), or longer pulses of vibration (pattern D) to the roughest surface texture (texture D). Similar perception to these types of vibration could be attained from reports in [25] and [66]. This clearly suggests that approximation of smoothness and roughness could be created by varying the pulses of the vibration.

Anecdotal evidence from discussions between participants and investigator implied that they had difficulties in differentiating between patterns B and C. The main reason for this matter could be due to the dimensions of the surface textures under investigation. Although the ridges of the surface textures differ by a double in width, both textures have almost the same groove width. According to research findings by Lawrence [20] and Lederman [104], groove widths play the strongest effect in providing the roughness sensation of a surface texture. Therefore, although the surface textures may have been correctly represented by the vibration patterns, the complexity in discriminating between the surface textures using a bare finger may have resulted in mismatched results between the two variables.

8.4 Summary

This chapter explained the procedures in conducting the psychophysics investigations, observations as well as evaluation from participants' feedback. This investigation was carried out to verify the capability of the chosen haptic actuator (the ERM motor) in providing vibration sensation to the residual arm. The twenty minutes test (per participant) to all fifteen participants showed that the participants were able to associate the vibration patterns with the surface textures, especially when they were provided with continuous vibration (associated with smooth texture) and longer pulses of vibrations (associated with the roughest texture).

Chapter 9 Conclusions and Future Work

9.1 Conclusions

The upgraded data acquisition strategies that include the construction of a voltage amplifier circuit and the deployment of a 16 bit, 200 kS/s data acquisition device have proven to produce reliable signal outputs from a piezoelectric sensor, with a very low signal-to-noise ratio (SNR) recorded at 3.6 dB. Four different types of surface textures have been tested and have shown distinctive FFT output patterns that enable discrimination between the surface textures.

The dimensions of the surface textures were also successfully determined using the dominant frequencies generated from the FFT plots. The data acquisition and signal processing system has shown repeatable and reliable performance in deciphering the grating widths for Texture B (repeating patterns of similar widths of grooves and ridges). The mean percentage difference between the measured and calculated grating widths of the texture was 2.55%. Similar to Texture B, Texture C (repeating patterns of different widths of ridges and grooves) produced highly repeatable, very unique FFT output plots. Interestingly, the plot showed occurrences of dominant harmonic frequencies which suggest additional information may be deciphered about the texture.

Although less distinctive FFT plots were obtained for Texture D (repeating patterns of increasing widths of grooves and constant widths of ridges) as compared to the other simpler surface textures, the data acquisition system was able to attain low percentage differences between the measured and calculated grating widths (2.08% mean difference). Currently, the grooves and ridges for this texture were identified by the locations of the peak frequencies (above or below the pre-set threshold values).

Equipped with the information gathered by the piezoelectric sensor, the sensation felt by sliding a finger across the textured surface were recreated by providing vibration supplementary sensation at the upper arm. Results from the MATLAB simulations show that the selected vibration actuator (eccentric rotation mass) exhibits linear relationship between the input voltage and its driving frequency. Through the relationship, the vibration produced by the actuator could be efficiently predicted. The transient responses obtained via the simulation showed that the actuator was able to reach the desired speed within 42 milliseconds, which is 2.8% of the overall period deemed adequate for prosthetic hands. The transient responses also provided some estimation in preparing the next haptic event, such as the time it may take to decrease the amplitude of vibration.

The experimental results on the selected vibration actuator show the expected theoretical logarithmic relationship between the frequency and voltage. Through adjustments of input voltage, frequencies could be generated between 76 Hz to 320 Hz, which is within the frequency bandwidth of the sensitive mechanoreceptors in the human hairy skin. At 250 Hz, which is the optimum frequency of the mechanoreceptors at the skin of the upper arm, the effective vibration energy in the X and Z axes were 0.5 g_{rms} and 0.2 g_{rms} respectively, which also are within the vibration detection threshold of the human hairy skin.

A prototype has been fabricated to work at the optimum frequency of 250 Hz. With reference to input pulses applied to the haptic actuator, it has produced vibration output with less than 90 milliseconds time delay in total. This was achieved by using the data acquisition device to channel out pulses that were generated from the frequency information gathered from the surface texture.

The implementation of the frequency measurement technique has improved the accuracy of the vibration actuator to produce a 250 Hz optimum frequency. Although care has been taken to ensure the actuator will supply the required vibration frequency through the manipulation of input voltage, factors such as the way the actuator is mounted have a substantial effect on the vibration frequency. Therefore using the information of the commutation poles of the eccentric rotation mass (the selected vibration actuator), a vibration frequency of 255±7.83 Hz have been obtained when the actuator was held stationary on the table, and 249.6±6.62 Hz when mounted on specially designed brass platform (mean ± standard deviation). This developed technique ensures consistent setting of the vibration stimuli on the upper arm and is

therefore not a factor to be considered having an influence during testing human responses.

For this application, the selection of the eccentric rotation mass (ERM) as the vibration actuator has also proven to be the most appropriate as compared to piezoelectric and linear resonant actuators. Although the ERM has slightly longer transient responses as compared to the other vibration actuators, the construction of the ERM enables direct measurement of vibration frequency, which allows accurate amount of vibration stimuli to be supplied to the upper arm.

Through a psychophysical investigation that comprises of 300 samples (4 types of vibration patterns x 5 repetitions x 15 participants), the hypothesis that the vibrations generated and perceived at the upper arm should have association with the surface textures has been validated. The investigation has revealed that there is a statistically significant relationship between the vibration patterns and the surface textures (probability value, $p < 0.001$). In particular, patterns with distinctive features produced higher matching scores as compared to the less distinct ones.

As the widths of the textures were calculated prior to supplying input pulses to the actuator, it imparts confidence that the generated vibration signals represent the surface textures accordingly. This is also an advantageous feature for maintenance and troubleshooting purposes as the calculated widths of the acquired signals could be compared with the actual dimensions of the surface textures.

The results from this research have shown promising implementation of sensory feedback to upper prosthetic device users. By providing a supplementary sensation, the users will be able to 'touch' and 'feel' objects held by the prosthetic hand. The enhancement of sensory feedback feature, along with other existing features in prosthetic devices, promotes a sense of embodiment to the users, and should be able to provide greater satisfaction and encourage users to fully utilize the device.

9.2 Recommendations for Future Work

The research work that has been presented in this thesis has successfully met the research objectives outlined in Section 1.2. However further improvements could be

carried out and oriented towards deciphering wider sets of daily-life surfaces, real-time feedback control as well adaptability to user requirements.

The recurrences of dominant harmonic frequencies at different scanning velocities for Texture C suggest that there may be more information that could be gathered about the texture. Further investigations will be essential for these consistent findings to gain greater validation about the texture. This could be done by acquiring signals on different types of surface texture in an organized sequence. The ratio of the groove width to the ridge width of Texture C is 1 to 2.2. Further tests could be done on textures with an inverted ratio of 2.2 to 1 as well as with increasing ratios (1 to 2.2N; N >1). This systematic assessment may reduce the percentage errors between the measured and calculated widths values, and ultimately will provide improved knowledge about the textures.

The experimental outcomes have shown potential in generating vibration feedback in real-time. In this study, the vibration patterns were generated using the post-processed signals, manually selected from the data samples of the surface textures. The factor that limited the capability of the designed system to automatically generate vibration patterns during the surface exploration was the requirement of constant velocity to produce dominant vibration frequencies which is used to calculate grating widths. The software could be programmed to automatically select the constant velocity from the overall dataset, but this too, may consume long processing time. Therefore, with suitable design of controllers, a constant velocity during the surface exploration process could be maintained. Also, the test rig may be further improved to achieve a constant sliding velocity throughout the acquisition process. This will undeniably reduce the processing time as the task for selecting constant velocity is eliminated.

As previously discussed in Chapter 6, the data acquisition device produced best output when the prosthetic finger moved in a constant velocity. Apart from training the users to manipulate the exploratory tasks in a constant velocity, a different calculation method that do not rely on FFT analysis may also be adopted so that the device could provide useful information even when moving at a non-constant velocity. This could be achieved by including more variables as part of the calculation method, in addition to the signals already gathered from the piezoelectric sensor and encoder.

In this study, a 250 Hz frequency was pre-set to the vibration actuator before being attached onto the upper arm. Although there were no complaints from the

participants about dizziness or skin irritation during the psychophysical investigation, it would be an added advantage if the users are able to adjust the frequency of vibration according to their comfort level. This could be achieved by implementing a closed loop control to the system to provide user input to the data acquisition system. Also, another opto-isolator should also be included in the circuit for isolation from the mains supply for the frequency adjustment purpose. This way, the user could fine-tune the vibration frequency as desired while the actuator remains affixed on his/her upper arm.

Moving even further ahead, this study could be extended to acquire information about diverse properties of surface textures that are common in everyday life, such as softness, warmness and stickiness. The reliability of the system to measure the widths of the surface gratings also opens various possibilities for applications in industries, where exact dimensions of surface textures are required.

References

[1] Uustal H; Baerga E., *Physical Medicine and Rehabilitation Board Review*, 2nd ed. New York: Demos Med. Publishing, 2004.

[2] "BeBionics3 Product Brochure," *RSLSteeper*, 2012. [Online]. Available: http://bebionic.com/distributor/documents/bebionic3_Product_Brochure.pdf. [Accessed: 31-Dec-2012].

[3] "Active Prostheses," *Touch Bionics*, 2012. [Online]. Available: http://www.touchbionics.com/products/active-prostheses/i-limb-ultra/. [Accessed: 31-Dec-2012].

[4] "OttoBock Arm Prosthesis Products," *OttoBock*, 2012. [Online]. Available: http://corporate.ottobock.co.uk/cps/rde/xchg/ob_uk_en/hs.xsl/3170.html. [Accessed: 31-Dec-2012].

[5] E. A. Biddiss and T. T. Chau, "Upper limb prosthesis use and abandonment: A survey of the last 25 years.," *Prosthet. Orthot. Int.*, vol. 31, no. 3, pp. 236–257, Sep. 2007.

[6] J. T. Belter and A. M. Dollar, "Performance characteristics of anthropomorphic prosthetic hands.," *IEEE Int. Conf. Rehabil. Robot. [proceedings]*, vol. 2011, p. 5975476, Jan. 2011.

[7] R. Vinet, Y. Lozac'h, N. Beaudry, and G. Drouin, "Design methodology for a multifunctional hand prosthesis.," *J. Rehabil. Res. Dev.*, vol. 32, no. 4, pp. 316–24, Nov. 1995.

[8] J. Gonzalez, H. Soma, M. Sekine, and W. Yu, "Psycho-physiological assessment of a prosthetic hand sensory feedback system based on an auditory display: A preliminary study.," *J. Neuroeng. Rehabil.*, vol. 9, p. 33, Jan. 2012.

[9] G. K. I. M. Bigley, "Sensation," in *Clinical Methods: The History, Physical, and Laboratory Examinations*, 3rd ed., H. J. Walker HK, Hall WD, Ed. Boston: Butterworth, 1990, pp. 343–350.

[10] S. Raspopovic and M. Capogrosso, "Restoring Natural Sensory Feedback in Real-Time Bidirectional Hand Prostheses," *Sci. Transl. Med.*, vol. 6, no. 222, 2014.

[11] D. S. Childress, “Closed-loop control in prosthetic systems: historical perspective.,” *Ann. Biomed. Eng.*, vol. 8, no. 4–6, pp. 293–303, Jan. 1980.

[12] R. R. Riso, “Strategies for providing upper extremity amputees with tactile and hand position feedback--moving closer to the bionic arm.,” *Technol. Health Care*, vol. 7, no. 6, pp. 401–409, Jan. 1999.

[13] A. Cranny, D. P. J. Cotton, P. H. Chappell, S. P. Beeby, and N. M. White, “Thick-film force, slip and temperature sensors for a prosthetic hand,” *Meas. Sci. Technol.*, vol. 16, no. 4, pp. 931–941, Apr. 2005.

[14] A. Chatterjee, P. Chaubey, J. Martin, and N. Thakor, “Testing a Prosthetic Haptic Feedback Simulator With an Interactive Force Matching Task,” *JPO J. Prosthetics Orthot.*, vol. 20, no. 2, pp. 27–34, Apr. 2008.

[15] K. Kim and J. Colgate, “On the design of miniature haptic devices for upper extremity prosthetics,” *IEEE/ASME Trans. Mechatronics*, vol. 15, no. 1, pp. 27–39, 2010.

[16] D. Cotton, P. Chappell, and A. Cranny, “A novel thick-film piezoelectric slip sensor for a prosthetic hand,” *IEEE Sens. J.*, vol. 7, no. 5, pp. 752–761, 2007.

[17] L. Beccai, S. Roccella, L. Ascari, P. Valdastri, A. Sieber, M. C. Carrozza, A. Member, and P. Dario, “Development and Experimental Analysis of a Soft Compliant Tactile Microsensor for Anthropomorphic Artificial Hand,” vol. 13, no. 2, pp. 158–168, 2008.

[18] Y. Visell, “Tactile sensory substitution: Models for enaction in HCI,” *Interact. Comput.*, vol. 21, no. 1–2, pp. 38–53, Jan. 2009.

[19] T. Mano and M. Ohka, “Mechanisms of fine-surface-texture discrimination in human,” *J. Accoust. Soc. Am.*, vol. 105, no. 4, pp. 2485–2492, 1999.

[20] M. A. Lawrence, R. Kitada, R. L. Klatzky, and S. J. Lederman, “Haptic roughness perception of linear gratings via bare finger or rigid probe,” *Perception*, vol. 36, no. 4, pp. 547–557, 2007.

[21] J. Scheibert and S. Leurent, “The role of fingerprints in the coding of tactile information probed with a biomimetic sensor,” in *Science*, vol. 323, March, pp. 1503–1506, 2009.

[22] B. J. P. Mortimer, G. A. Zets, and R. W. Cholewiak, “Vibrotactile transduction and transducers,” *J. Acoust. Soc. Am.*, vol. 121, no. 5, pp. 2970-2977, 2007.

[23] A. A. Stanley and K. J. Kuchenbecker, “Design of body-grounded tactile actuators for playback of human physical contact,” in *2011 IEEE World Haptics Conference*, Istanbul, 2011, pp. 563–568.

[24] L. M. Brown, S. A. Brewster, and H. C. Purchase, “A First Investigation into the Effectiveness of Tactons,” *First Jt. Eurohaptics Conf. Symp. Haptic Interfaces Virtual Environ. Teleoperator Syst.*, Pisa, 2005, pp. 167–176.

[25] L. Brown and T. Kaaresoja, “Feel who’s talking: using tactons for mobile phone alerts,” *CHI'06 Ext. Abstr. Hum. Factors Comput. Syst.*, pp. 604–609, 2006.

[26] F. De Vignemont, “Embodiment, ownership and disownership,” *Conscious. Cogn.*, vol. 20, no. 1, pp. 82–93, 2011.

[27] J. A. Berg, F. V Tenore, L. Jessica, R. J. Vogelstein, and S. J. Bensmaia, “Restoring the sense of touch with a prosthetic hand through a brain interface,” *Proc. Natl. Acad. Sci.*, vol. 111, no. 2, pp. 18279–18284, 2014.

[28] “Orthotics and Prosthetics - Global Pipeline Analysis, Competitive Landscape and Market Forecasts to 2017,” NY, Rep. 1604176, 2011.

[29] G. Mcfadden, “Freedom of Information Survey Report 2011-2012,” LimbCare Corp.., Berkshire, Survey Rep., 2012.

[30] “Amputation,” *The UK Limb Loss Information Centre*, 2013. [Online]. Available: http://limblossinformationcentre.com/rehabilitation/amputation/what-is-amputation/. [Accessed: 20-Feb-2013].

[31] O. Gibson, “Paralympics closing ceremony review: an emotional and fiery finale,” *The Guardian*, 10-Sep-2012. [Online]. Available: http://www.guardian.co.uk/sport/2012/sep/09/paralympics-closing-ceremony-finale-coldplay.

[32] “London 2012 Paralympic athletes: the full list of competitors and disciplines,” *The Guardian*, 2013. [Online]. Available: http://www.guardian.co.uk/news/datablog/2012/aug/30/every-paralympic-athlete-and-their-sport-data. [Accessed: 12-Apr-2013].

[33] P. Kyberd and C. Wartenberg, “Survey of Upper-Extremity Prosthesis Users in Sweden and the United Kingdom,” *JPO J. Prosthetics Orthot.*, vol. 19, no. 2, pp. 55–62, 2007.

[34] C. Antfolk, M. D’Alonzo, M. Controzzi, G. Lundborg, B. Rosén, F. Sebelius, and C. Cipriani, “Artificial redirection of sensation from prosthetic fingers to the phantom hand map on transradial amputees: vibrotactile versus mechanotactile sensory feedback.,” *IEEE Trans. Neural Syst. Rehabil. Eng.*, vol. 21, no. 1, pp. 112–20, Jan. 2013.

[35] K. Kim and J. E. Colgate, “Haptic feedback enhances grip force control of sEMG-controlled prosthetic hands in targeted reinnervation amputees.,” *IEEE Trans. Neural Syst. Rehabil. Eng.*, vol. 20, no. 6, pp. 798–805, Nov. 2012.

[36] G. Di Pino and A. Benvenuto, “Implant of Intraneural Multielectrodes in Human for Controlling a 5-fingered Hand Prosthesis, delivering sensorial feedback and producing rehabilitative neuroplasticity,” in *The Fourth IEEE RAS/EMBS International Conference on Biomedical Robotics and Biomechatronics*, 2012, pp. 1831–1836.

[37] D. M. Rager, D. Alvares, I. Birznieks, S. J. Redmond, J. W. Morley, N. H. Lovell, and R. M. Vickery, “Generating tactile afferent stimulation patterns for

slip and touch feedback in neural prosthetics," *Proc. Annu. Int. Conf. IEEE Eng. Med. Biol. Soc. EMBS*, pp. 5922–5925, 2013.

[38] J. Kim, M. Lee, H. J. Shim, R. Ghaffari, H. R. Cho, D. Son, Y. H. Jung, M. Soh, C. Choi, S. Jung, K. Chu, D. Jeon, S.-T. Lee, J. H. Kim, S. H. Choi, T. Hyeon, and D.-H. Kim, "Stretchable silicon nanoribbon electronics for skin prosthesis.," *Nat. Commun.*, vol. 5, p. 5747, 2014.

[39] N. Muridan, P. H. Chappell, D. P. J. Cotton, A. Cranny, and N. M. White, "Detection of slip from multiple sites in an artificial finger," *J. Phys. Conf. Ser.*, vol. 178, pp. 1–6, Jul. 2009.

[40] N. Muridan, P. H. Chappell, A. Cranny, and N. M. White, "Texture sensor for a prosthetic hand," in *Eurosensors XXIV*, 2010, vol. 5, pp. 605–608.

[41] J. Baits, R. Todd, and J. Nightingale, "The Feasibility of an Adaptive Control Scheme for Artificial Prehension," in *Proceedings of the Instrumentaion Mechanical Engineers*, 1968, vol. 183, no. 3, pp. 54–59.

[42] P. J. Kyberd, N. Mustapha, F. Carnegie, and P. H. Chappell, "A clinical experience with a hierarchically controlled myoelectric hand prosthesis with vibro-tactile feedback," *Prosthet. Orthot. Int.*, vol. 17, no. 1, pp. 56–64, Apr. 1993.

[43] R. M. Crowder, "Tactile Sensing," 1998. [Online]. Available: http://www.southampton.ac.uk/~rmc1/robotics/artactile.htm. [Accessed: 15-Mar-2013].

[44] T. Pritchard and K. Alloway, Eds., *Medical neuroscience*, 1st ed. Connecticut: Hayes Barton Press, 1998.

[45] E. Kandel, J. Schwartz, and T. Jessell, *Principles of neural science*, 4th ed., McGraw Hill, 2000.

[46] S. J. Bensmaïa and M. Hollins, "The vibrations of texture," *Somatosens. Mot. Res.*, vol. 20, no. 1, pp. 33–43, 2003.

[47] J. Raisamo. (2009) . *Tactile Sensing & Feedback*, [Online] Available: *pervasive.jku.at*.

[48] T. Kawamura, K. Tani, and H. Yamada, *Measurement System of Fine Step-Height Discrimination Capability of Human Finger's Tactile Sense*. InTech, 2012.

[49] L. Jones and N. Sarter, "Tactile displays: Guidance for their design and application," *Hum. Factors J. Hum. Factors Ergon.*, vol. 50, no. 1, pp. 90–111, 2008.

[50] T. Kaaresoja and J. Linjama, "Perception of Short Tactile Pulses Generated by a Vibration Motor in a Mobile Phone," *First Jt. Eurohaptics Conf. Symp. Haptic Interfaces Virtual Environ. Teleoperator Syst.*, pp. 471–472, 2005.

[51] R. D. Howe and M. R. Cutkosky, “Sensing Skin Acceleration for Slip and Texture Perception,” in *IEEE International Conference in Robotics and Automation*, 1989, pp. 145–150.

[52] T. Wescott, “Sampling : What Nyquist Didn’t Say, and What to Do About It,”,Wescott Des. Serv., Oregon City, OR., Sem. Rep., 2015.

[53] N. Jamali and C. Sammut, “Majority Voting : Material Classification by Tactile Sensing Using Surface Texture,” *IEEE Trans. Robot.*, vol. 27, no. 3, pp. 508–521, 2011.

[54] X. Song, H. Liu, J. Bimbo, K. Althoefer, and L. D. Seneviratne, “Object Surface Classificaiton based on Friction Properties for Intelligent Robotic Hands,” in *World Automation Congress*, 2013, pp. 1–5.

[55] N. Muridan, P. Chappell, A. Cranny, and N. White, “Texture Sensing at a Fingertip,” in *Biomedical Engineering*, 2011.

[56] N. Mohamad Hanif, I. Elamvazuthi, S. Sulaiman, and S. S O, “Simulation and Control of Sensory-Mode Interaction in Haptic Systems,” *Int. J. Eng. Technol.*, vol. 9, no. 10, pp. 73–79, 2009.

[57] G. Merrett and C. Metcalf, “Design and qualitative evaluation of tactile devices for stroke rehabilitation,” in *Institution of Engineering (IET) Assisted Living 2011*, London, 2011.

[58] C. Basdogan, M. Lum, J. Salcedo, E. Chow, S. A. Kupiec, and A. Kostrewski, “Autostereoscopic and Haptic Visualization for Space Exploration and Mission Design,” in *Haptic Interfaces for Virtual Environment and Teleoperator Systems*, 2002, pp. 271–276.

[59] C. Basdogan, S. De, J. Kim, M. Muniyandi, H. Kim, and M. a Srinivasan, “Haptics in minimally invasive surgical simulation and training,” *IEEE Comput. Graph. Appl.*, vol. 24, no. 2, pp. 56–64, 2004.

[60] R. S. Dahiya, G. Metta, M. Valle, and G. Sandini, “Tactile Sensing—From Humans to Humanoids,” *IEEE Trans. Robot.*, vol. 26, no. 1, pp. 1–20, Feb. 2010.

[61] J. Pasquero, “Survey on communication through touch,” Dept. Elect. Comp. Engr, McGill Univ., Montreal, Canada, Tech. Rep. TR-CIM 06.04, 2006.

[62] E. Y. Chen and B. A. Marcus, “EXOS Slip Display Research and Development,” *Dyn. Syst. Control*, vol. 1, no. 55, pp. 265–270, 1994.

[63] P. M. Taylor, A. Moser, and A. Creed, “A sixty-four element tactile display using shape memory alloy wires,” *Displays*, vol. 1, no. 18, pp. 163–168, 1998.

[64] Y. Makino, N. Asamura, and H. Shinoda, “Multi primitive tactile display based on suction pressure control,” in *Proceedings - 12th International Symposium on Haptic Interfaces for Virtual Environment and Teleoperator Systems, HAPTICS*, 2004, pp. 90–96.

[65] M. A. Srinivasan and K. Dandekar, “An investigation of the mechanics of tactile sense using two-dimensional models of the primate fingertip.,” *J. Biomech. Eng.*, vol. 118, no. 1, pp. 48–55, 1996.

[66] S. Demain, C. D. Metcalf, G. V Merrett, D. Zheng, and S. Cunningham, “A narrative review on haptic devices: relating the physiology and psychophysical properties of the hand to devices for rehabilitation in central nervous system disorders.,” *Disabil. Rehabil. Assist. Technol.*, vol. 8, no. 3, Jul. 2012.

[67] J. Sinapov, V. Sukhoy, R. Sahai, and A. Stoytchev, “Vibrotactile Recognition and Categorization of Surfaces by a Humanoid Robot,” *IEEE Trans. Robot.*, vol. 27, no. 3, pp. 488–497, 2011.

[68] K. Bark, J. W. Wheeler, S. Premakumar, and M. R. Cutkosky, “Comparison of Skin Stretch and Vibrotactile Stimulation for Feedback of Proprioceptive Information,” *2008 Symp. Haptic Interfaces Virtual Environ. Teleoperator Syst.*, Reno, pp. 71–78, Mar. 2008.

[69] H.N. Ho and L. A. Jones, “Contribution of thermal cues to material discrimination and localization.,” *Percept. Psychophys.*, vol. 68, no. 1, pp. 118–28, Jan. 2006.

[70] E. Kandel, J. Schwartz, and T. Jessell, “Coding of Sensory Information,” in *Principles of neural science*, 4th ed., McGraw Hill, 2000, pp. 411–429.

[71] M. D’Alonzo, F. Clemente, and C. Cipriani, “Vibrotactile stimulation promotes embodiment of an alien hand in amputees with phantom sensations.,” *IEEE Trans. Neural Syst. Rehabil. Eng.*, vol. 23, no. 3, pp. 450–457, 2014.

[72] “AB-004-Understanding ERM Vibration Motor Characteristics,” *Precision Microdrives TM*, 2012. [Online]. Available: http://www.precisionmicrodrives.com/application-notes-technical-guides/application-bulletins/ab-004-understanding-erm-characteristics-for-vibration-applications. [Accessed: 24-Aug-2012].

[73] S. Rao, “High-definition haptics: Feel the difference!,” *Texas Instruments Inc.*, 2012. [Online:]. Available: http://www.ti.com/lit/an/slyt483/slyt483.pdf. [Accessed: 20-Dec-2012]

[74] F. Wang, “Haptic Energy Consumption,” , Texas Instr. Inc., Dallas, TX., App. Rep., SLOA194, 1–17, 2014.

[75] T. (Maxim) Blankenship, “Tactile Feedback Solutions Using Piezoelectric Actuators,” 2011. [Online]. Available: http://www.maxim-ic.com/app-notes/index.mvp/id/4706.

[76] “Product Data Sheet : 5mm Vibration Motor (Model 304-109),” *Precision Microdrives TM*, 2012. [Online]. Available: https://catalog.precisionmicrodrives.com/order-parts/product/304-109-5mm-vibration-motor-8mm-type. [Acessed: 22-Aug-2012].

[77] "Product Data Sheet - 10mm Linear Resonant Actuator (C10-100)," *Precision Microdrives TM*, 2012. [Online]. Available: https://catalog.precisionmicrodrives.com/order-parts/product/c10-100-10mm-linear-resonant-actuator-4mm-type. [Accessed: 20-Aug-2012].

[78] E. Seigel, "Haptics technology: Picking up good vibrations," *EE Times*, 2011. [Online]. Available: http://www.eetimes.com/design/medical-design/4218132/Haptics-technology--picking-up-good-vibrations [Accessed: 15-Jan-2013].

[79] "Haptics: Touch Feedbacks that Really Moves You." *Texas Instruments*, 2013. [Online]. Available: http://www.ti.com.cn/cn/lit/ml/slyt418/slyt418.pdf [Accessed: 12-Jan-2013].

[80] M. Levin and A. Woo, "Making displays work for you Tactile-Feedback Solutions for an Enhanced User Experience," in *Information Display*, Campbell, CA., Society for Information Display, 2009, pp. 18–21.

[81] "Pico Vibe ^{TM} Model : 304-111," *Precision Microdrives*, 2013. [Online]. Available: https://catalog.precisionmicrodrives.com/order-parts/product/304-111-5mm-vibration-motor-11mm-type [Accessed: 22-Dec-2012].

[82] R. C. Dorf and R. H. Bishop, *Modern Control Systems*, 10th ed. , Upper Saddle River, NJ: Prentice Hall Inc., 2005.

[83] K. H. Nam, "Preliminaries for Motor Control," in *AC Motor Control and Electrical Vehicle Applications*, CRC Press, 2010, pp. 3–4.

[84] D. H. Shreve, "Introduction to vibration technology," , IRD Mech. Inc., Columbus, OH., Tech. Rep., 1994.

[85] J. C. Makous, R. M. Friedman, and C. J. Vierck, "A critical band filter in touch.," *J. Neurosci.*, vol. 15, no. 4, pp. 2808–18, Apr. 1995.

[86] N. S. Nise, *Control Systems Engineering*, 6th ed. , Hoboken, NJ : John Wiley & Sons, Inc., 2011.

[87] N. H. H. M. Hanif, P. H. Chappell, A. Cranny, and N. M. White, "Vibratory feedback for artificial hands," in *2013 International Conference on Electronics, Computer and Computation (ICECCO)*, Ankara, 2013, pp. 247–250.

[88] *Ultra High Accuracy Laser Displacement Meter LC-2400 Series*, Keyence Corp., Osaka, Japan, pp. 43–44, 1994.

[89] *Shimmer3: Wireless Sensor Platform*, Shimmer, Dublin, Ireland, pp. 1–2, 2013.

[91] *MEMS INERTIAL SENSOR : 3Axis - 2g/6g Linear Accelerometer*, ST Microelectronics, pp. 1–14, 2005.

[92] *Decoupling Techniques*, Analog Devices Inc., Norwood, MA., pp. 1–14, 2009.

[93] S. Sabin and R. Chitwood, "Understanding Discrepancies in Vibration Amplitude Readings Between Different Instruments," *Orbit*, no. 1, March 1994, pp. 40–57, 2006.

[94] N. Doertenbach, "The Calculation of Grms." QualMark Corp., Denver, CO., Tech. Rep., 2001.

[95] N. H. H. M. Hanif, P. H. Chappell, A. Cranny, and N. M. White, "Development of Vibrotactile Sensory Feedback For Prosthetic Hand Users," in *IASTED International Conference Biomedical Engineering (BioMed 2014)*, 2014.

[96] N. Muridan, "Sensing Texture Using An Artificial Finger," PhD dissertation, Elec. Comp. Sci., University of Southampton, 2013.

[97] "NI DAQPad 6015 / 6016 Family Specifications." *National Instruments*, pp. 1–10, 2005, [Online]. Available: http://www.ni.com/pdf/manuals/370969b.pdf [Accessed: 4-Jan-2014]

[98] C. M. Light and P. H. Chappell, "Development of a lightweight and adaptable multiple-axis hand prosthesis," *Med. Eng. Phys.*, vol. 22, no. 10, pp. 679–684, 2000.

[99] J. Karki, "Signal Conditioning Piezoelectric Sensors," Texas Inst. Inc., Applic. Rep. SLOA033A, 2000.

[100] I. Altinay, A. Muralidhar, "Phoenix Ambulatory Blood Pressure Monitor Project,", Halberg Chr. Centr., Univ. of Minnesota, Roseville, MN., Tech. Rep., 2007.

[101] *Interfacing Piezo Film to Electronics*, Measurement Specialties Inc., Hampton, VA., pp. 1–8, 2006.

[102] P. H. Chappell, N. Muridan, A. Mohamad Hanif, N. Hazrin H., Cranny, and N. M. White, "Sensing texture using an artificial finger and a data analysis based on the standard deviation," *IET Sci. Meas. Technol.*, pp. 1–9, 2015.

[103] S. J. Lederman, M. M. Taylor, "Fingertip force,surface geometry and the perception of roughness by active touch," *Percept. Psychophys.*, vol. 12, no. 5, pp. 401–408, 1972.

[104] S. J. Lederman, R. L. Klatzky, C. L. Hamilton, and G. I. Ramsay, "Perceiving roughness via a rigid probe : Psychophysical effects of exploration speed and mode of touch," *Haptics-e Electron. J. Haptic Res.*, vol. 1, no. 1, pp. 1–21, 1999.

[105] B. Messner and D. Tilbury, "DC Motor Speed: PID Controller Design," Mathworks, Applic. Rep., 2014. .

[106] N. H. H. M. Hanif, P. H. Chappell, A. Cranny, and N. M. White, "Surface Texture Detection with Artificial Fingers," in *37th Annual International*

Conference of IEEE Engineering in Medicine and Biology Society, 2015, pp. 8018–8021.

[107] "DRV2603 Haptic Drive with Auto-Resonance Detection for Linear Resonance Actuators (LRA)." *Texas Instruments Inc*, 2012 [Online]. Available: http://www.ti.com/lit/ds/symlink/drv2603.pdf. [Accessed: 5-Jan 2014] .

[108] "Psychophysics,n," *OED Online, Oxford University Press*, 2015. [Online]. Available: http://www.oed.com/view/Entry/238083?redirectedFrom=psychophysics. [Accessed: 22-Jan-2016].

[109] G. Gescheider, "Psychophysical Measurement of Thresholds: Differential Sensitivity," in *Psychophysics: The Fundamental*, 3rd ed., New Jersey: Lawrence Erlbaum Associates, 1997, pp. 1–15.

[110] J. R. Warmbrod, "Calculating, Interpreting, and Reporting Estimates of 'Effect Size' (Magnitude of an Effect or the Strength of a Relationship)." Texas Tech. University, Texas, pp. 1–22, 2001.

[111] D. Sharpe, "Your Chi-Square Test Is Significant: Now What?," *Pract. Assesment, Res. Eval.*, vol. 20, no. 8, 2015.

[112] "Chi-Square Test for Association using SPSS Statistics," *Laerd Statistics*, 2013. [Online]. Available: https://statistics.laerd.com/spss-tutorials/chi-square-test-for-association-using-spss-statistics.php.

[113] "Chi-Square Test for Independence," *StatTrek.com*, 2015. [Online]. Available: http://stattrek.com/chi-square-test/independence.aspx?Tutorial=AP.

Appendix A: Product Data Sheet for Pico Vibe™ 5mm Vibration Motor

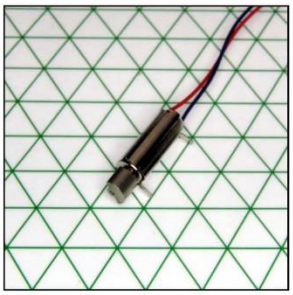

5mm Vibration Motor - 11mm Type
Shown on 6mm Isometric Grid

PRECISION MICRODRIVES™

Product Data Sheet
Pico Vibe™
5mm Vibration Motor - 11mm Type

Model: 304-111

Ordering Information

The model number 304-111 fully defines the model, variant and additional features of the product. Please quote this number when ordering.
For stocked types, testing and evaluation samples can be ordered directly through our online store.

Datasheet Versions

It is our intention to provide our customers with the best information available to ensure the successful integration between our products and your application. Therefore, our publications will be updated and enhanced as improvements to the data and product updates are introduced.
To obtain the most up-to-date version of this datasheet, please visit our website at:
www.precisionmicrodrives.com
The version number of this datasheet can be found on the bottom left hand corner of any page of the datasheet and is referenced with an ascending R-number (e.g. R002 is newer than R001). Please contact us if you require a copy of the engineering change notice between revisions.

If you have any questions, suggestions or comments regarding this publication or need technical assistance, please contact us via email at:
enquiries@precisionmicrodrives.com or call us on +44 (0) 1932 252 482

Key Features

Body Diameter:	4.5 mm [+/- 0.2]
Body Length:	11 mm [+/- 0.2]
Counterweight Radius:	2 mm [+/- 0.2]
Counterweight Length:	3 mm [+/- 0.2]
Shaft Orientation:	Inline
Rated Operating Voltage:	3 V
Rated Vibration Speed:	15,000 rpm [+/- 3,750]
Typical Rated Operating Current:	50 mA
Typical Normalised Amplitude:	1 G

Typical Vibration Motor Performance Characteristics

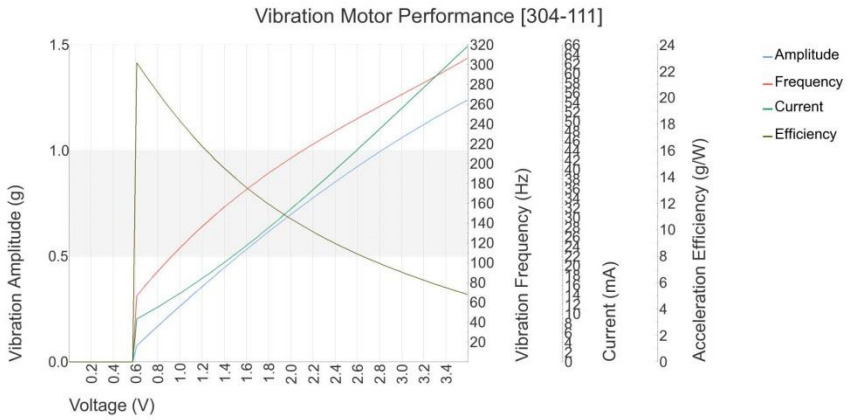

Physical Specification

PARAMETER	CONDITIONS	SPECIFICATION
Body Diameter	Max body diameter or max face dimension where non-circular	4.5 mm [+/- 0.2]
Body Length	Excl. shafts, leads and terminals	11 mm [+/- 0.2]
Unit Weight		1.1 g
No. of Output Shafts		1
Counterweight Radius	Radius from shaft for non-cylindrical weights	2 mm [+/- 0.2]
Counterweight Length		3 mm [+/- 0.2]
Shaft Orientation		Inline

Construction Specification

PARAMETER	CONDITIONS	SPECIFICATION
Motor Construction		Coreless
Commutation		Precious Metal Brush
No. of Poles		3
Bearing Type		Sintered Bronze

Leads & Connectors Specification

PARAMETER	CONDITIONS	SPECIFICATION
Lead Length	Lead lengths defined as total length or between motor and connector	100 mm [+/- 2]
Lead Strip Length		1.5 mm [+/- 0.5]
Lead Wire Gauge		32 AWG
Lead Configuration		Straight

Operational Specification

PARAMETER	CONDITIONS	SPECIFICATION
Rated Operating Voltage		3 V
Rated Vibration Speed	At rated voltage using the inertial test load	15,000 rpm [+/- 3,750]
Max. Rated Operating Current	At rated voltage using the inertial test load	90 mA
Rated Inertial Test Load	Mass of standard test sled	100 g
Max. Start Voltage	With the inertial test load	2 V
Min. Vibration Amplitude	Peak-to-peak value at rated voltage using the inertial test load	0.7 G
Max. Operating Voltage		3.6 V
Max. Start Current	At rated voltage	110 mA
Min. Insulation Resistance	At 50V DC between motor terminal and case	10 MOhm

Important: The characteristics of the motor is the typical operating parameters of the product. The data herein offers design guidance information only and supplied batches are validated for conformity against the specifications on the previous page.

Typical Performance Characteristics

PARAMETER	CONDITIONS	SPECIFICATION
Typical Rated Load Power Consumption	At rated voltage and load	150 mW
Typical Rated Operating Current	At rated voltage using the inertial test load	50 mA
Typical Vibration Amplitude	Peak-to-peak value at rated voltage using the inertial test load	1 G
Typical Start Current	At rated voltage	90 mA
Typical Vibration Efficiency	At rated voltage using the inertial test load	6.7 G/W
Typical Normalised Amplitude	Peak-to-peak vibration amplitude normalised by the inertial test load at rated voltage	1 G
Typical Start Voltage	With the inertial test load	0.6 V
Typical Terminal Resistance		33 Ohm
Typical Terminal Inductance		80 uH

Typical Haptic Characteristics

PARAMETER	CONDITIONS	SPECIFICATION
Typical Lag Time	At rated voltage using the inertial test load	16 ms
Typical Rise Time	At rated voltage using the inertial test load	28 ms
Typical Stop Time	At rated voltage using the inertial test load	36 ms
Typical Active Brake Time	Time taken from steady-state to 0.04 G under inverse polarity at max. voltage	18 ms

Typical Durability Characteristics

PARAMETER	CONDITIONS	SPECIFICATION
Typical Min. Counterweight Pullout		9.8 N

Environmental Characteristics

PARAMETER	CONDITIONS	SPECIFICATION
Max. Operating Temp.		60 Deg.C
Min. Operating Temp.		-20 Deg.C
Max. Storage Temp.		80 Deg.C
Min. Storage Temp.		-40 Deg.C

Typical Packing Conditions

PARAMETER	CONDITIONS	SPECIFICATION
Carton Type		Boxed Trays

Appendix B: Relationship between input voltages to the vibration amplitude

Voltage, V (V)	Transient Response		Speed, ω (rad/s)	Frequency, f (Hz)	Amplitude of Vibration (peak-to-peak)		
	Rise Time, T_r (ms)	Settling Time, T_s (ms)			Displace-ment (μm)	Acceleration (ms^{-2})	Gravitational Acceleration (G)
0.6	23.5	41.9	263	41.86	0.82	0.056	0.0056
1.0	24.0	41.9	439	69.87	1.42	0.27	0.028
1.5	23.5	41.9	658	104.72	2.16	0.92	0.10
2.0	23.5	41.9	878	139.74	2.84	2.16	0.22
2.5	23.5	41.9	1100	175.07	3.62	4.24	0.42
3.0	23.8	41.9	1320	210.08	4.2	7.2	0.76
3.5	23.5	41.9	1540	245.1	5.0	11.4	1.12
3.6	23.5	41.9	1580	251.46	5.2	13.0	1.5

Appendix C: Effects of Output Voltage to Acceleration and Frequency

Effects of Voltage Supply to Acceleration (g_{rms})

Voltage (V)	*X-axis(g_{rms})*	*Y-axis (g_{rms})*	*Z-axis (g_{rms})*
1	0.0935	0.1518	0.0819
1.5	0.2568	0.1907	0.131
2	0.4789	0.4131	0.2466
2.5	0.9212	0.4994	0.4969
3	1.424	0.6914	1.0386
3.5	1.81	0.7066	1.5377

Effects of Voltage Supply to Frequency (Experiment & Simulated)

Voltage (V)	*Frequency (Hz) (Experiment)*	*Frequency (Hz) (Simulation)*
1	152.6	69.87
1.5	190.7	104.72
2	248	139.74
2.5	286.1	175.07
3	305.2	210.08
3.5	324.2	245.1

Appendix D: Circuitry of Movement Mechanism of the Sliding Block

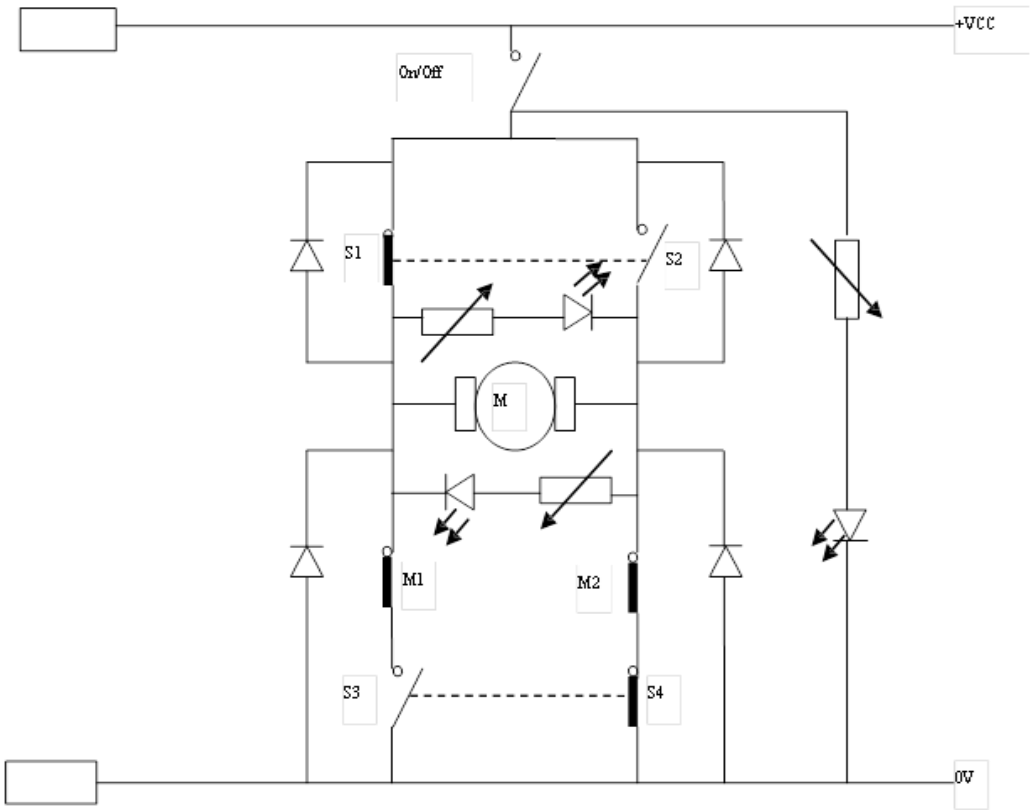

The diodes provide reverse EMF protection for the circuit; the LED's give an indication for motor direction. S1, 2, 3 and 4 are all part of a Double Pole Double throw (DPDT) ON-ON switch. M1 and 2 are the end stop micro switches which are mounted to the rig to stop the moving block before it reaches the end of travel.

Appendix E: Voltage Amplifier

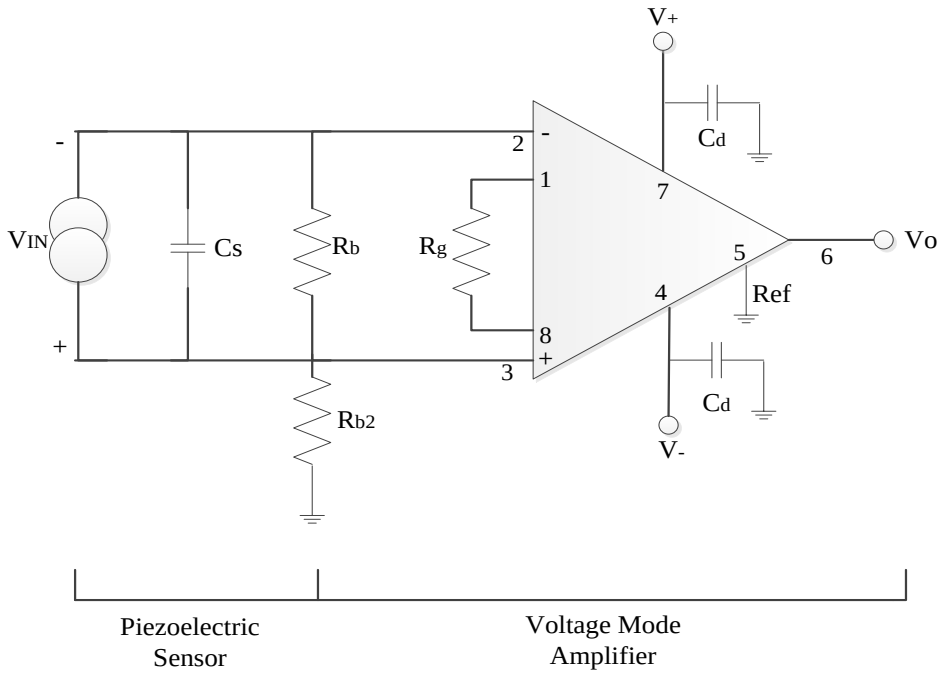

Input bias resistors, R_b, = 100 kΩ , R_{b2} = 240 Ω.

Sensor capacitance, C_s, = 1.786 nF (measured using an LCR meter)

External gain resistor R_g = 240Ω.

Amplifier Gain = 200

Appendix F: Measurement of Encoder Size

Measurement	*Block displacement (mm)*	*Data length*	*Number of pairs*	*Encoder pair widths*
1	111.98	138130	1312	0.08535061
2	109.99	1.75E+05	1258	0.087432432
3	103.13	2.06E+05	1185	0.087029536
4	98.16	1.78E+05	1156	0.084913495
5	109.19	1.39E+05	1246	0.087632424
				0.086471699

Appendix G: Measurements of Surface Gratings

Measurements were done using a microscope (Motic B3 Professional Series). The microscope was calibrated by measuring a calibration dot (1 mm diameter) printed on a slide provided by the manufacturer. The microscope is properly calibrated if the measured diameter matches the diameter of the calibration dot.

Surface Texture B

	Groove (µm)	*Ridge (µm)*	*Depth (µm)*
	196.9	195.7	151.2
	192.7	195.8	157.1
	193.3	196.6	148.1
	188.5	205.5	144.9
	191.5	206.9	143.8
Mean	**192.58**	**200.1**	**149.02**
in mm	**0.19258**	**0.2001**	**0.14902**

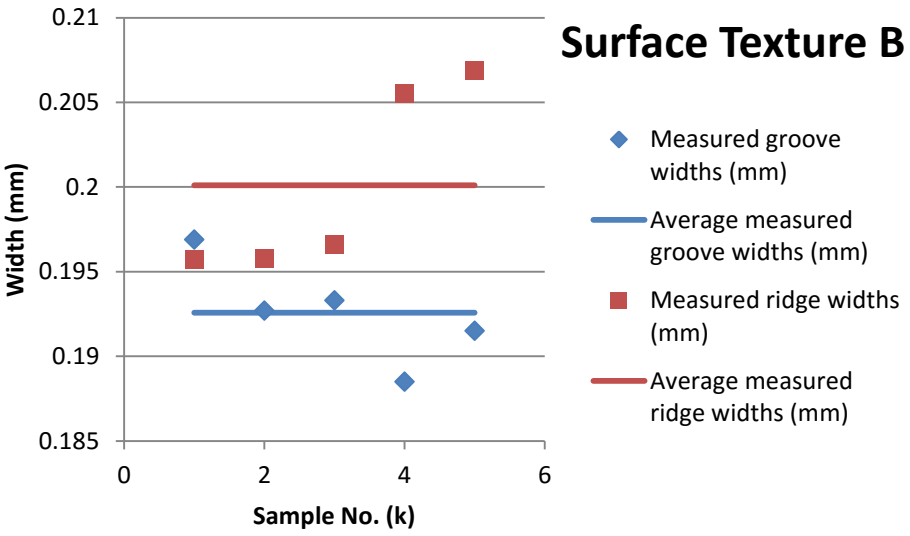

Surface Texture C

	Groove (µm)	*Ridge (µm)*	*Depth (µm)*
	311.9	675.8	241.7
	297	681.7	247
	301.5	671.4	249.8
	303	686.3	236.5
	304.5	672.8	240.9
	292.6	668.3	240.9
Mean	**301.75**	**676.05**	**242.8**
in mm	**0.30175**	**0.67605**	**0.2428**

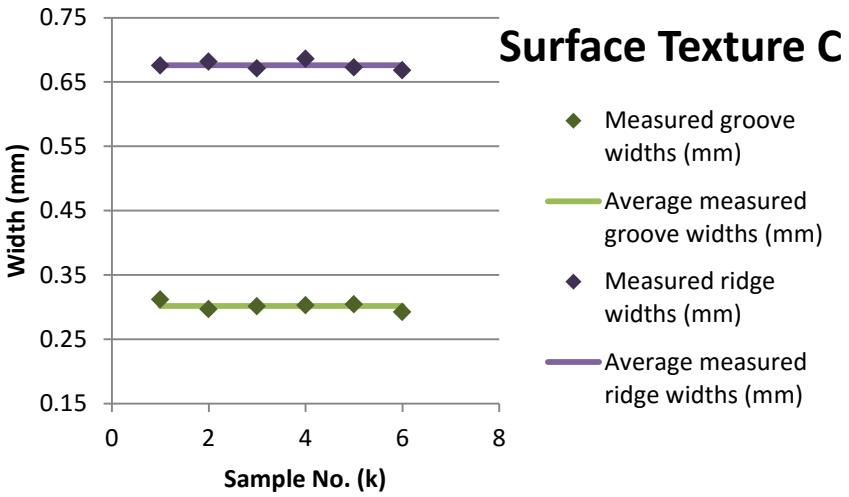

Surface Texture D

	a	*b*	*c*	*d*	*e*	*f*	*g*	*h*
	180	230.2	179.7	417.3	209.4	603	206.4	778.3
	172.4	208	191.7	409.9	203.5	609	200.5	777
	176.7	222.8	190.1	414.4	200.5	597.1	203	796.2
	167.8	218.4	190.1	415.9	202	611.9	216.8	788.8
	175.2	193.1	184.2	406.9	225.7	583.7	210.9	763.4
	212.4	188.6	228.7	408.4	209.4	562.9	231.7	760.4
Mean	**180.75**	**210.1833**	**194.083**	**412.133**	**208.417**	**594.6**	**211.55**	**777.35**
in mm	**0.18075**	**0.210183**	**0.19408**	**0.41213**	**0.20842**	**0.5946**	**0.21155**	**0.77735**

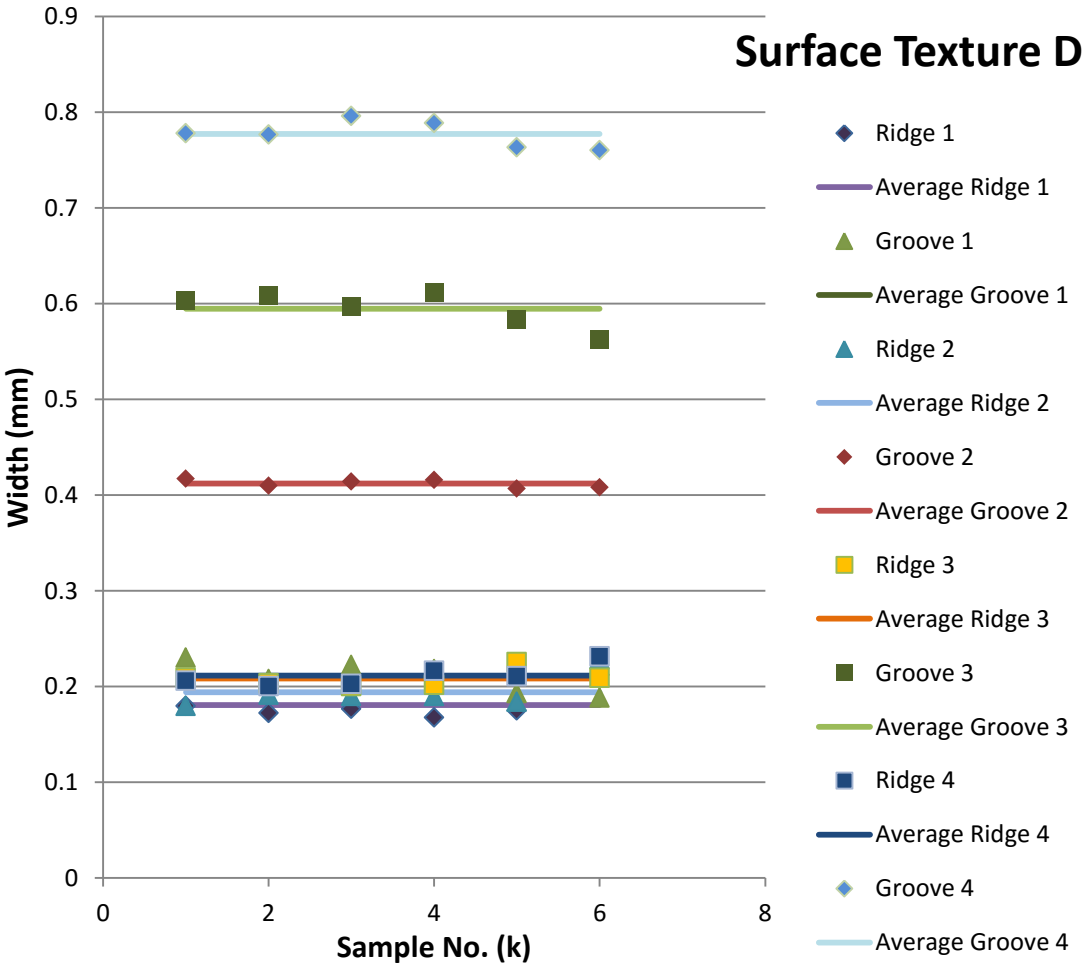
Surface Texture D
Width (mm)
Sample No. (k)
0.9
0.8
0.7
0.6
0.5
0.4
0.3
0.2
0.1
0
0
2
4
6
8
Ridge 1
Average Ridge 1
Groove 1
Average Groove 1
Ridge 2
Average Ridge 2
Groove 2
Average Groove 2
Ridge 3
Average Ridge 3
Groove 3
Average Groove 3
Ridge 4
Average Ridge 4
Groove 4
Average Groove 4

Appendix H: Output Plots for Vibration Motor for Different Vibration Patterns

Pattern A

Plot of g acceleration vs time

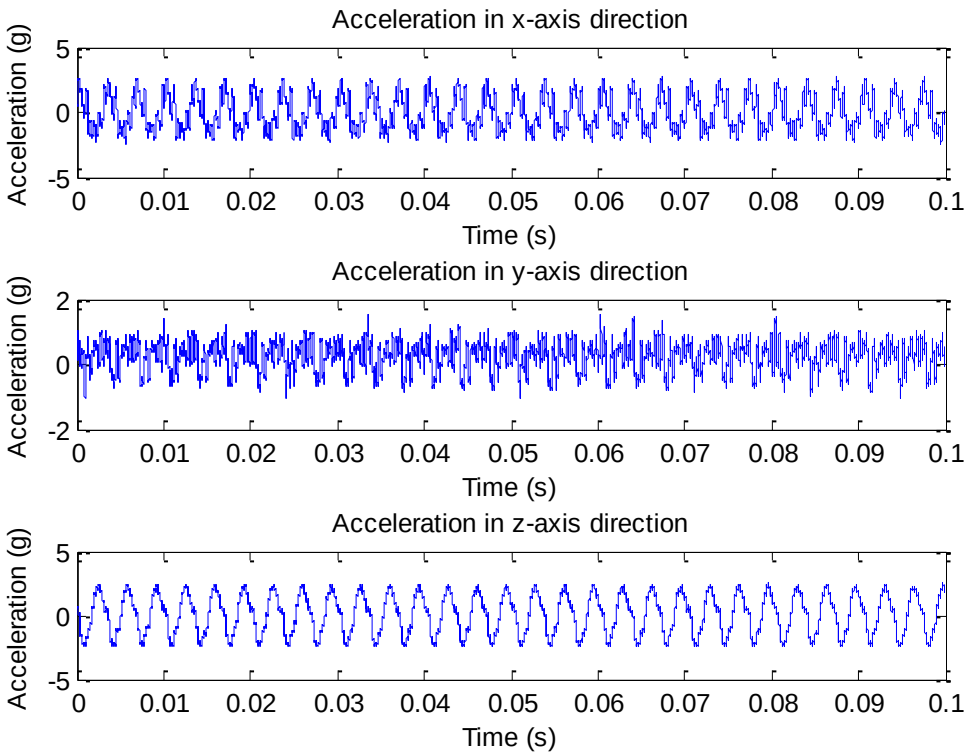

FFT Plot

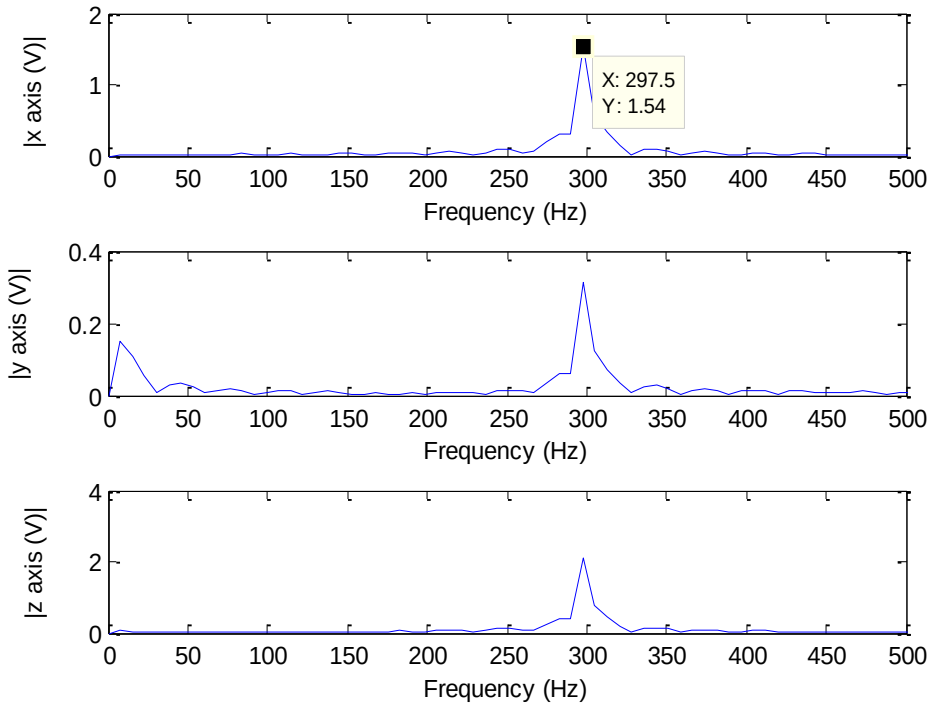

Pattern B

Plot of g acceleration vs time

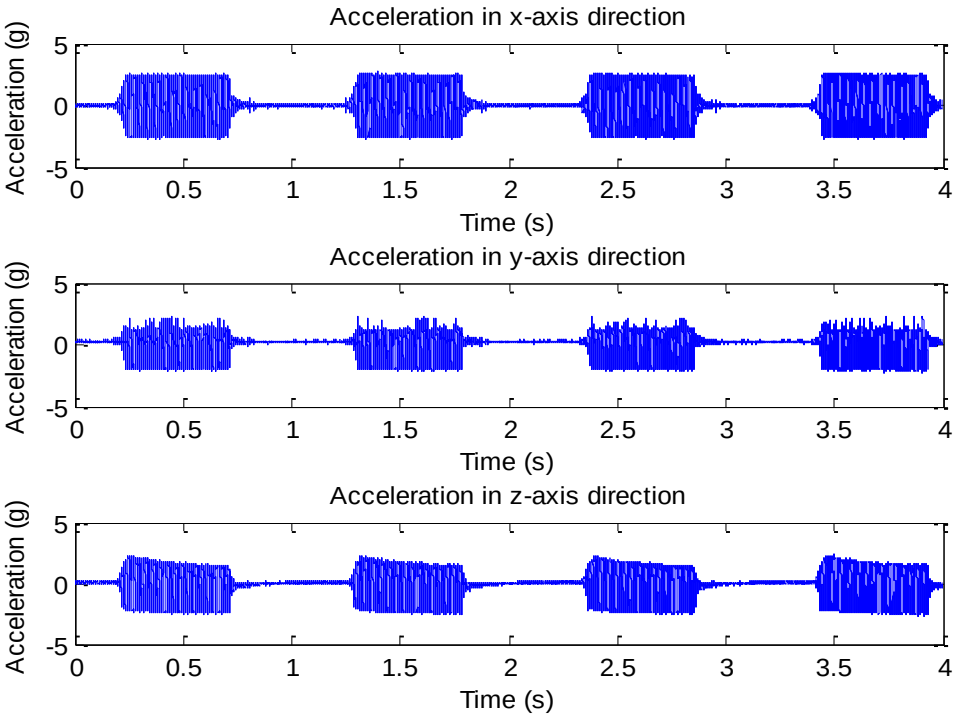

FFT Plot

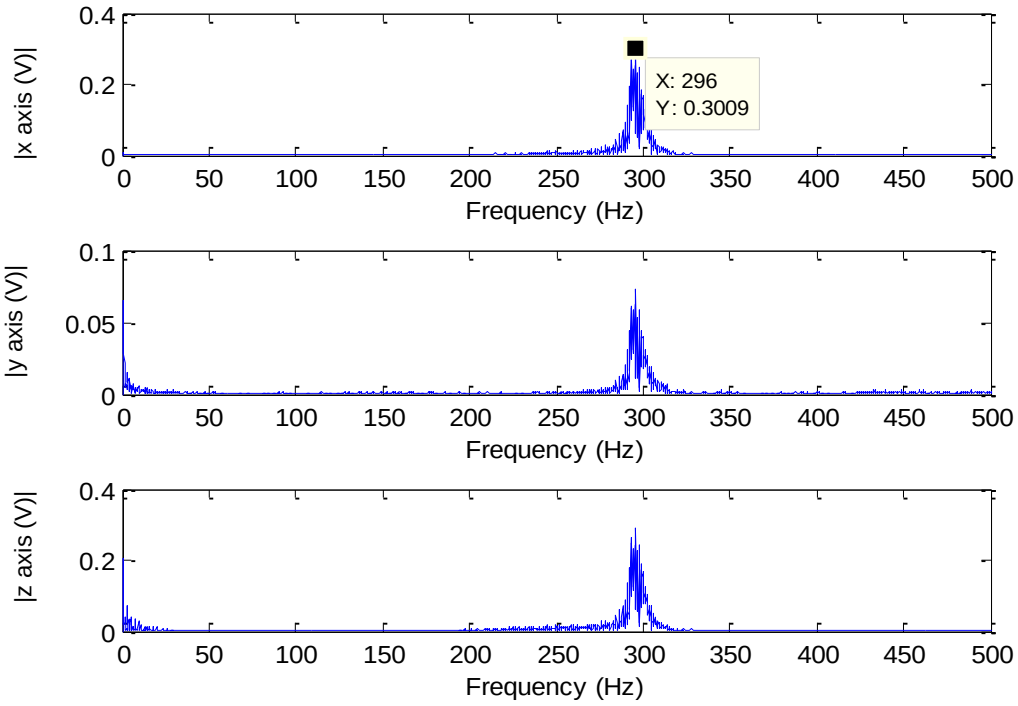

Pattern C

Plot of g acceleration vs time

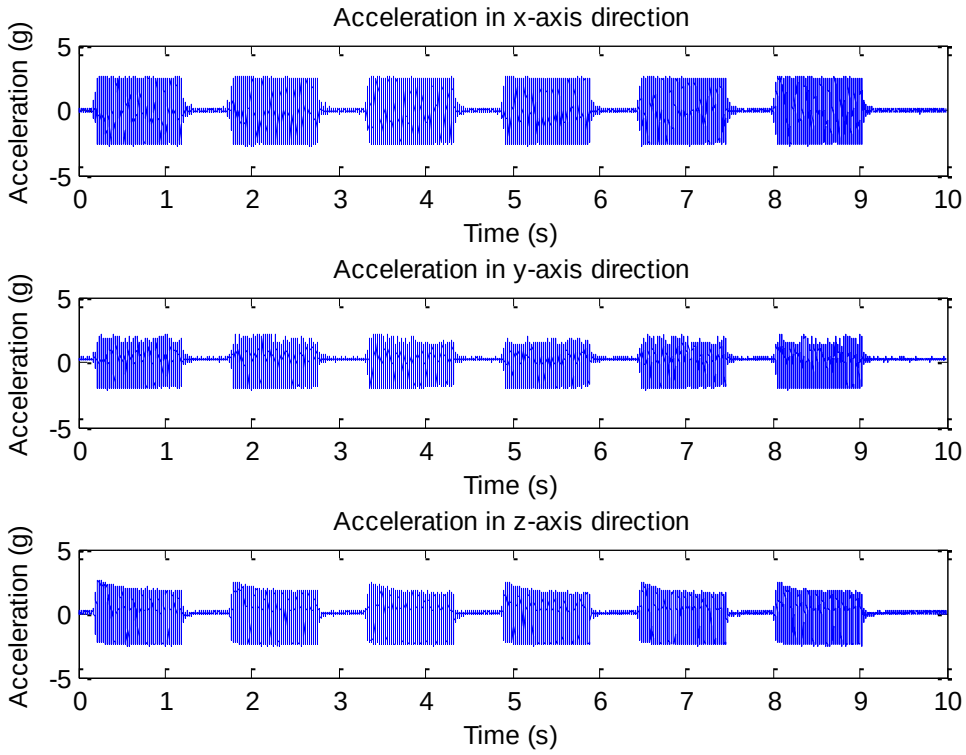

FFT Plot

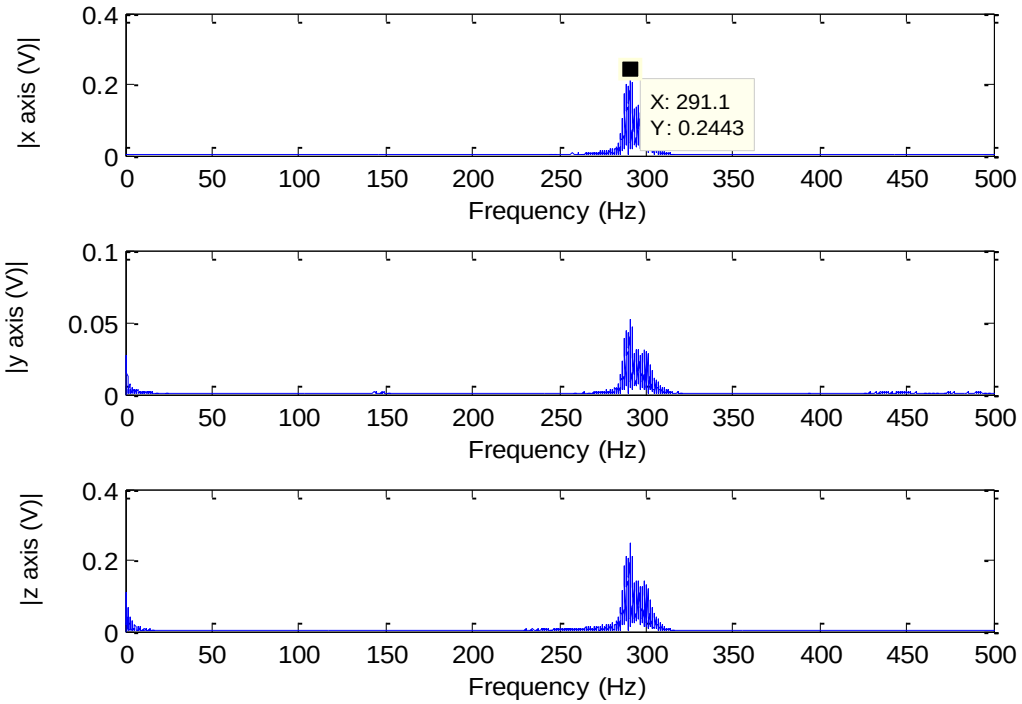

Pattern D

Plot of g acceleration vs time

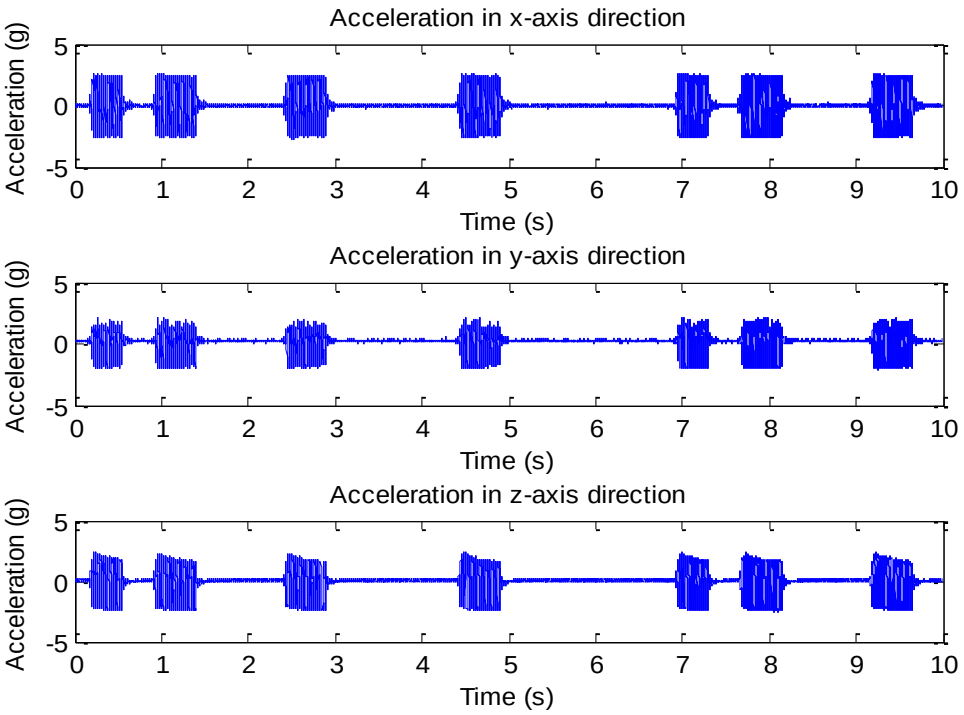

FFT Plot

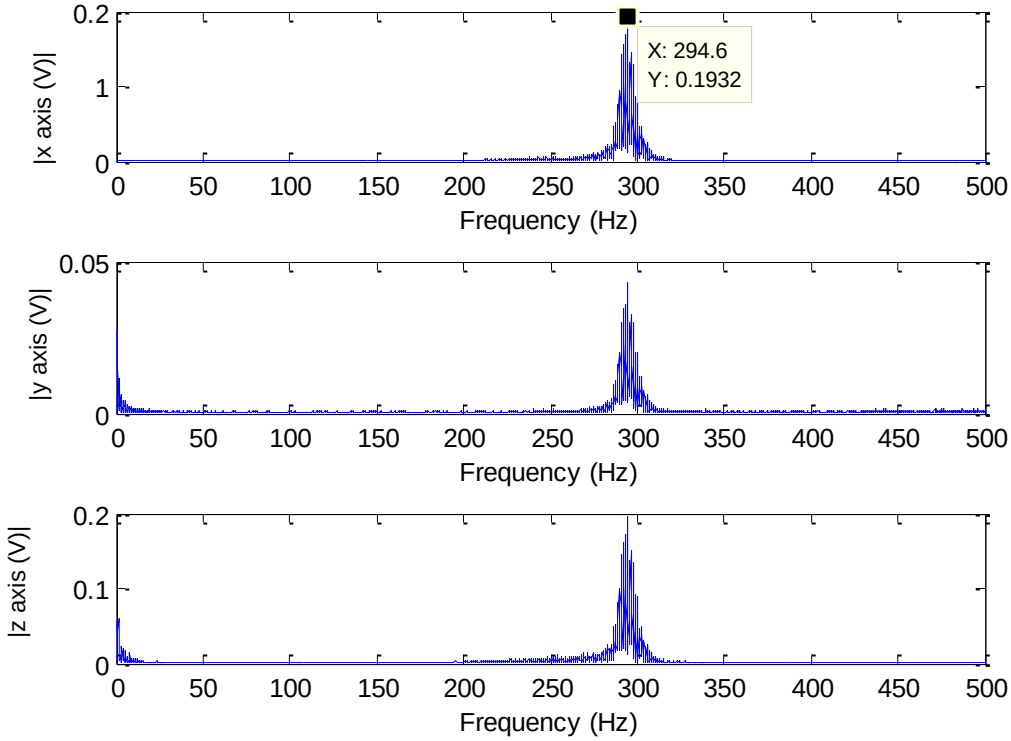
|x axis (V)|
0.2
1
0
X: 294.6
Y: 0.1932
0 50 100 150 200 250 300 350 400 450 500
Frequency (Hz)
|y axis (V)|
0.05
0
0 50 100 150 200 250 300 350 400 450 500
Frequency (Hz)
|z axis (V)|
0.2
0.1
0
0 50 100 150 200 250 300 350 400 450 500
Frequency (Hz)

Appendix I: Ethics Documentation (ERGO/FPSE/15290)

FPSE Ethics Committee
FPSE EC Application Form Ver 6.6d

Refer to the *Instructions* and to the *Guide* documents for a glossary of the key phrases in **bold** and for an explanation of the information required in each section. The *Templates* document provides some text that may be helpful in presenting some of the required information.

Replace the highlighted text with the appropriate information.

Note that the size of the text entry boxes provided on this form does **not** indicate the expected amount of information; instead, refer to the *Instructions* and to the *Guide* documents in providing the complete information required in each section. Do **not** duplicate information from one text box to another.

Reference number: ERGO/FPSE/15290	Version: 1.1	Date: 2015-05-10
Name of **investigator**(s): Noor Hazrin Hany Binti MOHAMAD HANIF		
Name of supervisor(s) (if student **investigator**(s)): 1. Paul CHAPPELL 2. Neil WHITE 3. Andy CRANNY		
Title of study: Psychophysics investigations in associating surface textures with vibrations		
Expected study start date: 22/6/2015	Expected study end date: 14/8/2015	
Note that the dates requested on the "IRGA" form refer to the start and end of *data collection*. These are not the same as the start and end dates of the study for which approval is sought. Note that approval must be obtained before the study commences; retrospective approval cannot be given.		

The investigator(s) undertake to:

- Ensure the study Reference number ERGO/FPSE/15290 is prominently displayed on all advertising and study materials, and is reported on all media and in all publications;
- Conduct the study in accordance with the information provided in the application, its appendices, and any other documents submitted;
- Conduct the study in accordance with University policy governing research involving human **participants** (http://www.southampton.ac.uk/ris/policies/ethics.html);
- Conduct the study in accordance with University policy on data retention (http://www.southampton.ac.uk/library/research/researchdata/);
- Submit the study for re-review (as an amendment through ERGO) or seek FPSE EC advice if any changes, circumstances, or outcomes materially affect the study or the information given;
- Promptly advise an appropriate authority (Research Governance Office) of any adverse study outcomes, changes, or circumstances (via an adverse event notification through ERGO);
- Submit an end-of-study form as may be required by the Research Governance Office upon completion of the study.

REFER TO THE INSTRUCTIONS DOCUMENT WHEN COMPLETING THIS FORM.

PRE-STUDY

Characterise the proposed **participants**
Number of participants required: Fifteen (15) The participants will be recruited amongst friends of the main investigator as the study requires some level of time commitment. It is also easier to have participation amongst friends as they could be approached face-to-face.

Describe how **participants** will be approached
Prospective participants will be approached personally by the investigator. The investigator will give a detailed description of the study, the time requirements, and the aims of the research, before asking whether the prospective participant might be interested in taking part. If they express interest, they will be given a copy of the participant information sheet and asked contact the investigator if they wish to take part.

Describe how inclusion and/or exclusion criteria will be applied (if any)
Participants will be recruited on a first-come, first-served basis, subject to the following inclusion and exclusion criteria. Inclusion criteria: 1. Male and female participants over the age of 18 2. Able to understand and follow simple instructions 3. Able to tolerate to the sensation of haptic vibrations transcutaneously applied to the upper arm 4. Medically stable 5. Intact skin condition of upper limb such that necessary haptic actuators can be placed using a Velcro strap Exclusion criteria: 1. Allergic to plastic material / micropore tape / Velcro band 2. Contra – indications to vibrations at the skin surface 3. Pacemaker users 4. Poorly controlled epilepsy 5. Not on any long term medication 6. No history of upper motor neuron (UMN) injury / condition /treatment

Justifications on the inclusion and exclusion criteria:

1. This study requires participants to identify different patterns of vibrations felt on their upper arms. The maximum duration per vibration is 10 seconds depending on the vibration patterns. It would be harmless to healthy participants, but it may inflict slight discomfort and cause possible side effects to those listed in the exclusion criteria.

2. The participants should also be medically stable and able to tolerate to haptic vibrations trancutaneously applied to the upper arm to ensure reliability and accuracy of the data collected during this study.

3. The haptic actuator that generates the vibration will be strapped to the participants' upper arms using Velcro band and micropore tape during the study. Although the vibration test could be done on a thin layer of clothing, strapping the motor on a bare skin is more preferred. It is therefore important that the participants have intact skin condition on the upper limb and are not allergic to the materials used for strapping the actuators.

Describe how **participants** will decide whether to take part

Participants will likely first consider whether the research sounds interesting, followed by consideration of the amount of time required, and then may go on to consider the invasiveness of the study. If they have expressed some interest, a copy of the participant information form will be given to them by hand. After receipt of the form, the participant is left with a period of not less than one day to consider participation before a verbal reply is required. No further effort will be made to encourage participation. This strategy is believed to be sufficient to permit informed consent to participation in the study.

Participant Information

Provide the **Participant Information** in the form that it will be given to **participants** as an appendix. All studies must provide **participant information**.

Consent Form

Provide the **Consent Form** (or the request for consent) in the form that it will be given to **participants** as an appendix. All studies must obtain **participant** consent. Some studies may obtain verbal consent, other studies will require written consent, as explained in the *Instructions* and *Guide* documents.

DURING THE STUDY

Describe the study procedures as they will be experienced by the **participant**

The purpose of this study is to associate the vibrations perceived on the posterior upper arm with the sensation felt when sliding a finger across a fabricated textured surface. The participants will experience 4 different patterns of vibrations that will be randomly repeated for 5 times (hence number of perceived vibrations is 20). The vibrations will be provided by a 11 mm miniature motor with a maximum supply of 2V, 120 mA (vibration frequency of 250 Hz). The motor will be battery powered and opto-electronically coupled to provide isolation with the main power supply. As a safety precaution, a first-aider will be on standby in the building throughout this psychophysics test.

In each activity session, an individual participant will arrive, and then follow as closely as possible the following schedule:

1. Welcome and introduction. Participant will be given 4 textured surfaces to feel and touch with his/her index finger (**5 min**)

2. Participants will be requested to put their arms on their sides. The length of the dominant upper arm (between the tip of shoulder (scapular acromion) and the elbow (humeral coronid fossa)) of the participant will be measured using a measuring tape, and the motor will be strapped on the posterior of the upper arm at ¼ of the total length from the tip of shoulder. The participant will then be introduced to the 4 different types of vibration to become familiar before the test begins. (**10 minutes**)

The 4 vibration patterns (*Patterns A – D*) are introduced in the following sequence:

Pattern A – continuous vibration (associated with smooth sensation)

Pattern B – repeated 500 millisecond* pulses with 500 millisecond* pauses in between (associated with surface Type B – repeating patterns of similar widths of grooves and ridges)

Pattern C – repeated 1000 millisecond* pulses with 500 millisecond* pauses in between (associated with surface Type C - repeating patterns of different widths of ridges and grooves)

Pattern D – repeated 500 millisecond* pulses with 500 millisecond* pause in between, then 500 millisecond* pulses with 1000 millisecond pause in between, then 500 millisecond* pulses with 1500 millisecond* pauses in between, and finally 500 millisecond* pulses with 20000 millisecond* pauses in between (associated with multiple roughness sensation)

* Approximate duration

3. **Psychophysic Test** – The 20 vibrations (**4** patterns, randomly repeated 5 times) will be provided to the participant one at a time. Participant will be asked to associate the provided surface textures with the generated vibration. For each vibration patterns perceived at the upper arm, the participants will verbally state the type of textures closely represented by the vibration. The information will be gathered by the investigator by using a specially prepared data collection form. (The form is as attached in Appendix (ii)) (**20 minutes**)

Finally, the participant will be thanked for his / her participation and invited to contact the investigator if they have any questions about the study, or the research more generally. They will be offered the opportunity to leave their e-mail address if they wish to receive a report on the findings of the study.

Identify how, when, where, and what kind of data will be recorded (not just the formal research data, but including all other study data such as e-mail addresses and signed consent forms)

The participants will be required to provide their name and signature on the consent information.

The study will be done in Room 4235 (Test Lab) of Building 59 (Zepler) on weekdays during normal office hours (9 a.m. to 5 p.m.). The only data that will be recorded is the relationship between the surface texture and the perceived vibration. This information will be verbally provided by the participant, and the investigator will gather this information using the prepared data collection form (Appendix ii).

After completing the test, the participant may opt to leave their email address should he/she wish to receive a report on the findings of the study.

Participant questionnaire

As an appendix, if using a questionnaire, reproduce any and all **participant** questionnaires or data gathering instruments in the exact forms that they will be given to or experienced by **participants**. If conducting less formal data collection, provide specific information concerning the methods that will be used to obtain the required data.

POST-STUDY

Identify how, when, and where data will be stored, processed, and destroyed
Contingency tables, scatter plots and chi-square test will be performed on the collected vibration pattern – texture surface data. Please see the DPA plan (Appendix iv) on how, when and where data will stored, processed and destroyed.

STUDY CHARACTERISTICS

(L.1) The study is funded by a commercial organisation: ~~**Yes /**~~ **No** (delete or highlight one) If 'Yes', provide details of the funder or funding agency here

(L.2) There are **restrictions** upon the study: ~~**Yes**~~ **/ No** (delete or highlight one) If 'Yes', explain the nature and necessity of the **restrictions** here

(L.3) Access to **participants** is through a third party: ~~**Yes**~~ **/ No** (delete or highlight one) If 'Yes', provide evidence of your permission to contact them as a separate appendix. Do not provide explanation or information on this matter here

(M.1) **Personal data** is collected or processed: **Yes /** ~~**No**~~ (delete or highlight one) Data will be processed outside the UK: ~~**Yes**~~ **/ No** (delete or highlight one) If 'Yes' to either question, provide the **DPA Plan** as a separate appendix. Do not provide information or explanation on this matter here. Note that using or retaining e-mail addresses, signed consent forms, or similar study-related **personal data** requires M.1 to be "Yes"

(M.2) There is **inducement** to **participants**: ~~**Yes**~~ **/ No** (delete or highlight one) If 'Yes', explain the nature and necessity of the inducement here

(M.3) The study is **intrusive**: ~~**Yes**~~ **/ No** (delete or highlight one) If 'Yes', provide the **Risk Management Plan** and the **Debrief Plan** as appendices, and explain here the nature and necessity of the intrusion(s)

(M.4) There is **risk of harm** during the study: ~~**Yes**~~ **/ No** (delete or highlight one) If 'Yes', provide the **Risk Management Plan**, the **Contact Information**, and the **Debrief Plan** as appendices, and explain here the necessity of the risks

(M.5) The true purpose of the study will be hidden from **participants**: ~~**Yes**~~ **/ No** The study involves **deception** of **participants**: ~~**Yes**~~ **/ No** (delete or highlight one) If 'Yes' to either question, provide the **Debrief Plan** as an appendix, and explain here the necessity of the deception

(M.6) **Participants** may be minors or otherwise have **diminished capacity**: ~~**Yes**~~ **/ No** If 'Yes', AND if one or more Study Characteristics in categories M or H applies, provide the **Risk Management Plan** and the **Contact Information**, as appendices, and explain here the special arrangements that will be put in place that will ensure informed consent

(M.7) **Sensitive data** is collected or processed: ~~**Yes**~~ **/ No** (delete or highlight one) If 'Yes', provide the **DPA Plan** as a separate appendix. Do not provide explanation or information on this matter here

(H.1) The study involves: **invasive** equipment, material(s), or process(es); or **participants** who are not able to withdraw at any time and for any reason; or animals; or human tissue; or biological samples: ~~**Yes**~~ **/ No** (delete or highlight one) If 'Yes', provide further details and justifications as one or more separate appendices. Do not provide explanation or information on these matters here. Note that the study will require separate approval by the Research Governance Office

Technical details

If one or more Study Characteristics in categories M.3 to M.7 or H applies, provide the description of the technical details of the experimental or study design, the power calculation(s) which yield the required sample size(s), and how the data will be analysed, as separate appendices. Do not provide explanation or information on these matters here.

APPENDICES (AS REQUIRED)

While it is preferred that this information is included here in the Study Protocol document, it may be provided as separate documents.

If provided separately, be sure to name the files precisely as "Participant Information", "Questionnaire", "Consent Form", "DPA Plan", "Permission to contact", "Risk Management Plan", "Debrief Plan", "Contact Information", and/or "Technical details" as appropriate.

Appendix (ii): Data Collection Plan

The purpose of this data collection is to investigate whether the vibration generated and perceived at the upper arm could be associated with the surface texture provided. There will be 4 types of vibration patterns that will be randomly repeated 5 times. The participants are required to associate the vibration patterns with the given surface textures (4 types – A, B, C and D). For each vibration patterns perceived at the upper arm, the participants will verbally state the type of textures closely represented by the vibration. The information will be gathered by the investigator by using this form.

Length of Upper Arm: ___ cm ¼ Length of Upper Arm: ___ cm

No of trials	Vibration Patterns (randomly generated)	Type of Texture (to be selected by participants)
1	Pattern B	
2	Pattern B	
3	Pattern A	
4	Pattern D	
5	Pattern A	
6	Pattern C	
7	Pattern A	
8	Pattern D	
9	Pattern B	
10	Pattern D	
11	Pattern C	
12	Pattern D	
13	Pattern A	
14	Pattern C	
15	Pattern C	
16	Pattern D	
17	Pattern C	
18	Pattern B	
19	Pattern A	
20	Pattern B	

Appendix J: Dimensions of the Fabricated Brass Platform

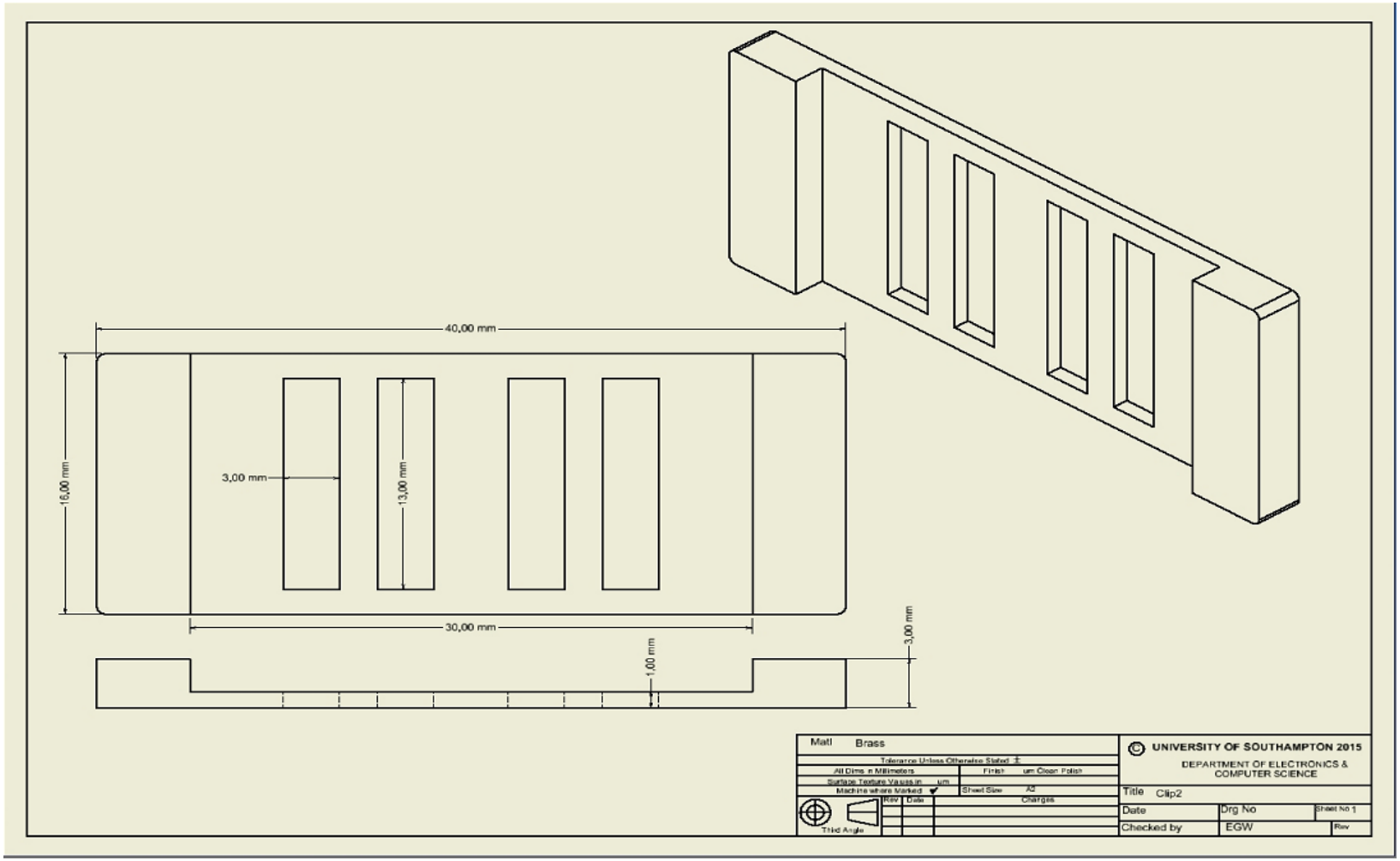
40,00 mm
16,00 mm
3,00 mm
13,00 mm
30,00 mm
1,00 mm
3,00 mm
Matl Brass
Tolerance Unless Otherwise Stated ±
All Dims. in Millimeters
Finish um Clean Polish
Surface Texture Values in um
Machine where Marked
Sheet Size A2
Rev Date Changes
Third Angle
© UNIVERSITY OF SOUTHAMPTON 2015
DEPARTMENT OF ELECTRONICS & COMPUTER SCIENCE
Title Clip2
Date
Drg No
Sheet No 1
Checked by EGW
Rev